UNIVERSITÀ
DEGLI STUDI
FIRENZE

PhD in
Atomic and Molecular Photonics

CYCLE XXXV

COORDINATOR
Prof. Diederik Wiersma

MESOSCALE CALCIUM IMAGING OF FREELY MOVING MICE ENGAGED IN SOCIAL INTERACTION REVEALS WIDESPREAD INTER-BRAIN SYNCHRONY

Academic Discipline (SSD) FIS/03

Doctoral Candidate
Dr. Lucchesi Jessica

Supervisor
Prof. Pavone Francesco

Co-Supervisor
Dr. Allegra Mascaro Anna Letizia

Coordinator
Prof. Diederik Wiersma

Years 2019/2022

ABSTRACT

The natural inclination to engage or associate with others is referred social interaction. The mechanisms involved in social behavior are extremely complex but are important for the health and well-being of every individual. When social interactions are compromised, they are a clear sign in several psychiatric disorders such as autism, schizophrenia, depression, and social anxiety disorder. Identifying the neural and behavioral mechanisms underlying these conditions would be important to improve their treatment.

In mice, studies of social interaction are primarily based on examining behavior in individual animals by analyzing a single brain region at a time. In addition, monitoring neural activity using optical imaging techniques requires keeping the subject in a head-fixed condition, greatly limiting the behavioral repertoire.

In humans, conversely, the neural activity of two or more subjects is acquired simultaneously using non-invasive techniques such as EEG, fMRI, or fNIRS during the execution of the behavioral paradigm. This type of study called Hyperscanning provides information about brain organization and the level of synchrony between the two participants' brain signals during the performance of various types of social activities.

Recently, with the advent of miniaturized optical devices, it is possible to perform optical imaging in freely moving rodents, however, currently developed systems have fields of view limited to a few mm^2 or require implantation of GRIN lenses in the brain site to be investigated. All of this precludes the study of neural dynamics distributed over large cortical areas associated with complex behaviors.

In this Ph.D. project to overcome these problems, a new miniaturized wide-field optical system "Miniscope" was developed to perform calcium imaging, distributed over both hemispheres, in freely moving mice. Given the importance of social interactions in individual well-being, an innovative experimental paradigm was developed to study the behavioral repertoire exhibited by rodents. By combining this novel miniaturized optical system and the developed behavioral paradigm, a study of Hyperscanning in mice engaged in social interaction was conducted. This allowed simultaneous investigation of both the behavioral repertoire and neuronal activity distributed over the entire cortex. The results obtained show that the developed system allows the monitoring of calcium activity with a large wide field of view and sufficient optical resolution to perform mesoscale neuronal imaging. Design improvements made it possible to develop a system light enough to perform free-moving imaging without hindering animal behavior.

Using the Miniscope, it was possible to record the neural activity distributed over the entire cortex mantle while two subjects are interacting in freely moving conditions. Wavelet Coherence Transform analysis was used to analyze the neural signal since this technique is widely employed in Hyperscanning studies in humans and provides information on how similar a pair of signals are as a function of frequency and time.

Wavelet analysis conducted over the whole cortex revealed inter-brain coupling in two frequency bands (infra-slow and slow) modulated by the type of behavior. In detail, when two subjects simultaneously participate in the interaction (Gap Interacting), two coherence peaks in two frequency bands at 1/16 Hz (infra-slow) and about 4 Hz (slow) are evident. However, when only one of the two subjects in the dyad goes to the gap to interact (Gap Non-Interacting) a single coherence peak emerged in the infra-slow frequencies of lower intensity than in the previous behavioral condition, while the peak in the slow frequencies disappears. These results show that inter-brain coupling in slow frequencies is a characteristic event of the Gap Interacting condition, however, the Gap Non-Interacting is a sufficient behavioral condition to determine inter-brain coupling although there is no physical contact between dyad members.

Moreover, when the synchrony of parceled brain regions is examined, it is found that not all cortical regions exhibit the same inter-brain coupling in the two frequency bands. Analysis of parcellated coherence maps by area highlights inter-brain coherence coupling of all cortical regions in the infra-slow band of the interacting dyad, while slow frequency analysis showed coupling between the two neural signals mainly in the somatosensory and visual area of both hemispheres and the associative area of the right hemisphere only.

In conclusion similar to the results obtained in Hyperscanning experiments, we found that social interaction in mice modulates the coupling among the brains of interacting subjects and that this coupling is dependent on both the cortical areas and the frequency band. This matches the observations done in humans and therefore this platform provides an experimental framework to study social interactions in an animal model.

List of Contents

I. Introduction 1
  1. Social Interaction 3
    1.1. Behavioral Paradigms for Studying Social Interaction 4
    1.2. Neuroscience of Social Interaction: Animal Studies 14
  2. Neuroscience of Social Interaction: Human Studies 21
    2.1. Hyperscanning Techniques for the Study of Brain Dynamics 22
    2.2. Analysis Techniques for the Study of Biomedical Signals 24
  3. Calcium Fluorescence Indicators 32
    3.1. Genetically Encoded Calcium Indicator (GECI): GCaMP Family 34
    3.2. Development of Thy1-GCaMP6 Transgenic Mice 37
  4. Wide-field Fluorescence Microscopy 38
  5. Miniscope 40
    5.1. Single-photon Miniaturized Devices based on GRIN lens 42
    5.2. Miniaturized Wide-field Microscopy 46
  6. Aim of the study 48
II. Methods 51
  1. Surgery for the Realization of the Optical Window 53
  2. Transgenic Animals 56
  3. Wide-field Epifluorescence Microscope and Behavioral Platform 57
  4. Visual Stimulation Experiment 61

5. Social Interaction: Timeline of the Experiment 63

III. Results 67

1. Miniscope 69

1.1. Mechanical and Optical Design 69

1.2. Miniscope: Optical Characterization 70

1.3. Miniscope Compared to Widefield Microscope: Visual Stimulation Experiment 72

2. Behavioral Setup 76

3. Miniscope Validation 79

3.1. Behavioral Tracking in Mice with and without Miniscope 79

3.2. Image Processing and Fluorescence Signal 83

4. Social Interaction: Behavioral Analysis 86

4.1. Quantification of Nose Pokes Events in Interacting vs Solitary Subject…..87

4.2. Behavioral Segmentation 90

5. Social Interaction: Wavelet Coherence Transform Analysis 92

5.1. Coherence Spectrum Distributed over the Entire Cortex 95

5.2. Coherence Spectrum Parceled for Cortex Brain Region 98

V. Discussion 101

VI. Future Perspective 115

1. Hemodynamic Contribution: Measurement of Reflectance.............117

2. The New Generation of Miniscopes..121

2.1. Miniscope v2: Mechanical and Optical Design 123

2.2. Miniscope v2: Optical Characterization 125

3. Toward the Wire-free Version 127

Bibliography..129

Ringraziamenti 155

List of Figures

Figure 1: Three-Chamber Test. 6
Figure 2: Representation of the V-soc Maze Test. 7
Figure 3: Visible Burrow System. 8
Figure 4: Representation of the U-Shaped Two-Choice Test. 9
Figure 5: Experimental Setup to Study Social Interactions in the Home Cage. 11
Figure 6: Representation of the Linear Chamber Test. 13
Figure 7: Mouse Brain Areas (sagittal plane). 16
Figure 8: Graphical Representation of Wavelet Transform Analysis. 25
Figure 9: Graphical representation of the Number of Cycles of the Gaussian Function. 27
Figure 10: Wavelet Scaling. 28
Figure 11: Wavelet Transform Coherence Graphical Representation. 31
Figure 12: GECI Indicator Based on Single Fluorescent Protein "GCaMP". 35
Figure 13: Miniscope History. 41
Figure 14: Single-photon Miniaturized Devices. 44
Figure 15: mini-mScope Design. 47
Figure 16: Illustration Showing the Steps of Surgery to Create the Optic Window. 55
Figure 17: Widefield Epifluorescence Microscope. 60
Figure 18: Timeline of the Experiment. 65
Figure 19: Miniscope Design: Mechanical and Optical Characterization. 71
Figure 20: Visual Stimulation: Comparison between Widefield and Miniscope. 74

Figure 21: Experimental Setup for Performing Social Interaction Recordings. 77
Figure 22: Miniscope Validation: Behavioral Tracking in mice with and without Miniscope. 82
Figure 23: Miniscope Validation: Image Processing and Fluorescence Signal. 84
Figure 24: Social Interaction: Quantification of Nose Pokes Events. 89
Figure 25: Behavioral Segmentation. 91
Figure 26: Wavelet Coherence Analysis: Interacting vs Surrogate Dyads. ...94
Figure 27: Coherence Spectrum Distributed over the Entire Cortex. 97
Figure 28: Coherence Spectra Segmented by Brain Region and Coherence Map. 99
Figure 29: Oxy- and Deoxy-Hemoglobin Absorption Spectrum. 119
Figure 30: Miniscope v2. 126

List of Formulas

Equation 1: Wavelet Transform 26
Equation 2: Morlet Wavelet 26
Equation 3: Gaussian Function 27
Equation 4: Number of cycles 27
Equation 5: Cross-wavelet Transform 29
Equation 6: Wavelet Coherence 30
Equation 7: Equation for Calculating Magnification and Focal Length 58
Equation 8: Equation for Calculating the Focal Length of the Tube Lens 58

I. Introduction

1. Social Interaction

Social interactions are defined as how we act and react to those around us; they form the basis of any relationship between two or more individuals, regardless of age, gender, or ethnicity. Physical movements, body language, coordination, competition, conversation, sharing thoughts and emotions, playing, and more are all part of these interactions. Positive social contacts provide several physical and mental advantages. These include enhanced mental and physical health, greater communication skills, and increased cognitive capacity. The natural inclination to engage or associate with others is defined as social interaction. The neural mechanisms involved in social behavior are only partially known so understanding them would help improve the health and well-being of every individual (Kim et al. 2019). When social interactions are compromised, they are a clear sign, in several psychiatric disorders such as autism spectrum disorder (ASD), schizophrenia, depression, and social anxiety disorder (Acikgoz, Dalkiran, and Dayi 2022; Bove et al. 2018; Kaidanovich-Beilin et al. 2011), for this reason, identifying the mechanisms underlying these conditions is important to ameliorate their treatments (Gunaydin et al. 2014).

Numerous tests have been conducted on rodents (mice and rats) as they are prosocial animals exhibiting a wide behavioral repertoire (Kim et al. 2019). They are colonial animals that generally live in groups with a large number of members establishing hierarchies, show parental behaviors, affiliation, juvenile play, social dominance, memory, and social communication, sometimes exhibit aggressive behavior, and finally, they have an innate instinct to explore new environments (Crawley 2007; Ricceri, Michetti, and Scattoni 2016). These are just some of the features of the wide behavioral repertoire of rodents, a suitable animal model to generate experimental paradigms to enable a greater understanding of the disorders of social recognition and social behavior that can occur in humans (Crawley 2004).

1.1. Behavioral Paradigms for Studying Social Interaction

Rodents represent a widely used model for studying social interaction because they are prosocial animals that tend to live in large groups. Various experimental paradigms have been developed over the years to study behavior under physiological conditions and to understand what behavioral dynamics are altered under pathological conditions such as the autism spectrum. Starting from the classic Three-Chambered test to open field arena, dyadic tests are performed to study behavior between both same-sex couples (female-female or male-male) or mixed (male-female) (Ricceri et al. 2016).

A series of behavioral paradigms used throughout history for the study of social interactions in mice will be described below.

1.1.1. Three-Chambered Apparatus

Several sociability tests have been designed to test and compare different behavioral aspects of social interactions in rodents (Bove et al. 2018; Crawley 2004; Kim et al. 2019; E. Lee et al. 2016; Lee et al. 2018; Moy et al. 2004; Nadler et al. 2004; Silverman et al. 2010).

The first studies to investigate social behavior began in the early 2000s with the development of the Three-Chambered apparatus (Nadler et al. 2004), to evaluate sociability and the preference for social novelty to conduct studies in physiological conditions and subsequently in contexts of behavioral deficits characteristic, for example, the autism spectrum (Crawley 2004).

The apparatus consists of a large arena divided by two clear plexiglass barriers, with an open middle section, to generate three communicating chambers allowing the animal to explore the environment (**Figure 1**). In the two lateral chambers, two round wire cages could be empty or contain an unfamiliar subject. The paradigm includes four phases: the Habituation of the mouse to the center chamber where the animal explores only this part of the setup for 10 minutes. The habituation of the mouse to all three chambers, where the animal is allowed to explore all the apparatus (without the empty cages) for 10 minutes. Sociability test [1](“Stranger 1” vs “Empty”): in which in one of the lateral chambers an unfamiliar subject (“Stranger 1”) is placed inside the round wire cage while the other chamber remains with an empty cage and the mouse is left free to move for 10 minutes. Preference for social novelty test [2] (“Stranger 1” vs “Stranger 2”): after 10 minutes of sociability, a second unfamiliar animal (“Stranger 2”) was placed inside the previously empty wire cage and the preference for the two subjects was evaluated (**Figure 1**) (Nadler et al. 2004; Yang, Silverman, and Crawley 2011). At the end of all the sessions, the parameters of time spent in the two chambers, number of entrances, and time spent sniffing the wire cages were evaluated to determine the levels of sociability and preference for social novelty.

---

[1] **Sociability** is defined as the tendency of the experimental subject to spend more time exploring an unfamiliar mouse than exploring an empty chamber.

[2] **Preference for Social Novelty** is defined as the tendency to spend more time exploring a second unfamiliar subject than the unfamiliar mouse previously entered (Moy et al. 2004; Yang, Silverman, and Crawley 2011).

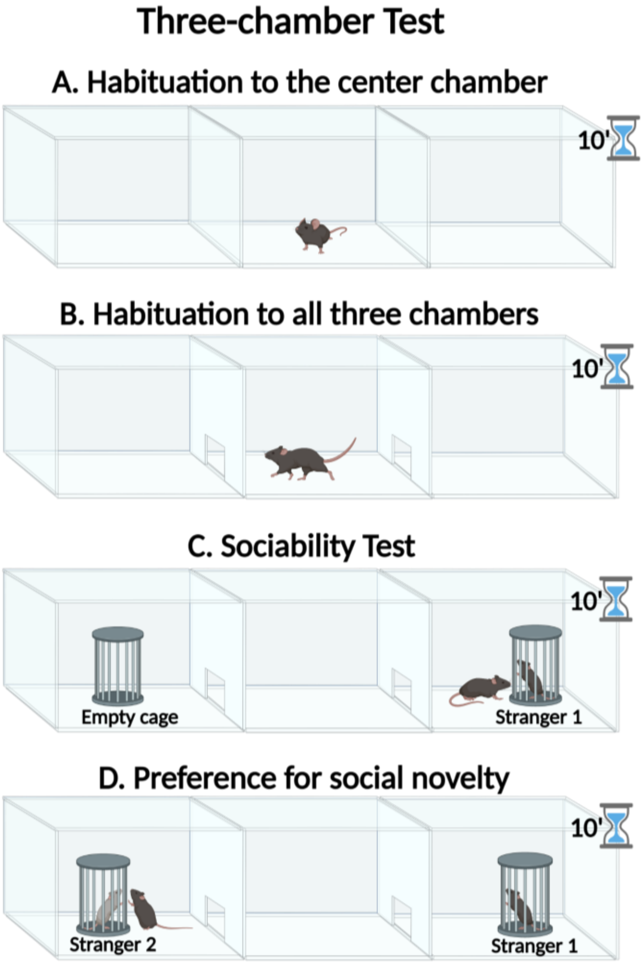

Figure 1: Three-Chamber Test.

Representation of the experimental apparatus of the Three-Chamber test. Panel (**A)** shows the Habituation phase to the central chamber followed by the Habituation to the three chambers in panel **(B)**. In **(C)**, a stranger subject was placed in one of the two lateral chambers to evaluate Sociability while in **(D)**, the Preference for Social Novelty was assessed by placing a second foreign subject in the opposite side chamber. Each phase lasts 10 minutes.

1.1.2. Vsoc-maze Test

The Three-Chamber test is the progenitor of experimental apparatus for studying social behavior. Starting from this model, different types of setups have been developed such as the Vsoc-maze (**Figure 2**), a modified version of the V-shaped maze, used to test sociability and the preference for social novelty (Martínez-Torres et al. 2019). The different shape of the setup is designed to reduce behavioral variability, compared to the Three-Chamber test, for this reason, the duration of the sessions was shortened from 10 to 5 minutes. Nadler and colleagues observed that most social approach behaviors occur within the first 5 minutes of the sociability test (Nadler et al. 2004). The reduction of the duration of the behavioral sessions could improve the reproducibility of the experiments by reducing the stress on the animal (Martínez-Torres et al. 2019).

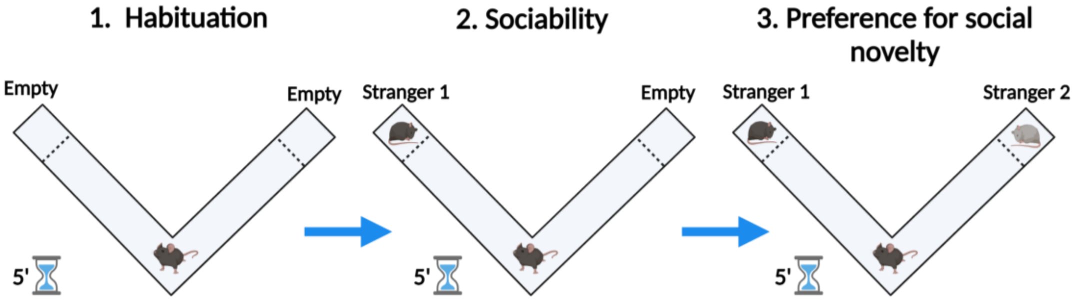

Figure 2: Representation of the V-soc Maze Test.

In this paradigm, the shape of the experimental setup was modified to limit behavioral variability. In this test Habituation (1), Sociability (2), and Preference for Social Novelty (3) are assessed. The duration of sessions is reduced from 10 to 5 minutes to reduce the animal's stress.

1.1.3. Visible Burrow System

Given the wide behavioral repertoire of rodents and particularly the normal development of large colonies with the establishment of hierarchies, one behavioral paradigm employed in the study of behavioral alterations in different rodent strains is the Visible Burrow System (VBS) (**Figure 3**) (Bove et al. 2018). The VBS simulates the natural environment in which rodents live, this apparatus consists of an open arena with a defined light/dark cycle (12h light and 12h dark), connected to a second arena kept constantly in the dark, equipped with chambers and burrows where animals have the opportunity to nest (**Figure 3**). Both male and female animals are housed in this setup, and although it was previously developed to investigate the effects on brain mechanisms related to dominance/submission behavior (Herman and Tamashiro 2017), today this paradigm is being used to improve the translational validity of sociability in rodents in a more natural-like habitat (Bove et al. 2018).

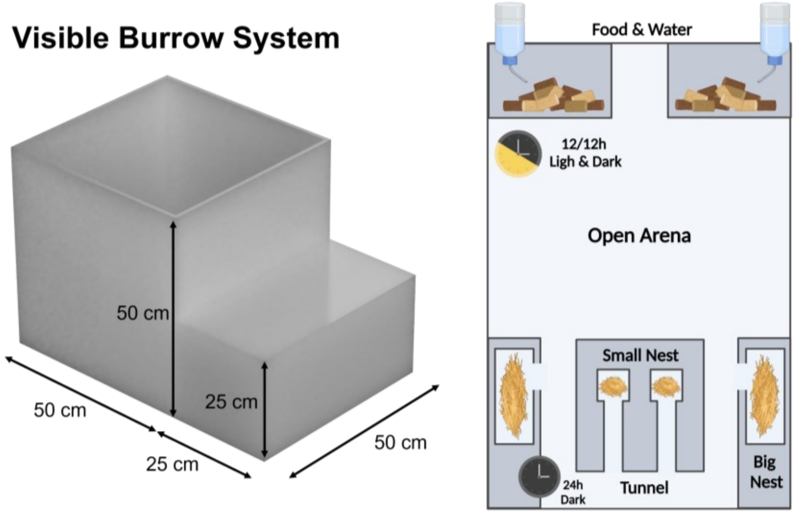

Figure 3: Visible Burrow System.

On the left. CAD diagram of the experimental apparatus consisting of two communicating arenas, the first open field with dimensions of 50 x 50 x 50 cm and the second kept constantly in the dark with dimensions of 25 x 50 x 50 cm. The right internal representation of the Visible Burrow System. A 12/12 h light-dark cycle is maintained in the open field arena with food and water ad libitum. The dark arena contains a series of tunnels in which animals can nest.

1.1.4. U-Shaped Two-Choice Field

Inspired by the Three-Chamber test, among the paradigms we find the U-shaped two-choice field to study sociability and understand the different behavioral states of sociality in rodents (Lee et al. 2018). This test has as its basic structure an open field square arena in which a central wall is inserted on one side to create two symmetrical rectangular fields that generate a U-shaped structure seen from above (**Figure 4**). The wall leaves the arena partially open providing the possibility for rodents to choose the area to explore. Using the U-shaped two-choice paradigm it is possible to study different aspects of sociability by comparing contrasting behavioral options, such as the choice between a social target vs an inanimate target or empty wire cage, an earlier stranger vs a new stranger, or finally the choice between a cage-mate and a non-mate (familiar vs non-familiar) (**Figure 4**) (Lee et al. 2018).

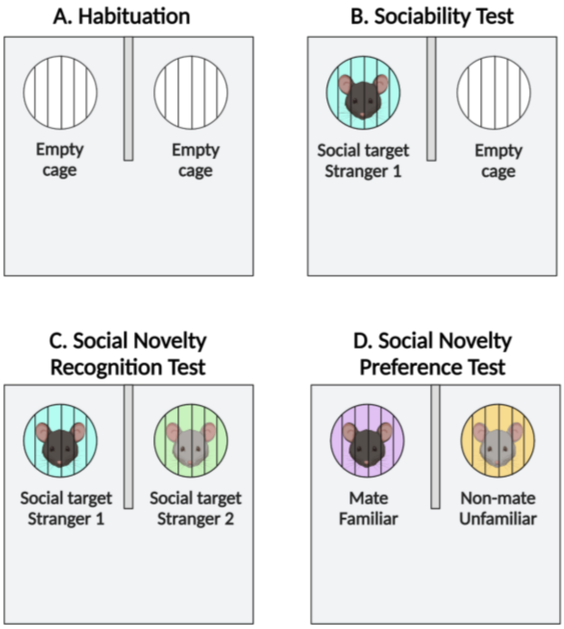

Figure 4: Representation of the U-Shaped Two-Choice Test.

This test consists of a square arena with a central barrier to generating a U-shaped field. This setup leaves the animal free to choose which area to explore **(A)**. The parameters of Sociability **(B)**, Social Novelty Recognition **(C)**, and Social Novelty Preference **(D)** are evaluated. In the paradigm, the Social Novelty Preference is assessed between a familiar and unfamiliar subject

1.1.5. Social Interaction Test in Home Cage

Although the Three-Chamber test remains the progenitor of behavioral tests from which numerous versions have been developed, in most of the studies listed in the previous paragraphs, we tend to investigate and compare the reaction between two or a maximum of three subjects at the same time, the recording sessions generally are long to obtain a large data output and all setups require the animal to be moved from their cage into a foreign environment generally made of Plexiglass. The aim of the study conducted by Kim and colleagues is always focused on the analysis of the time spent by the subjects sniffing an empty wire cage or with a stimulus inside, but with the difference of conducting the test in their home cage with the bedding and all the olfactory stimuli normally present (Kim et al. 2019). This is to limit the novelty effect of the environment and conduct the experiment in a less stressful and ethologically valid context. With these settings, it is possible to test the behavior of several subjects simultaneously obtaining a high throughput of information and data in a shorter amount of time.

The subjects who took part in the study were housed together in a large cage in groups of 5 animals. Using the home cage, following the habituation phase in which an empty circular wire cage was placed in the center for 30 minutes, a stranger mouse (stimulus) was placed inside to assess sociability (**Figure 5**). In the present study, they chose to develop two different home-cage setups to measure the degree of sociability and preference for social novelty. In addition to the previous one, two further behavioral tests were conducted in which two small cages (one on each side) of the same material as the home cage were added to the ends of the cage, closed by a transparent barrier during the habituation phase and replaced from a wire grid for social interaction sessions. The stimulus (stranger mouse) and an inanimate object were placed in their respective structures. The inanimate object was subsequently replaced by a second stimulus, a new stranger mouse to assess the degree of sociability and preference for social novelty (**Figure 5**) (Kim et al. 2019). Excluding the habituation phase, each sociability level assessment test lasted 15 minutes.

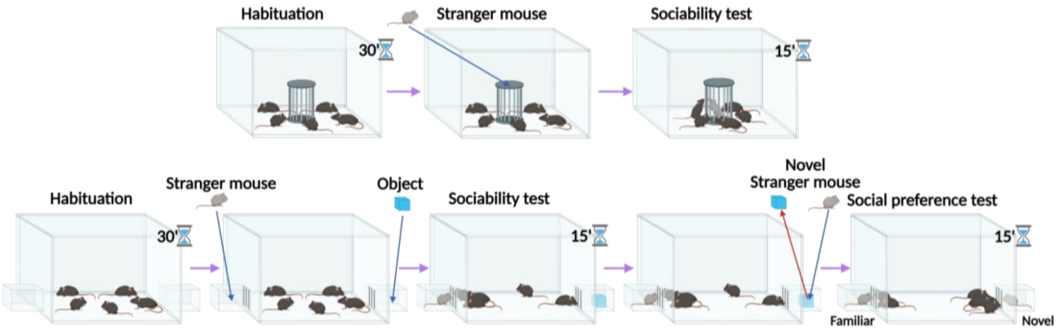

Figure 5: Experimental Setup to Study Social Interactions in the Home Cage.

In this paradigm, evaluating the social interaction of many animals simultaneously increases the data output. Furthermore, conducting the test in one's home cage allows one to evaluate the behavior of the subjects in more naturalistic conditions.

1.1.6. Modified Version of the Three-Chamber Test to Assess Social Approach Behavior

The studies reported until now are mainly focused on the analysis of behavior in different contexts and experimental setups. Instead, Lee and colleagues (E. Lee et al. 2016) focus only on social approach behavior while recording the activity of a population of neurons in the medial Prefrontal Cortex using a modified version of the Three-Chamber test (E. Lee et al. 2016). This three-linear apparatus (45 x 10 x 21 cm) made of transparent plexiglass (**Figure 6**), differs from the classic Three-Chamber test as it is formed by a single rectangular arena without the possibility of exploring the side chambers, this minimizes the exploration of superfluous areas and to encourage the mechanism of social interaction with the target. The social targets were placed in two additional chambers (10 x 10 x 20 cm) placed at the ends of the apparatus (**Figure 6**). The target chambers could remain empty (empty chamber "E"), contain a stranger mouse (social stimulus "S"), or an inanimate object (non-social stimulus "O"). Each animal was tested several times by exposing it to a different stranger mouse with an interval of 4 days between each experimental session since it is known that social isolation improves social interaction (Crawley 2004). To allow the animals to interact, the lower 10 cm of the side walls of the linear chambers communicated with the target chambers with thin metal wires. Similarly to the various paradigms, in this test, there are three experimental sessions: the first is for habituation in which the mouse is placed in the linear chamber with the target chambers empty for 10 minutes to explore the environment ("Habituation" or "E-E" session). Subsequently, a stranger mouse (social stimulus "S") and an inanimate object (non-social stimulus "O") are placed simultaneously in the target chambers and the interaction session is performed for 10 minutes. At the end of the latter, the two stimuli were switched in position (“S-O”,“O-S”) (always keeping the same stranger mouse) and the test was repeated for another 10 minutes. The repeated session of interaction (“O-S”) between an inanimate object and social stimulus has the goal to separate the neuronal dynamics dependent on the social objective from those of spatial position (right-left) (Lee et al. 2015).

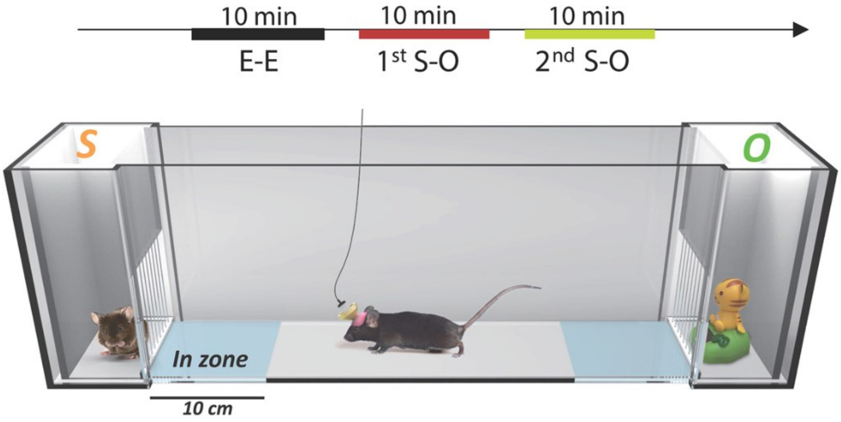

Figure 6: Representation of the Linear Chamber Test.

This paradigm, inspired by Crawley's Three-Chamber test, consists of three phases: one of Habituation in which the two lateral chambers are empty (E-E), the first phase of Social Interaction where a stranger mouse is placed into one of the two chambers versus an inanimate object (S-O) and the third phase where the stranger mouse and the inanimate object are swapped between the two chambers (O-S). Image from E. Lee et al. 2016.

1.2. Neuroscience of Social Interaction: Animal Studies

Considering the importance of social interactions in the modern community and the wide repertoire of behavioral paradigms in the literature and trying to understand the neural mechanisms underlying social interactions, or more broadly in social cognition, it is important to ameliorate the conditions in which these processes are impaired. Throughout history, using different tools of investigation, the field of neuroscience is trying to gain more information about neuronal circuitry and the mechanisms involved in social interaction at different levels of resolution starting from the examination of a few neuronal units to larger brain areas (Miura et al. 2020).

As previously discussed, both rats and mice exhibit a wide behavioral repertoire including engagement in reciprocal interactions with conspecifics, pro-social behaviors, emotional contagion, and empathic responses (Atsak et al. 2011; Ben-Ami Bartal et al. 2014).

Whether we talk about the behavioral approach, social interaction, or generally about social cognition in animal models, the brain area most involved is the medial prefrontal cortex (mPFC). This area is connected with several sub-cortical structures such as the amygdala for emotional processing, hippocampus for memory processing, hypothalamus for stress modulation and regulation, nucleus accumbens (NAc) involved in social incentive, olfactory bulbs for receiving and processing olfactory signals, and finally cortical regions for processing sensory and motor inputs and outputs (Ko 2017).

1.2.1. Brain Areas Related to Social Interactions: Role of the medial Prefrontal Cortex

The medial prefrontal cortex (mPFC) together with its projections (**Figure 7**) plays an important role in modulating social behavior not only in rodents but also in humans (Ernst and Fudge 2009). Anatomically, the prefrontal cortex in humans is divided into different regions which include: the orbitofrontal, dorsolateral, ventrolateral, and medial prefrontal cortex. All of these regions mediate cognitive behavior, decision-making, and goal-directed social behaviors (Amodio and Frith 2006), therefore it is not surprising that patients with PFC lesions exhibit a reduced or less flexible behavioral repertoire (Anderson et al. 1999).

Although anatomically between humans and rodents there is no direct similarity between the structures, a significant functional homology between the mPFC in the two species is reported in the literature. In human studies, it was found that mPFC has projections with subcortical structures such as the amygdala and hypothalamus (Insel and Fernald 2004). Analyzing the levels of sociability and preference for social novelty with the Three-Chamber test in rodents, it was observed that neurons in the mPFC exhibit a high rate of discharge when a mouse interacts with a foreign subject but not with an inanimate object or a simple empty chamber. This suggests that the neuronal activity of the mPFC is involved with the social approach behavior in mice (E. Lee et al. 2016). In the study by Lee and colleagues (Lee et al. 2015), a functional asymmetry was reported between neuronal activity in the two hemispheres of the mPFC. According to this study, neurons in the right hemisphere of the mPFC appear to process stress during dangerous experiences while the left hemisphere plays its role in translating stress into social behavior (Lee et al. 2015).

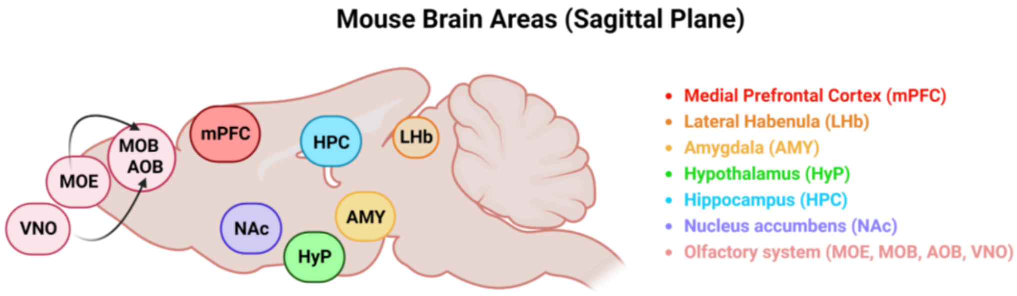

Figure 7: Mouse Brain Areas (sagittal plane).

Representation of mouse brain areas involved in social interactions. Starting from the rostral region we find the olfactory system which includes Main Olfactory Epithelium (MOE), Main Olfactory Bulb (MOB), Accessory Olfactory Bulb (AOB), Vomeronasal Organ (VNO), medial Prefrontal Cortex (mPFC), Nucleus accumbens (NAc), Hypothalamus (HyP), Hippocampus (HPC), Amygdala (AMY) and Lateral Habenula (LHb).

1.2.2. Role of the Amygdala

Combining optogenetic manipulation techniques and electrophysiological recordings, the amygdala has been documented to exert modulatory effects on social behaviors by processing emotionally and socially relevant information through the numerous subcortical networks that interact with the mPFC (Yizhar et al. 2011); this information is typically detected in rodents through olfactory-based perception (Adolphs 2010). There are more than 20 different subnuclei in the amygdala, many of which are involved in specific social behaviors through significant anatomical and functional interactions with other brain regions. There are three amygdaloid subnuclei mainly involved in social behavior: a more superficial group made up of the cortical nuclei and the nucleus of the lateral olfactory tract, a centromedial group made up of the medial (MeA) and central (CeA) nuclei. Finally, the basolateral complex (BLA) group, includes the lateral, basal nucleus, and accessory basal nucleus (Sah et al. 2003). The primary sensory input into the amygdala occurs in the BLA, whereas the CeA is the main output structure that responds to physiological fear reactions and social behavioral responses. Olfactory inputs are received by the MeA, which then transmits this information to other hypothalamic regions to affect a range of social behaviors, including defensive, aggressive, mating, and parenting behaviors (Canteras et al. 1995). Finally, the lateral nucleus of the amygdala receives somatosensory, auditory, and visual inputs that will be conveyed to the CeA nuclei, in turn, is connected with the hypothalamus, brainstem, and finally to the mPFC to coordinate social behaviors such as aggression or mating (Ko 2017). Using recent neuroimaging techniques, it is possible to investigate the connections between the amygdala and the mPFC to understand their role in behaviors related to fear and anxiety. Theta range (4-12 Hz) oscillatory behavior and synchrony in the mPFC-BLA circuit in mice have been linked to the discrimination of aversive versus safe cues in fear-conditioning and open-field test paradigms (Likhtik et al. 2014).

Finally, several neurotransmitters such as dopamine and serotonin, neuropeptides like oxytocin (OXT), arginine vasopressin (AVP), corticotropin-releasing hormone (CRH), and neuropeptide Y, related to social behavior are released by the amygdala (Ko 2017).

1.2.3. Role of the Hypothalamus

The hypothalamus regulates a variety of innate survival behaviors and related internal motivational states, such as eating, drinking, defending against predators, and engaging in social behaviors like mating and combat. It has several nuclei, each of which is believed to be involved in one or more behavioral processes (Lo et al. 2019). In rodents, the hypothalamus gets multimodal sensory inputs from the PFC and hippocampus as well as olfactory inputs from the brainstem, amygdala, and other olfactory organs. In response to these inputs and the reception of hormonal stimuli such as oxytocin and arginine vasopressin, from the posterior pituitary, hypothalamic neurons regulate several complicated homeostatic mechanisms correlated with social behaviors (Ervin et al. 2015).

1.2.4. Role of the Hippocampus

The hippocampal tri-synaptic circuit connects the entorhinal cortex EC, the dentate gyrus (DG), and Cornu Ammonis regions 3 and 1 (CA3 and CA1) (Lehr et al. 2021). The small subregion of the hippocampus between CA3 and CA1 is named CA2, this turns out to be closely connected with the other hippocampal regions playing the role in hippocampal information processing. Pyramidal neurons in CA2 receive excitatory input from CA3 and DG and a strong excitatory connection from the entorhinal cortex, located outside the hippocampus. Pyramidal neuron silencing studies conducted on this region show that CA2 plays a crucial role in social recognition memory (Hitti and Siegelbaum 2014; Lehr et al. 2021). Consequently, CA2 has become an area that is predominantly linked to the processing of social information.

Given the crucial role of the hippocampus in memory formation, it is not surprising that mPFC neurons establish strong connections with the hippocampus to mediate social cognition in mice (Kogan, Franklandand, and Silva 2000). According to several researches, the mPFC and hippocampus activity during social cognition is correlated or synchronized in a specific frequency range (Bicks et al. 2015). In particular, social memory, and emotional behaviors traits like fear and anxiety have been linked to the ventral hippocampus (vHPC) (Keysers et al. 2022; Okuyama et al. 2016). In addition, strong connections between vHPC and the amygdala are important for the expression of social behaviors in rodents (Ko 2017).

1.2.5. Role of the Lateral Habenula

A vast range of behaviors, including maternal care, sleep, and different types of cognition, are influenced by the lateral habenula (LHb) (Baker et al. 2015). As a component of the epithalamus, the Lateral Habenula through both the dopamine and 5-hydroxytryptamine (5-HT) systems sends information about the emotional/internal state. Several studies have suggested that the LHb is involved in olfactory processing, mating behavior, painful or rewarding learning, and the execution of complicated goal-directed activities (Baker et al. 2015; Ko 2017).

According to projection neuron targets or neuronal types, the LHb can be divided into at least 10 regions, but it is unclear what exactly each subregion contributes. The basal ganglia, lateral hypothalamus, ventral tegmental area (VTA), basal forebrain (BF), and medial raphe nuclei are just a few of the brain areas that the LHb receives input from, all of this suggesting that it contributes to behavioral flexibility (Ko 2017). Also, the lateral LHb receives inputs from the anterior cingulate cortex and insular cortex, while the medial LHb receives inputs from the prelimbic and infralimbic regions of the mPFC (Baker et al. 2015). Together with a recent study reporting the role of LHb in social play behavior (Baarendse et al. 2013), suggest that this brain region is involved with various aspects of social behavior.

1.2.6. Role of the Olfactory System

Social behavior is an extremely complex phenomenon orchestrated by numerous brain components. In describing the areas classically involved in these processes, the olfactory system has often been mentioned. For most of their social interactions, mice heavily rely on olfaction. Olfactory cues help in choosing a partner, distinguishing other subjects or individuals, and assessing health status (Ryan et al. 2008). Mice with anosmia exhibit unusually aggressive, affiliative, and sociable behavior. Both the main and the accessory olfactory systems in mice are capable of detecting olfactory cues (Jakupovic, Kang, and Baum 2008).

For social interaction, rodents use body odor, studies suggest that the main olfactory epithelium (MOE) (**Figure 7**) is involved in the detection of volatile components of urine, which will be processed later in the main olfactory bulb (MOB).

Receptor neurons in the vomeronasal organ (VNO), on the other hand, would pick up nonvolatile components of urine and extra-orbital secretions from the lacrimal glands and then process the signal in the accessory olfactory bulb (AOB) (Jakupovic et al. 2008).

2. Neuroscience of Social Interaction: Human Studies

Although the social nature of human beings has been discussed for many years from countless perspectives starting from the philosophical one in which, paraphrasing Aristotle, "Man is a social animal", the field of neuroscience has begun to study only in the last few decades the brain structures necessary to understand personal and other people's information, including the rules underlying interactions with other human beings (Babiloni and Astolfi 2014; Hari and Kujala 2009). In the past, the study of these circuits was based only on the neural analysis of a single individual while interacting with other subjects, however, this involves the limitation of having only a limited portion of the information that we could obtain from the simultaneous recording of two or more interacting individuals.

The idea of performing Hyperscanning studies is born: the simultaneous measurement in real time of the brain activity of two or more subjects involved in social interactions to investigate neuronal correlations (Astolfi et al. 2011; Babiloni and Astolfi 2014; Dumas et al. 2010; Konvalinka and Roepstorff 2012), contrary to the classic behavioral paradigms in which the brain activity of the single individual was studied, using Hyperscanning studies we can obtain information about inter-cerebral synchrony by going to deeper and broadening previous studies on the neuroscience of social interactions.

2.1. Hyperscanning Techniques for the Study of Brain Dynamics

Throughout history, various tools have been developed to investigate brain dynamics, later used for Hyperscanning studies. Among the various techniques, we mention the most relevant in recent years such as Electroencephalography (EEG) (Babiloni et al. 2006), Magnetoencephalography (MEG) (Baillet 2017), functional Magnetic Resonance (fMRI) (Montague et al. 2002) and finally the most recent: functional Spectroscopy in the Near Infrared (fNIRS) (Cui, Bryant, and Reiss 2012).

Functional magnetic resonance (fMRI) is a widely used technique in the study of cognitive neuroscience and Hyperscanning (Koike et al., 2016; Montague et al., 2002; Spiegelhalder et al., 2014). It detects changes associated with blood flow and perceives the difference in contrast between the oxygenated and non-oxygenated form of hemoglobin (blood-oxygen-level-dependent BOLD contrast) therefore it is a technique that measures brain activity indirectly. The good spatial resolution, generally 3 mm, except for some special types of High-Resolution fMRI that go down to the sub-millimeter level (Goense, Bohraus, and Logothetis 2016), is its main advantage. It is a non-invasive method with the ability to study the deeper structures and allows you to understand where something happened in the brain. Despite these advantages, the use of the BOLD signal to estimate brain activity does not make it an excellent tool for temporal resolution compared to other systems such as EEG or MEG, however, to obtain images with a good signal-to-noise, subjects must remain stable and lying down inside the scanner while moving as little as possible (Glover 2011). This complicates the study of brain dynamics and the generation of experimental paradigms in which verbal or physical interaction is required between participants in naturalistic contexts. Also not to be underestimated are the physical dimensions of the instrument and the complexity of synchronizing multiple systems while performing imaging sessions (Czeszumski et al. 2020).

Electroencephalography (EEG) is the oldest method to investigate brain activity. Using electrodes applied to the scalp, the EEG directly measures neuronal activity therefore, compared to techniques that use the BOLD signal (such as fMRI), the EGG has a much higher temporal resolution (in the order of milliseconds), but having electrodes on the skin as an investigation tool, it is only suitable for the study of the cerebral cortex or the superficial structures without being able to go deep (Michel and Brunet 2019). Although fMRI was the first technique to perform Hyperscanning and in ancient times EEG systems were low mobility systems, in recent years thanks to the development of portable EEG systems it has become a commonly used tool to perform social interaction experiments between two or more subjects and study neuronal changes with good temporal resolution (Babiloni et al. 2006; Barraza, Pérez, and Rodríguez 2020; Lindenberger et al. 2009). All this made it possible to generate experimental paradigms in more naturalistic contexts (Müller and Lindenberger 2014).

Functional near-infrared spectroscopy (fNIRS) is the newest neuroimaging technique employed to conduct Hyperscanning (Cui et al. 2012; Funane et al. 2011; Quaresima and Ferrari 2019; Scholkmann et al. 2013). The fNIRS is capable of detecting brain activity indirectly using the BOLD signal (as for the fMRI) but unlike the latter, the fNIRS has a good spatial resolution (about 1 cm) allowing it to record the activity of the superficial brain areas for the EEG. However, having a resolution between 0.1 and 1s compared to the EGG, it has a lower temporal resolution (Czeszumski et al. 2020). Given these characteristics, the fNIRS is used in the study of cognitive neuroscience and social interaction as the measured signal has good resistance to movement artifacts so it allows the creation of experimental sessions in which the participants have greater freedom of movement and the paradigms developed resemble real-life contexts (Scholkmann et al. 2013).

2.2. Analysis Techniques for the Study of Biomedical Signals

Inspired by human studies conducted with EEG (Barraza et al. 2020), fMRI (Montague et al. 2002), or fNIRS (Cui et al. 2012) techniques, we decided to analyze the calcium profile recorded from the whole cortex correlated with neuronal activity, as a biomedical signal by performing a spectral analysis as a function of time and frequency.

Biomedical signals can be divided into two categories: stationary and non-stationary.

The main difference between these is that in the first, all the properties of the signal, such as its mean or its variance, remain constant over time, while in non-stationary signals this does not happen (Ramirez Pacheco, Torres Román, and Toral Cruz 2012). A useful tool to investigate biomedical signals is represented by spectral analysis: a representation of the signal in terms of its frequency components (amplitude vs frequency) which provides a complementary view to the temporal analysis (amplitude vs time). To analyze biomedical signals among the most widely used techniques we found the Fourier Transform (FT), which provides frequency information but assumes that the signal is stationary and therefore coherent in its properties over time (Harikrishna et al. 2021). Although the FT provides information on the frequency, it is known that signals related to the neuronal activity are non-stationary and highly dynamic signals over time.

To overcome this limitation, the Short Time Fourier Transform (STFT) was developed which provides a time-frequency representation of the signal (Baba 2012). The underlying assumption when performing the STFT is that in the short time window of observation, the signal is stationary. A Fourier Transform of each stationary part is then performed along the signal and finally concatenated together. With the STFT it is possible to take a window function of fixed length and scroll it along the signal from start to end by calculating the FT in each stationary section. Although STFT provides a higher resolution in the frequency and time domain because it uses fixed-length windows, due to the Heisenberg uncertainty principle it is not possible to know exactly at which instant in time that frequency exists. It follows that uncertainty remains in time and frequency (Addison 2005; Rajoub 2020).

This is the main motivation for why the Wavelet Transform (WT) was introduced. WT can analyze a signal in different frequencies at different resolutions: this is known as multi-resolution analysis. Looking at the frequency over time graph for the WT (**Figure 8**), we will notice a good time resolution and poor frequency resolution at high frequencies. In the opposite condition, we will have a good frequency resolution and poor time resolution at low frequencies.

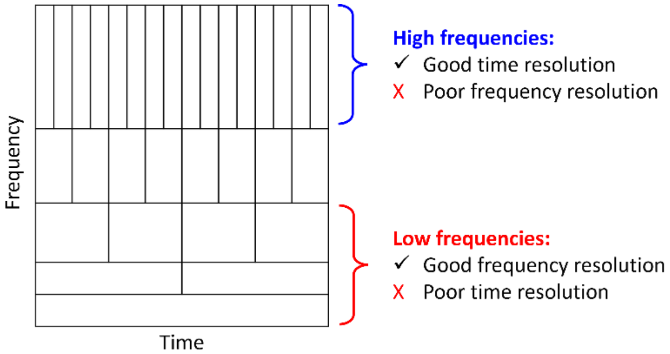

Figure 8: Graphical Representation of Wavelet Transform Analysis.

Time-Frequency graph to represent the multi-resolution analysis of the Wavelet Transform. At high frequencies the vertical lines are greater than at low frequencies, this is to represent greater time resolution. At low frequencies the horizontal lines are denser than at high frequencies, this is to represent better frequency resolution.

The graphical representation simplifies this concept. As we can see (**Figure 8**), at high frequencies the vertical lines are denser, which means a higher temporal resolution; while at low frequencies we observe a greater number of horizontal lines to represent a better resolution in frequency.

The Wavelet Transform (**Equation 1**) of a signal $f(t)$ is defined as:

$$F(\tau, S) = \frac{1}{\sqrt{|S|}} \int_{-\infty}^{+\infty} f(t)\psi^* \left(\frac{t-\tau}{S}\right) dt$$

Equation 1: Wavelet Transform

where the signal $f(t)$ is not multiplied by an exponential but by the complex conjugate ψ^* which corresponds to the mother wavelet selected to decompose the signal. The output of the equation, in addition to τ, is S called the Scale parameter which corresponds to the reciprocal of the frequency.

In this analysis, the wavelet is used like a small wave that corresponds to the new base function, similar to the sine and cosine functions used for the FT or the window function for the STFT. The wavelet is a zero mean wave used for signal processing.

Among the various types of Wavelets, for time-frequency analysis of non-stationary biomedical time series, such as neuroelectrical signals like EEG, fNIRS, or fMRI, the Morlet wavelet (**Equation 2**) is often used (Addison 2005).

$$\psi(t) = e^{2j\pi ft} e^{\frac{-t^2}{2\sigma}}$$

Equation 2: Morlet Wavelet

This wavelet is obtained from the product of a Gaussian with a complex sinusoid, the width of the Gaussian that tapers the sine wave is a critical characteristic of the Morlet wavelet. This width parameter controls the trade-off between temporal precision and frequency precision and it is typically defined as the “number of cycles" (Grinsted, Moore, and Jevrejeva 2004).

Given the Gaussian function (**Equation 3)**:

$$e^{\frac{-t^2}{2\sigma}}$$

Equation 3: Gaussian Function

The width of this function depends on the number of cycles (**Equation 4**) described by the relation:

$$\sigma = \frac{n}{2\pi f}$$

Equation 4: Number of cycles

Increasing n, the number of cycles, the width of the Gaussian increases (**Figure 9**), so when the Fourier Transform of the Gaussians is performed, the function with the lower number of cycles is wider in the frequency domain than the Gaussian with a greater number of cycles.

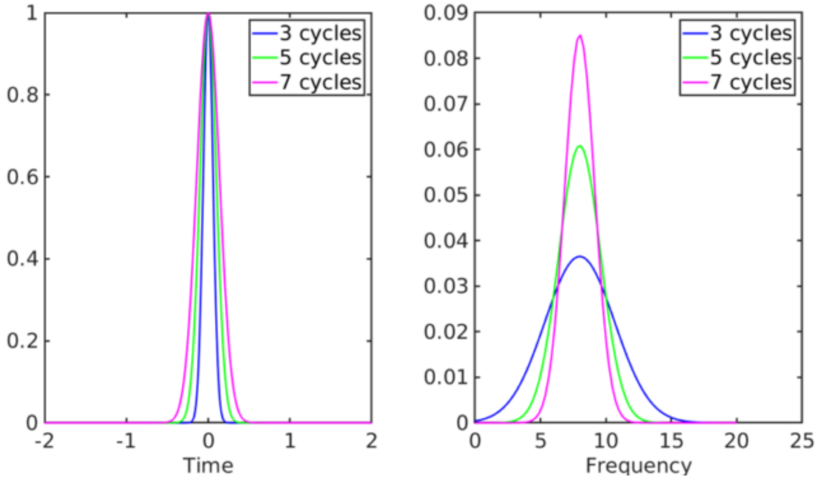

Figure 9: Graphical representation of the Number of Cycles of the Gaussian Function. The width parameter of the Gaussian is defined by the number of cycles, which controls the level of accuracy in both time and frequency.

For this reason, the Morlet wavelet is a suitable choice since it offers a fair balance between temporal and frequency localization (Grinsted et al. 2004).

The wavelet transform performs the convolution of the complex wavelet with the temporal signal allowing two mechanisms: scaling and translation.

By changing the scale parameter S, we can modify the width of the wavelet and its central frequency while we slide it along the signal. We have the possibility of increasing the values of S and expanding the wavelet (**Figure 10**). An expanded Wavelet is better for resolving the low-frequency components of the signal with bad temporal resolution. For small values of S, we get a shrunken Wavelet which is better at resolving high-frequency components of the signal with good temporal resolution (**Figure 10**) (Torrence and Compo 1998).

Figure 10: Wavelet Scaling.

Representation of the effect of Wavelet scaling. By varying the scaling parameter, the width of the Wavelet and the center frequency of oscillation can be changed. High values of S stretch the wavelet (left), and small values of S result in compression (right) of the wave function.

With this scaling flexibility and changing the width of the window function, the WT resolves high and low-frequency components with good resolutions. In addition to scaling, it is possible to translate the wavelet over the signal, by modifying τ, as for the window function of the STFT.

Coming back to the WT equation, in the conjugate complex the wavelet is translated along the signal by changing τ, as a window function, and it is also scaled by dividing by S, stretching, and compressing the wavelet. By setting all these parameters we obtain output values of F which represent the coefficients of the wavelet.

To analyze the similarity or coherence between two signals we can use the Wavelet Transform to perform Wavelet Transform Coherence (WTC) (Davis et al. 2017).

The research of cognitive neuroscience and the neuronal circuitry underlying social interactions are fields that have been increasingly explored in recent years. In particular, we wonder if there are possible connections between the brains of two or more interacting subjects (Dumas et al. 2010). In many human studies, they have used Hyperscanning as an investigative tool to simultaneously record the brain activity of multiple subjects (Babiloni and Astolfi 2014). The WTC is a type of analysis that was first applied to the study of EL-Nino-Southern Oscillation and other meteorological phenomena in the 1990s (Torrence and Webster 1999). Subsequently, it proved to be suitable also in the field of neuroscience as a method of studying the time-frequency dynamics of neural signals. Wavelet coherence has been used to investigate oscillatory dynamics in short-term memory (Payne and Kounios 2009) or pathological conditions such as autism spectrum disorder (ASD) (Catarino et al. 2013) or schizophrenia (Sakkalis et al. 2006).

The Wavelet Transform Coherence has the power to provide time coupling using variable length windows as short windows for analyzing high frequencies or longer windows for low frequencies. This makes it possible to measure the cross-correlation between two signals in the time-frequency space that could have a coherent phase relationship suggesting causality or a possible link between the two-time series. The WTC is capable of discovering locally locked-in phase events that may not be detectable with the analysis of time series such as the Fourier Transform (Grinsted et al. 2004; Torrence and Webster 1999). Giving as output a correlation coefficient localized in the time and space of the frequencies.

Given the X and Y time series, wavelet coherence also referred to as cross-wavelet transform (**Equation 5**) is defined as:

$$W_n^{XY}(s) = W_n^X(s)W_n^{Y*}(s)_X$$

Equation 5: Cross-wavelet Transform

Where $W_n^X(s)$, $W_n^Y(s)$ are the wavelet transform of X and Y , s indicates the wavelet scale, n the time index, and $(*)$ the conjugate complex of the wavelet transform. The cross-wavelet reveals the regions of the spectrum in the time and frequency domain where a common power is observed between the two signals. Since this idea is related to the notion of coherence, we may use the following equation to define wavelet coherence (**Equation 6**) (Torrence and Webster 1999):

$$R^2(s) = \frac{|<(s^{-1}W_n^{XY}(s))>|^{\,2}}{|<(s^{-1}W_n^{X}(s))>|^{\,2}|<(s^{-1}W_n^{Y}(s))>|^{\,2}}$$

Equation 6: Wavelet Coherence

We have the ratio of bi-spectrum divided by the product of the two spectra where <·> represent the smoothing operator in scale and time and the factors s^{-1} is used to convert an energy density.

This parameter is used to quantify the degree of a linear relationship between two non-stationary signals in both domains. It is a coefficient that assumes values between 0 and 1, where 0 indicates the absence of correlation and 1 is the perfect coherence between the two signals (**Figure 11**). The WTC reveals the region of the spectrum, in the time-frequency space, in which the two-time series are covariant and are coherent with each other even if they do not have high power. A statistical significance level of Wavelet Coherence is estimated using Monte Carlo simulations (Torrence and Compo 1998).

Since this analysis includes both the scaling and the translation of the wavelet on time series of finite length, errors will occur at the beginning and the end of the spectrum. To solve this problem, a possible solution is to fill the end and the beginning of the time series with zeros before performing the wavelet transform and remove them later (Torrence and Compo 1998). This limits what is called the "Boundary Effects". In this way, we will define the Cone of Influence (COI), the region of the spectrum in which the estimates of the Wavelet coefficients are reliable (**Figure 11**) (Zhang and Moore 2011).

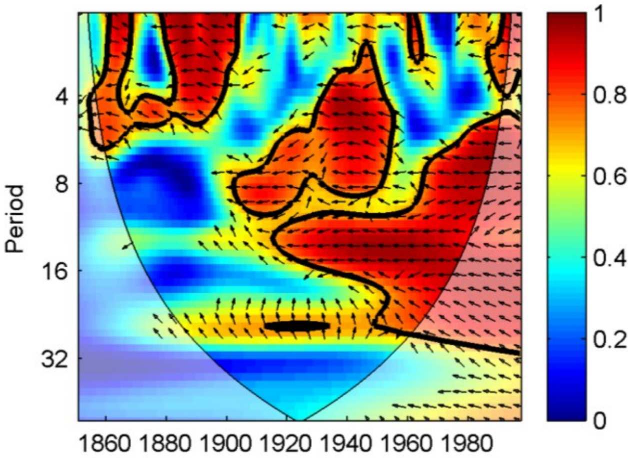

Figure 11: Wavelet Transform Coherence Graphical Representation.
The image shows a graphical example of Wavelet Transform Coherence (WTC). On the x-axis is generally shown the time, on the y-axis is the period or frequency, and on the color scale the level of coherence between 0 and 1 of the two signals under consideration. The funnel structure represents the Cone of Influence (COI) while the arrows represent the phase relationship between the two signals. Image from Grinsted et al. 2004.

In conclusion, wavelet coherence analysis allows for highlighting the existing synchrony between two signals that would not be visible from the analysis of the single time series relating to neuronal activity. As reported by the literature, the simultaneous analysis of brain activity from multiple interacting subjects can reveal information about the inter-brain synchrony and it has been used in many experimental paradigms as a study of cooperative and competitive tasks (Barraza et al. 2020; Cui et al. 2012), decision-making (Zhang et al. 2017), action monitoring (Dommer et al. 2012), verbal (Jiang et al. 2012) and non-verbal communication (Hirsch et al. 2017). The possibility to choose the scale of the mother function, not having a fixed length window, the best resolution in the time-frequency domain, and the ability to observe the covariation and phase coupling of the two-time series are just some of the characteristics that make this technique a powerful tool for the analysis of non-stationary biomedical signals such as those related to the brain activity of multiple subjects.

3. Calcium Fluorescence Indicators

Social interactions in rodents are studied mainly at the behavioral level by using different paradigms while in humans, Hyperscanning studies are highlighting the role of certain brain areas during social tasks (Babiloni and Astolfi 2014; Barraza et al. 2020; Crawley 2007; Montague et al. 2002; Nadler et al. 2004). To learn about neuronal mechanisms during social interactions in mice, we need an animal model to visualize brain dynamics. Due to its high sensitivity and stability, fluorescence is one of the most widely used physical phenomena in optical imaging for the study of biological mechanisms. Fluorescence, first described by George G. Stokes in 1852, is a physical phenomenon lasting a few nanoseconds in which the emission of photons in the visible spectrum by previously excited molecules is observed (Stokes 1852). From biology, we know that calcium is an essential intracellular messenger in synaptic transmission. At rest, the cytosolic concentration of calcium is about 50-100 nM, which can temporarily increase during action potentials by ten to one hundred times (Berridge, Lipp, and Bootman 2000). Using the change in concentration of this ion and combining it with the fluorescence mechanism, it is possible to generate a tool for conducting imaging capable of measuring calcium fluctuations. To investigate and monitor calcium activity using fluorescence instruments, chemical and Genetically Encoded Calcium Indicators (GECI) are two families used in the last years.

Chemical indicators are small fluorescent molecules such as fura-2, indo-1, and fluo-4, with the peculiarity of having a chemical compound with calcium chelating groups. This family of indicators is not easily applicable in live animal models due to the permeability issues of the chemical compound in the tissue, so they are generally employed in cultures or isolated cells (Redolfi et al. 2021).

3.1. Genetically Encoded Calcium Indicator (GECI): GCaMP Family

The development of GECIs made it possible to overcome the limitation of chemical indicators reason why they have been widely used in live animals for *in vivo* expression of Ca^{2+} sensitive proteins (Dana et al. 2014). GECIs are divided into two types: those involving Förster resonance energy transfer (FRET) such as Cameleons and single fluorescent protein-based indicators like GCaMP.

FRET-based GECIs, are indicators in which non-radiative energy transfer occurs between an excited donor fluorophore and an acceptor fluorophore without emitting a photon. However, their distance must be less than 10 nm to allow energy transfer (Jares-Erijman and Jovin 2003; Nagai et al. 2004). Using fluorescence microscopy, FRET signaling can be accurately revealed in small subcellular structures such as dendritic spines, allowing to deepen of the molecular mechanisms underlying synaptic plasticity or visualizing the activity of the neuronal network both in vitro and in vivo (Ueda, Kwok, and Hayashi 2013).

The first version of calcium indicators based on a single fluorescent protein was developed in the early 2000s under the name G-CaMP (Nakai, Ohkura, and Imoto 2001), which contains within it the circularly permutated form of the Enhanced Green Fluorescent Protein (cpEGFP) which expresses greater variation of fluorescence. The N- and C-terminal ends of the cpEGFP protein are linked to the peptide M13 and calmodulin (CaM), respectively. M13 is a synthetic peptide with a sequence similar to Myosin Light Chain Kinase (MLCK) (**Figure Figure** 12), while calmodulin is a calcium-binding protein with numerous functions in the homeostasis of this ion. When the concentration of this ion increases, such as during neuronal activity, and simultaneously an excitation wavelength of 496 nm is provided, calcium binds to calmodulin and the M13 peptide resulting in a conformational change of the cpEGFP protein and fluorescence emission at about 513 nm (**Figure 12**) (Nakai et al. 2001).

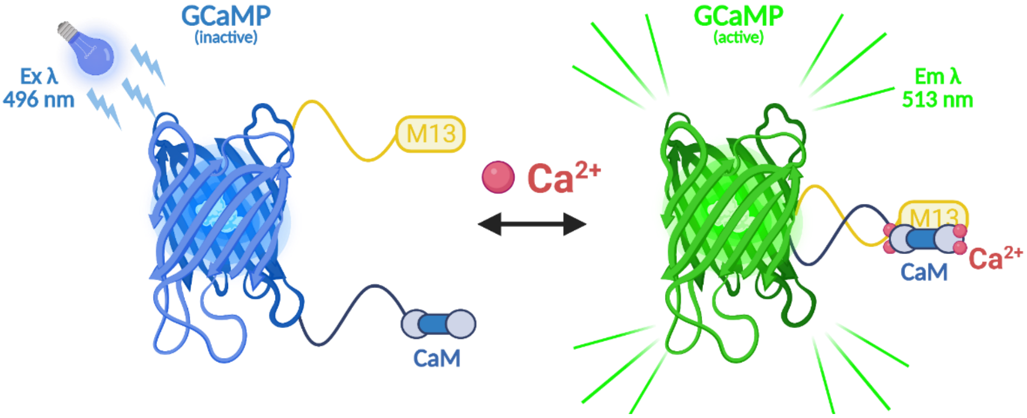

Figure 12: GECI Indicator Based on Single Fluorescent Protein "GCaMP".

Representation of the structure of cpEGFP with the connected peptide M13 and Calmodulin. When the GCaMP indicator is excited with a wavelength of 496 nm and in the presence of calcium, the latter binds to calmodulin and M13 peptide causing conformational changes of cpEGF, with emission of fluorescence at 513 nm.

Despite its usefulness, the first version of G-CaMP (Nakai et al. 2001) exhibited reduced fluorescence and high-temperature sensitivity, expressing its fluorescence around 28°C but not at a physiological temperature of 37°C. This has been a major limitation in vivo studies. Over the years, thanks to genetic engineering and the use of mutations, several variants of GCaMP have been developed in which various aspects have been optimized including the expression temperature, basal fluorescence, sensitivity, and calcium binding kinetics (Akerboom et al. 2012; Ohkura et al. 2005; Tallini et al. 2006; Tian et al. 2009).

In 2013, the GCaMP6 variant was developed (Chen et al. 2013) in which by mutagenesis of some amino acid residues at the interface between cpGFP, CaM, and M13 peptide, the affinity of the sensor for calcium was improved. There are three different forms of GCaMP6 (6s, 6m, and 6f for slow, medium, and fast) with different sensitivity and kinetics. The GCaMP6f indicator was used in this project for its rapid kinetics (rise and decay time of about 200 ms) for detecting free calcium at the cytoplasmic level making it an optical tool for our neuronal imaging studies. Testing the GCaMP6 indicator in layer 2/3 pyramidal neurons of the visual cortex in vivo rodent studies showed that this family can resolve neuronal activity and single action potentials with nearly 100% accuracy (Chen et al. 2013). The development of this marker has led to considerable use in neuroscience to monitor single action potentials or the activity of large brain areas in animal studies.

3.2. Development of Thy1-GCaMP6 Transgenic Mice

The development of GECIs makes it possible to investigate neuronal dynamics, previously the expression of these markers by viral transfection using adeno-associated viruses was preferred. This technique required complex surgeries with limited time windows to perform imaging stably and without altering cell structure (Tian et al. 2009).

To overcome these limitations, the development of transgenic animals has enabled the stable and homogeneous expression of the GCaMP indicator.

In this work, Thy1-GCaMP6f-WPRE transgenic mice expressing the GCaMP indicator under the control of the Thy1 promoter were used to drive fluorescent protein expression at the neuronal level. WPRE is the post-transcriptional regulatory element of the marmot hepatitis virus that together with the poly-adenylation (pA) tail increases mRNA stability and consequently GCaMP protein expression (Dana et al. 2014; Donello, Loeb, and Hope 1998). Using this gene cassette, the highest expression was detected in the hippocampus (CA1 and CA3 and dentate gyrus). In the cortex, GCaMP is uniformly expressed throughout the cortex with the highest expression in layers 5 and 6 (L5 and L6) compared to layer 2/3 (L2/3) while no expression was recorded in layer 4 (L4) cells. The marker was also detected in other brain structures such as the amygdala, thalamus, hypothalamus, etc., making it an excellent tool to investigate neuronal processes in mice in vivo (Dana et al. 2014).

4. Wide-field Fluorescence Microscopy

One of the main goals of neuroscience is to try to elucidate what brain mechanisms coordinate behavior. Advances in linear and nonlinear optical imaging combined with fluorescence indicators are making it possible to achieve this goal (Chen et al. 2013). The implementation of these techniques has enabled the recording of the activity of a few neuronal units in large brain populations *in vivo* in small animal models (Wallace and Kerr 2019; Yang and Yuste 2017).

Different types of microscopes have been developed to perform functional *in vivo* imaging. The main characteristics and physical problems that the systems have to solve are the same: to provide an adequate number of photons to the sample, reduce the photobleaching phenomenon, perform recordings with a high spatio-temporal resolution by expanding the field of view, and finally maintain a good signal-to-noise ratio (SNR) (Lichtman and Conchello 2005).

In the wide-field microscope, the fluorescence signal from the sample is captured by a high-speed scientific complementary metal oxide semiconductor (sCMOS) camera with a large field of view. However, these systems suffer from the problem of light scattering, which causes cross-talk between camera pixels. As a result, single-photon imaging does not allow scanning of deep structures (> 200 μm depth), so it is widely used for imaging superficial areas, such as studying cortical dynamics *in vivo* in rodents (Yang and Yuste 2017).

This system, also known as an epifluorescence microscope, illuminates a large portion of the sample by catching the re-emitted fluorescence in the focus plane using the same objective lens while the fluorescence of the out-of-focus planes contributes to the background of the image (Lichtman and Conchello 2005). Excitation and emission filters with a specific coating are implemented in the optical path of these microscopes to select the wavelength range of interest, and a dichroic mirror positioned at a 45° angle can reflect the excitation wavelength, convey it into the objective, and transmit the emission light (Jay Reichman: Handbook of optical filters for fluorescence microscopy).

Since a wide-field epifluorescence microscope uses a single photon as the excitation source, fluorophore emission increases linearly with excitation power until saturation. Despite all, to perform mesoscale imaging, wide-field microscopy with a low magnification objective is widely used. Although unable to achieve cellular resolution, this type of microscopy, thanks to its large field of view, is useful in mapping functional connectivity between different brain regions or across the entire dorsal cortex of the mouse (Ferezou et al. 2007; Makino et al. 2017; Montagni et al. 2018; Murakami et al. 2015; Quarta et al. 2022; Zatka-Haas et al. 2021).

5. Miniscope

Considering the current *in vivo* imaging techniques of mice that involve the use of complex and heavy microscopes that can be applied in anesthetized animals or head-fixed conditions, thinking of a new system to monitor neuronal activity while simultaneously studying animal behavior under more naturalistic conditions would open a new frontier in the field of neuroscience.

Traditional microscopy techniques are not easily implemented in behavioral paradigms such as spatial navigation, social interactions, and the study of natural sleep or circadian rhythms where a high degree of freedom of movement of the animal is required. To monitor neuronal activity in real-time, head-fixed conditions introduce stressors, limit the complexity of the behavioral repertoire, and alter brain activity compared with freely moving conditions (Chen et al. 2020).

The development of recent miniaturized fluorescence microscopes has made it possible to overcome the limitation of classical microscopes, enabling real-time recording of neural activity in free-moving animals (Chen, Tian, and Kong 2022). Optimization in weight and size has made it possible to apply these systems in freely moving animals such as mice, rats, birds, and bats (Aharoni and Hoogland 2019; Barbera et al. 2016; de Groot et al. 2020; Jacob et al. 2018; Liberti et al. 2017, 2022; Rynes et al. 2021; Scott et al. 2018).

In order not to affect animal behavior, commercial Miniscope must be compact and not exceed 15% of body weight (about 4 g for mice). Miniscope can be divided into single- and multi-photon fluorescence microscopes. The main differences between the two systems are given by the physical principle of excitation, the field of view, optical resolution, ability to penetrate tissues, scanning speed, and differences in the hardware system (Chen, Tian, and Kong 2022).

Despite the advantages of these systems, in single- and multi-photon Miniscope, imaging deep structures often require implanting a GRIN lens in the brain in the region of interest. Even though updated pharmacological protocols and the presence of less invasive surgical procedures, the insertion of these small lenses inevitably causes tissue damage that could alter animal behavior (S. A. Lee et al. 2016). A longer recovery time is required to ensure that inflammatory responses caused by GRIN lens implantation and craniotomy decrease (Bocarsly et al. 2015).

Over the past decade (**Figure 13**), several laboratories have helped improve and develop variants of single- and two-photon Miniscope, improving their weight, portability, ease of mounting, the field of view, and ability to penetrate tissues, making them compatible with GECIs to monitor calcium activity in the form of fluorescence. Since a single-photon optical system was developed in this project, the following is a discussion of recently developed miniature single-photon devices.

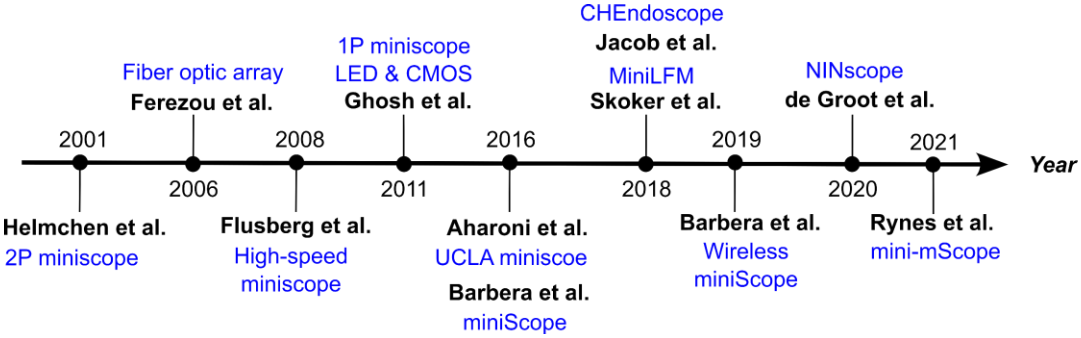

Figure 13: Miniscope History.

Timeline of major miniaturized optical systems developed since the beginning of the 21st century.

5.1. Single-photon Miniaturized Devices based on GRIN lens

Most of the currently developed miniaturized systems are GRIN lens-based devices for imaging small fields of view, with a resolution predominantly of a few hundred neuronal units.

An epifluorescence microscope capable of conducting high-speed imaging (<100Hz) was developed in 2008 (Flusberg et al. 2008). The miniaturized microscope weighing only 1.1 grams could be carried by mice to conduct imaging at the cellular level during movement. This device was initially used to monitor cortical microcirculation, the hippocampal area CA1, and subsequently to study the calcium dynamics of cerebellar Purkinje cells during locomotion (Flusberg et al. 2008).

This system was further improved in 2011 with the development of a miniaturized microscope weighing 1.9 grams capable of high-speed cellular resolution imaging over an area of about 0.5 mm^2 (**Figure 14A**) (Ghosh et al. 2011). Recordings with this system made it possible to monitor the activity of the cerebellum in real-time, highlighting the synchrony of cerebellar neurons during free locomotion activity (Ghosh et al. 2011).

In the era of miniaturized microscopes, the UCLA Miniscope (**Figure 14B**) is probably one of the systems with the greatest impact in the field of neurophotonics (Aharoni and Hoogland 2019) first employed in the study of memory formation in the CA1 hippocampal area (Cai et al. 2016). It has a field of view of 700 x 450 µm, a weight of about 3 grams, and a single-photon acquisition rate of 60 fps (Aharoni and Hoogland 2019). The optical design, inspired by a conventional epifluorescence microscope, using an achromatic lens combined with a GRIN lens made it possible to focus and collimate light on the CMOS sensor. In addition, by using one or two GRIN lenses it is possible to perform imaging of surface or deep brain structures.

The UCLA device presents excellent advances in electronics. The wiring system provides that power supply, data reception, and transmission are performed using a single flexible coaxial cable with a diameter of only 0.3 mm. This improvement minimizes the impact of cable resistance and heaviness on the animal's head, affecting normal behavior (Aharoni and Hoogland 2019).

At the same time as the development of the UCLA Miniscope, the National Institute on Drug Abuse (NIDA) also developed a miniaturized microscope called the miniScope (**Figure 14C**) (Barbera et al. 2016).

The miniScope has a total weight of 2.4 grams, a field of view of 1.1 x 1.1 mm, and a sampling rate of 10 Hz has been used to study neuronal dynamics in different brain regions during free behavior (Barbera et al. 2016; Liang et al. 2018; Zhang et al. 2019). Combined with a GRIN relay lens system allows imaging of deep layers. In contrast to other systems, to isolate the device from external light, the miniScope housing was built using a 3D printer with nickel plating.

Although the use of a GRIN lens allows imaging of deep structures, performing three-dimensional scans could help understand the dynamics of neuronal populations of complex behaviors. To solve this limitation, a research group has developed a miniaturized system called MiniLFM, capable of performing high-speed (16 fps) volumetric imaging (700 x 600 x 360 μm^3) of neuronal activity in freely moving rodents (Skocek et al. 2018). The device was combined with light-field microscopy (LFM) technology, generally applied for whole-brain imaging of small, transparent organisms (Prevedel et al. 2014); with Seeded Iterative Demixing (SID) (Nöbauer et al. 2017), a computational strategy based on constrained matrix factorization to resolve neuronal activity in a 3D volume.

The University of Toronto has developed a compact endoscope weighing 4.5 g, with a frame rate of 20 Hz and a field of view of 500 µm diameter called CHEndoscope (**Figure 14D**) (Jacob et al. 2018), compatible with behavioral paradigms to study neuronal activity. The system assembles in less than 6 hours, has a very low development cost, and is easily modified to fit the experimental setups of different laboratories, making it an advantageous option for research groups that prefer to use standard components (Jacob et al. 2018). The devices previously discussed have recorded neuronal activity with a cellular resolution of specific circumscribed brain regions. Given the complexity of behavior, understanding the neuronal networks that coordinate it requires expanding the number of brain areas to be studied. A Dutch research group, in response to these requirements, has developed a dual-site, cellular-resolution system called NINscope (**Figure 14E**) (named after the institute that developed it) that is light enough and has a small footprint, such that two Miniscopes can be affixed to rodent heads to simultaneously monitor two different brain areas. Weighing 1.6 g and with a field of view of 786 x 502 µm, the NINscope made it possible to monitor functional connections between the cortex and cerebellum in freely moving mice (de Groot et al. 2020).

Figure 14: Single-photon Miniaturized Devices.

Representation of some of the recently developed single-photon miniaturized systems for calcium imaging. Starting from the top **(A)** we find the single-photon miniscope developed by Ghosh et al in 2011. **(B)** the UCLA Miniscope developed by Aharoni in 2016. **(C)** miniScope by Barbera in 2016. **(D)** CHEndoscope by Jacob et al in 2018 and finally the NINscope by de Groot in 2019. Image modified by (Barbera et al. 2016; Cai et al. 2016; Ghosh et al. 2011; de Groot et al. 2020; Jacob et al. 2018).

A. One-Photon miniscope Ghosh et al. 2011

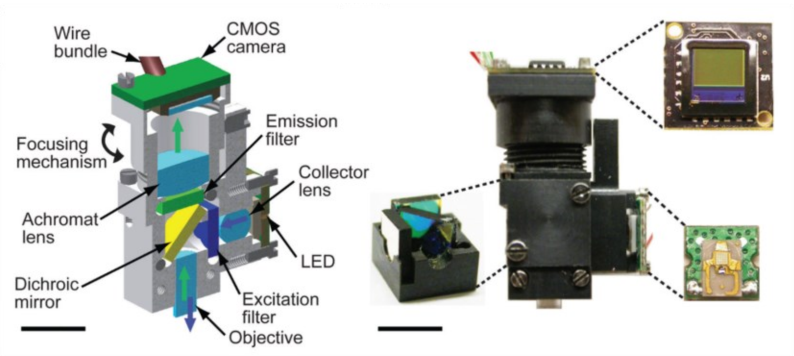

B. UCLA miniscope Aharoni et al. 2016

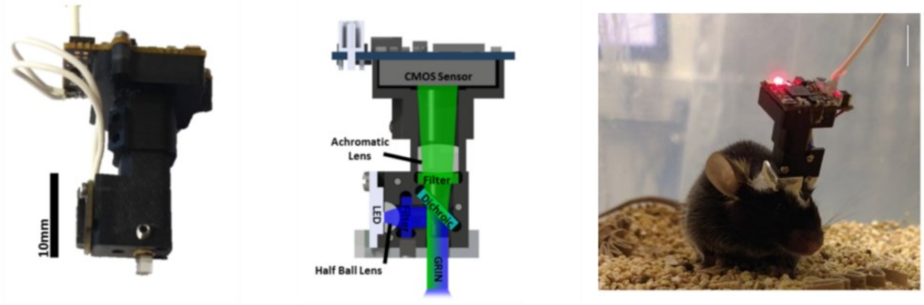

C. miniScope Barbera et al. 2016

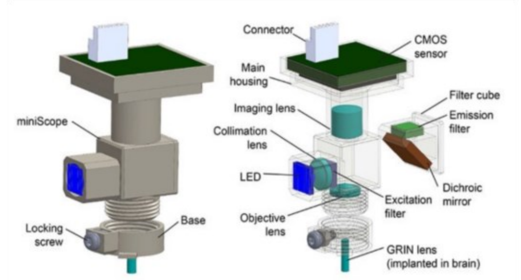

D. CHEndoscope Jacob et al. 2018

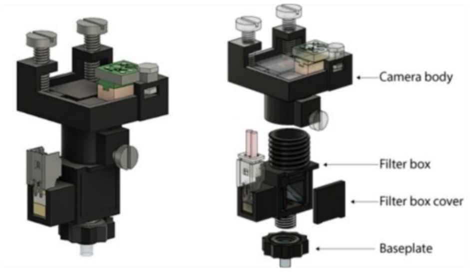

E. NINscope de Groot et al. 2019

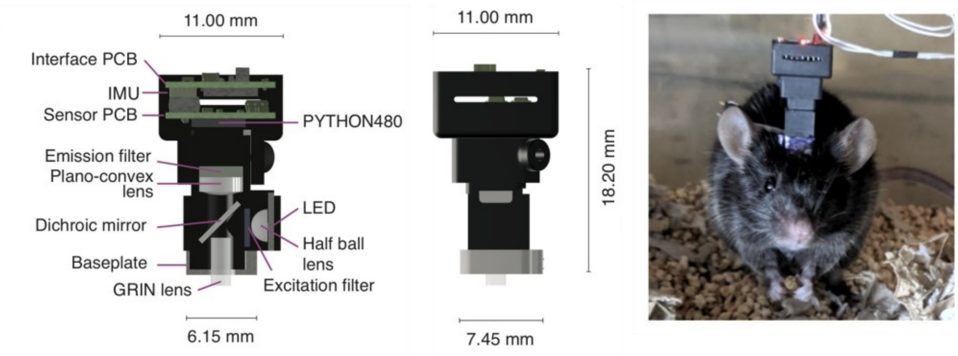

5.2. Miniaturized Wide-field Microscopy

Miniaturized head-mounted systems developed up to the last few years have very small fields of view spanning areas smaller than 1 mm^2 with mostly cellular resolution. In 2021, mini-mScope was developed (**Figure 15**), a miniaturized wide-field device with a large FOV of 8 x 10 mm, a resolution ranging from 39 to 56 µm, and weighing less than 4 grams (Rynes et al. 2021). Although the optical resolution of the system has enabled mesoscale imaging due to the wide field of view, mounting the mini-mScope on the heads of mice requires a craniotomy for the application of the previously developed See-Shells transparent polymer skulls (**Figure 15**) (Ghanbari et al. 2019). A craniotomy so extensive as to expose both hemispheres is a rather invasive procedure, with technical difficulties in execution, requiring longer recovery times to reduce pain and inflammatory processes. This system is currently the first device capable of recording cortical activity in both hemispheres with a sufficient field of view, however, it is only compatible with See-Shells-transparent polymer skulls. The research team validated the functionality and adaptability of mini-mScope in different experimental settings while keeping the animal under free-movement conditions (Rynes et al. 2021).

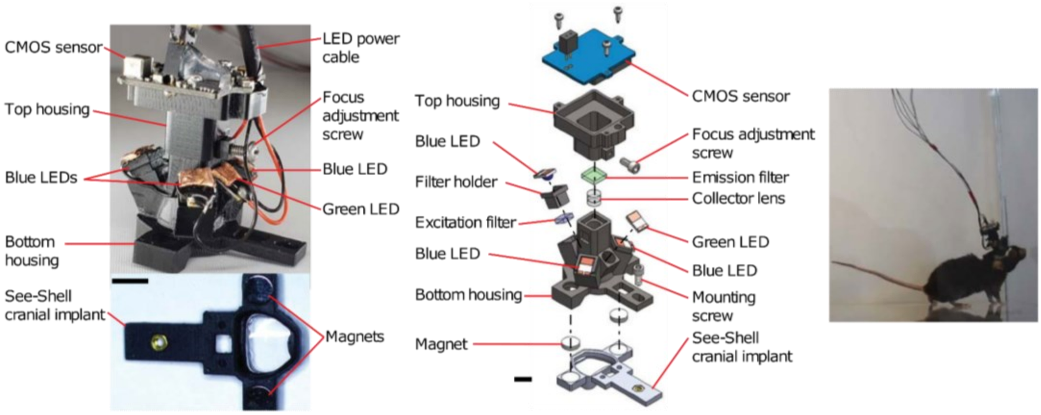

Figure 15: mini-mScope Design.

Component representation and assembly of the mini-mScope developed by Rynes and colleagues. The bottom image of the See-Shell cranial implant is to be attached following craniotomy to make the optical window. Right photo of a mouse bearing the mini-mScope.

6. Aim of the study

From the analysis of the current literature done in the previous chapters, it follows that simultaneously monitoring the activity of multiple brain areas during freely-moving behavior is a high-impact query in the field of neuroscience.

Behavior and particularly social interactions are extremely important components of individual life and well-being. No organism is capable of living and obtaining the resources necessary for its survival in complete solitude. Both humans and animals, spontaneously tend to aggregate in groups, and the development of social hierarchies is an innate characteristic of the individual.

The field of social interactions is something extremely complex that is expressed through various forms and modalities ranging from verbal to non-verbal language, during mechanisms of aggression or fear, it is present in interactions in peer and parental relationships. These are just some of the examples that we could mention when we address the issue of social interactions and the well-being of each of us. Given the complexity of social behavior, it would be reductive to think that there are only limited brain areas that orchestrate all these aspects. The advent of miniaturized optical systems finally opened a new frontier that allowed for the development of behavioral paradigms that are more ethologically valid compared to the conventional approach which requires constraining the subject limiting the behavioral repertoire and altering cortical activity. With this information, it would be important to expand the number of cortex areas to be investigated to try to answer the question of whether the coordinated activity of cortex networks controls behavior or whether there is inter-brain synchrony between two interacting subjects.

To date, in the era of miniaturized single-photon microscopes, despite great progress in improving electronics, optics, acquisition speed, and device size, most systems developed, lack a comprehensive view of how neuronal dynamics are distributed in the brain. The maximum field of view achieved allows the investigation of surfaces of very few mm^2, allowing imaging of small areas or brain structures at a different resolution. Humans studies conducted with techniques such as fMRI, EEG, or fNIRS suggest the involvement of cortical structures and inter-brain synchrony at different frequency bands (theta and gamma) and that this synchrony is modulated by the type of social tasks such as cooperation or competition. In rodents, imaging of small subcortical regions and structures revealed the key role of mPFC in modulating social interactions, while on other cortical structures, no information is reported.

This thesis addressed the unmet need of investigating inter-brain synchrony during social interaction. For this purpose, a wide-field miniaturized fluorescence microscope capable of investigating neuronal dynamics distributed across the cortex was developed, validating a behavioral paradigm to assess the impact of social interactions on cortical circuits by developing a Hyperscanning study in mice to examine possible inter-brain synchrony during this behavior.

II. Methods

1. Surgery for the Realization of the Optical Window

To visualize neural dynamics in vivo, mice involved in the experiments underwent surgery to create optical access to the cortical region of interest. All activities were performed by the ministerial protocol, all instruments were previously sterilized with 70% ethanol or at high temperatures to guarantee an excellent microbiological standard.

We proceed by turning on the oxygen and isoflurane dispenser for induction of anesthesia of the animal. The mouse after being weighed is placed in the induction chamber, where it is subjected to inhalation of isoflurane 5% until it is unconscious. The surgical procedure involved anesthetizing the mouse inside the stereotactic apparatus (Model 1900, Kopf Instruments, Tujunga, California, USA) and fixing the head to avoid movement that could affect the course of surgery.

Before the start of the surgery, the apparatus was calibrated to correctly align the animal's head to the rostral-caudal and mid-lateral planes. Suppression of the nociceptive reflex is evaluated to determine the optimal depth of general anesthesia. During surgery, isoflurane is lowered to 1-2% as maintenance. To reduce the risk of hypothermia, the animals were kept warm throughout the surgical procedure until complete recovery, using a heating pad under the mouse’s ventral area. Their body temperature was monitored continuously by a rectal probe and maintained in the range of 36.5-37°C (ThermoStar, RWD, San Diego, California, USA).

Mice were monitored by the operator (by observation of chest movements) to assess that the respiratory rate was in the optimal range of ~55-65 respirations per minute. To prevent the process of ocular dehydration, ophthalmic gel

(Lacrilube 42.5% Liquid Paraffin + 53.7% White Vaseline, AbbVie S.r.l., Latina, Italy) was applied to the eyeball to create a protective gel film.

We proceed by removing the hair using scissors initially and then depilatory cream exposing the dorsal surface of the animal's head and limiting the infectious processes. The depilated area was disinfected with ethanol 70% and Betadine 10% (Betadine 10%, Meda Pharma S.p.A, Milan, Italy) 3 times. A subcutaneous injection of corticosteroid anti-inflammatory (Dexamethasone sodium phosphate, 5mg/Kg) was performed to reduce phlogosis processes, and local application by subcutaneous inoculation of a solution of lidocaine chlorohydrate 2% was applied topically as a local anesthetic.

With the help of tweezers, a flap of skin was lifted and a cut was made with scissors to expose a window on the skull of about 2-2.5 cm^2 to expose both hemispheres (**Figure 16**). The exposed surface was kept hydrated with sodium chloride 0.9% (Sodium Chloride 0.9%, Eurospital S.p.A., Trieste, Italy), cleaned of any hairs, and finally dried. With the stereotaxic apparatus and the monocle, we positioned on Bregma (the midline bony landmark where the coronal and sagittal sutures meet, between the frontal and two parietal bones) and then on Lambda (point of conjunction between the two parietals and the occipital bone), which is generally -4.2 mm from Bregma (**Figure 16**). These two anatomical landmarks were stained with a permanent marker. A layer of transparent dental cement (Super-Bond Universal Starter Kit, Sun Medical, Furutaka, Japan) was spread over the entire cortex making sure that the edges were carefully covered and not to have left any flap of tissue exposed to the air to prevent any infection.

The implant ring with glued custom-made aluminum support bar (head-post) (**Figure 16**) previously disinfected with ethanol 70% was placed on the animal's head. The correct position of the implanted ring was determined to include in the field of view the inferior cerebral vein on the rostral-caudal axis and the transverse sinus on the mid-lateral axis. Another parameter to check is that the implanted ring is parallel to the surface of the skull to avoid introducing distortions on both axes. Additional transparent dental cement was applied to secure the implanted ring with the head post and seal the lateral margins between the ring and the skin to prevent external light from entering the field of view during imaging sessions.

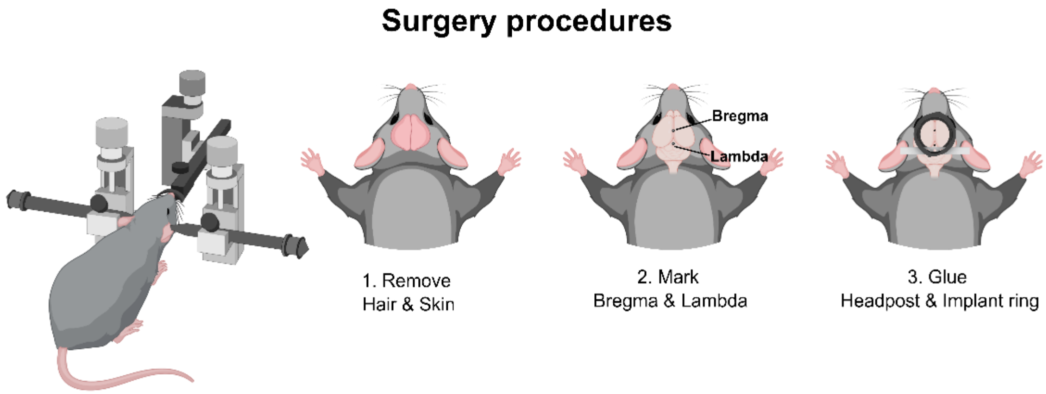

Figure 16: Illustration Showing the Steps of Surgery to Create the Optic Window. Starting from the left, the mouse in the head-fixed condition in the stereotactic apparatus was depicted. Following the removal of hairs and a flap of skin on the dorsal surface of the skull, two anatomical landmarks are marked: Bregma and Lambda. Finally, the optical window is covered with a layer of dental cement, and the head-post and implant ring are glued onto the dorsal surface.

At the end of the surgery, a subcutaneous injection of analgesic and non-steroidal anti-inflammatory (Carprofen, 5 mg/Kg) drugs and 0.2 ml lactated Ringer’s solution (Lactated Ringers, Eurospital S.p.A., Trieste, Italy) was given to facilitate recovery. At the end of the surgery, the mouse is placed in the induction chamber providing it only with oxygen until the first signs of awakening appear. Finally, it was placed in its home cage inside the animal facility on a heating pad for 1 hour until it was completely awakened. In the postoperative hours, the mouse was scrupulously followed to evaluate both the resumption of motor activity and the response to stimuli. To limit postoperative pain, multimodal analgesic therapy was administered daily for the first 3 days (Carprofen (5 mg/Kg) and Tramadol (20mg/kg), subcutaneously). The animals received 1 week of recovery from surgery where they were given *ad libitum* water and food.

2. Transgenic Animals

All animal experiments were authorized by the Italian Ministry of Health (authorization 241-2020-PR). A total of 10 non-sibling female GCaMP mice (C57BL/6J-Tg(Thy1-GCaMP6f)GP5.17Dkim/J) were used to perform visual stimulation experiments, characterize the Miniscope and investigate peer social interactions with a novel subject to incentivize interactions and avoid aggressive phenomena that might occur in male subjects. Mice were housed on a 12 h light/dark cycle with *ad libitum* access to water and food.

3. Wide-field Epifluorescence Microscope and Behavioral Platform

To validate the capabilities of the miniaturized optical system, visual stimulation experiments were performed by recording the cortical activity distributed on both hemispheres with the conventional widefield epifluorescence microscope and comparing it with the Miniscope developed in the laboratory. The widefield epifluorescence microscope used is a custom-made system developed in our laboratories consisting of a 470 nm LED (M470L5, 470 nm, 650 mW; Thorlabs Inc., Newton, New Jersey, USA) (**Figure 17A**) to excite the GCaMP6f indicator. Lighting and dimming of this LED are set by a USB Controller Hub and power supply (KCH301; Thorlabs Inc., Newton, New Jersey, USA) and a T-Cube LED Driver (LEDD1B; Thorlabs Inc., Newton, New Jersey, USA) (**Figure 17B**). The illumination emitted by the LED was collimated by an aspherical condenser (ACL2520U-A; Thorlabs Inc., Newton, New Jersey, USA) and reflected by an elliptical mirror (BBE1-E02, 1" Broadband Dielectric Elliptical Mirror; Thorlabs Inc., Newton, New Jersey, USA) (**Figure 17C**) placed in a right-angle mirror mount (KCB1EC/M, Kinematic Elliptical Mirror Mount; Thorlabs Inc., Newton, New Jersey, USA) to deflect light to a 100 mm focal lens (f=100 mm) (AC254-100-A-ML; Thorlabs Inc., Newton, New Jersey, USA) placed before the cube (DFM1/M) containing the filter and mirror kit for GFP (MDF-GFP; Thorlabs Inc., Newton, New Jersey, USA). Inside are: the 482/18 bandpass excitation filter (MDF-GFP; Thorlabs Inc., Newton, New Jersey, USA) to select only the wavelengths to excite GCaMP and the 495 nm dichroic mirror (DC FF 495-DI02 Semrock, Rochester, New York, USA) (**Figure 17D**) that is responsible for reflecting the excitation wavelength and directing it to the rear aperture of the objective (TL2X-SAP 2X Super Apochromatic Microscope Objective, 0.1 NA, 56.3 mm WD; Thorlabs Inc., Newton, New Jersey, USA) (**Figure 17E**). Since the objective has a 2X magnification and a 1X magnification is sufficient to study the cortical dynamics distributed on both hemispheres, using the following equation (Equation 7):

$$M_{eff} : f_{TLM}(mm) = M_{Des}: f_{TLO}(mm)$$

Equation 7: Equation for Calculating Magnification and Focal Length

Where M_{eff} is the Effective Objective Magnification, $f_{TLM}(mm)$ is the focal Tube Lens in Microscope of the microscope you are using, M_{Des} is the Design Magnification, which is the factory magnification printed on the objective, and $f_{TLO}(mm)$ is the focal Design Tube Lens of the Objective that the manufacturer of the objective used to calculate the design magnification. This focal length is given in a table by the manufacturer, in our case, using an objective 2X this focal length is 200 mm.

This equation (Equation 8) was used to calculate the focal distance of the tube lens $f_{TLM}(mm)$ to be inserted into the optical path to focus the sample image on the camera sensor.

$$f_{TLM}(mm) = f_{TLO}(mm)\ x\ \frac{M_{eff}}{M_{Des}}$$

Equation 8: Equation for Calculating the Focal Length of the Tube Lens

Knowing that the $f_{TLO}(mm)$ reported by the manufacturer is 200 mm, M_{Des} reported on the objective is 2X and the desired M_{eff} is 1X, we obtain a focal length of 100 mm.

Once the sample is illuminated, the emitted fluorescence is collected again by the objective lens and directed into the cube. The fluorescence, having a longer wavelength than the excitation light will pass through the dichroic mirror and be filtered by a 525/50 bandpass excitation filter for GFP (MDF-GFP; Thorlabs Inc., Newton, New Jersey, USA) (**Figure 17D**). At the top end of the cube, an achromatic Doublet lens with a 100 mm focal length was added before focusing the image on the CMOS sensor of the high-speed camera (Orca Flash 4.0 V2; Hamamatsu Digital camera; Bridgewater, New Jersey, USA) (**Figure 17F**). LED and camera synchronization for sample illumination and image recording were controlled by a National Instrument via a TTL signal**.**

In the lower part of the microscope was inserted a mechanical behavioral apparatus in which the animal could be inserted and recording sessions conducted under head-fixed conditions. This structure (**Figure 17G**) consisted of an aluminum breadboard with dimensions 200 x 200 x 12.7 mm (MB2020/M Aluminum Breadboard, M6 Taps; Thorlabs Inc., Newton, New Jersey, USA) on which 2 horizontal optical supports (TR30/M; Thorlabs Inc., Newton, New Jersey, USA) were attached to the base structure using 2 pedestal pillars posts with a height of 25 mm and diameter of 25 mm (RS1P/M; Thorlabs Inc., Newton, New Jersey, USA) and 2 clamping forks (CF125C/M; Thorlabs Inc., Newton, New Jersey, USA).

These two supports formed the anchor base of a custom-made structure, made in our machine shop, called "*sandwich*" (**Figure 17G**) because it consists of two metal plates that using a screw can be opened to insert the ends of the head-post and then closed. This system guarantees to perform imaging sessions in head-fixed conditions with excellent stability without introducing motion artifacts. To adjust the focus of the wide-field microscope objective, the behavioral platform was placed on a motorized stage (MLJ150/M; Thorlabs Inc., Newton, New Jersey, USA) (**Figure 17H**) that allowed the platform to move vertically by bringing it closer to or away from the objective.

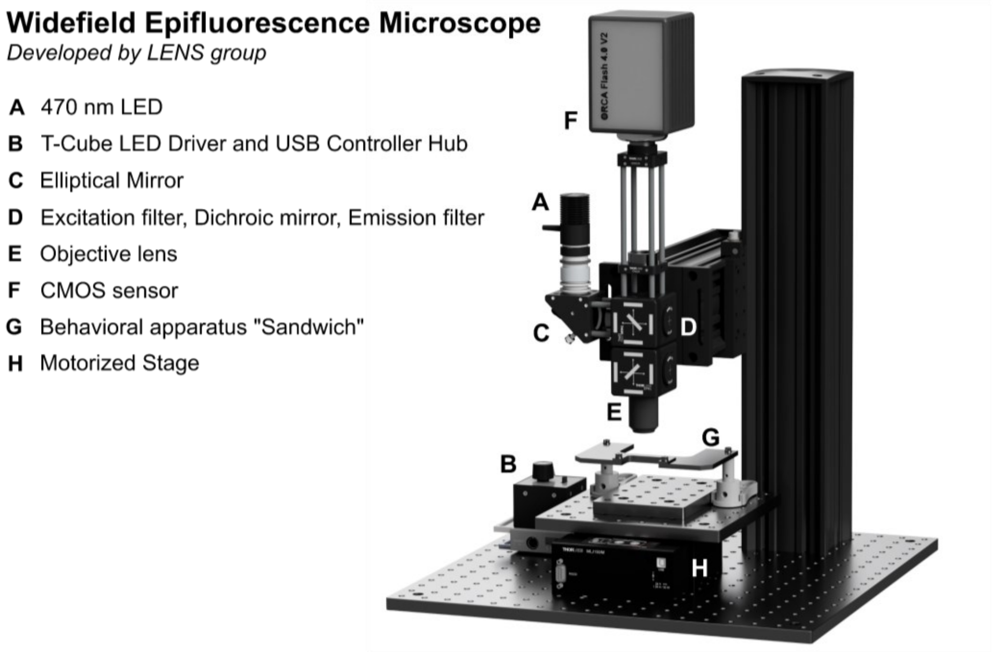

Figure 17: Widefield Epifluorescence Microscope.

CAD rendering of the Widefield Epifluorescence Microscope developed in our laboratory and behavioral "sandwich" apparatus to lock the animal and perform imaging sessions under head-fixed conditions.

4. Visual Stimulation Experiment

To verify the functionality and dependability of the developed miniaturized optical system, a visual stimulation experiment to compare the Miniscope to the conventional Widefield epifluorescence microscope was carried out. Recordings of cortical activity distributed over both hemispheres, in awake conditions, were conducted to record fluorescence signals and make a qualitative analysis of both systems.

A mouse expressing the fluorescent indicator “GCaMP6f” that underwent the same surgical procedures described in paragraph 1, chapter II, was used in this study. Following the recovery period, the animal was gently placed in the behavioral setup to perform recordings of cortical activity in head-fixed conditions. Through the aluminum head-post embedded in the implanted ring, it was locked into the anchor structure *“sandwich”* and positioned under the objective lens of the wide-field microscope. To habituate the animal to the “sandwich” and head-fixed condition, a few time-increasing sessions in the anchor structure were conducted in the previous days to experiment execution. This allows the animal to remain in a quiet state and perform the visual stimulation recordings in awake conditions under the best possible conditions.

A LED that emitted intermittent flesh of white light was chosen for stimulation. The LED was shielded by an optically isolated conical structure equipped with a terminal slit to let out a spot of light large enough to illuminate the entire eye of the animal. This conical structure was added to facilitate the directionality of the stimulus. In addition, given the proximity between the animal's eye and the optical window on the dorsal surface of the animal's head, this structure prevented the white light responsible for the visual stimulus from hitting the optical window and entering the optical path of the wide-field microscope going to distort the fluorescence measurements. To further reduce this phenomenon, an optical iris was interposed between the animal's head and the objective during widefield microscope acquisitions. In this experiment, a visual stimulus of white light lasting 100 ms with a frequency of 0.2 Hz (1 stimulus every 5 seconds) directed at the right eye was provided. The stimulation frequency and synchronization with the wide-field system and Miniscope were performed with a trigger controlled by coaxial cables and a National Instruments connected to a computer.

5. Social Interaction: Timeline of the Experiment

Following the surgery and for the entire duration of the experiment, to avoid aggressions and injuries that could affect the outcome of the experiment, in particular those affecting the area of optical access to the cerebral cortex, and to encourage social interactions during the experimental sessions, the animals were housed individually in an enriched environment ensuring visual and olfactory contact with conspecifics from the adjacent cages.

Before the start of the recording sessions, the experimental conditions and the dyads of the interacting subjects were defined. Social interaction experiments were conducted 2 times a week by allowing at least 2 days to elapse between one session and the next. The interacting dyads (subject A vs. subject B) were combined in a way that at each recording session subject A met a novel subject B, without combining animals from the same litter. Subjects of the interacting dyad were housed individually in separate animal facilities for at least 2 days before the experimental session (**Figure 18_Step 1**). On the days of recording, the subjects of the interacting dyad were individually moved from the animal facility to the experimental room and allocated to the opposite side of the room to minimize the level of interaction before the session. The Miniscope is mounted on the animals' heads and then they are housed in their cage for at least 15 minutes for the habituation phase (**Figure 18_Step 2**).

The recording session included 3 phases: in the first, subject A was placed alone in the behavioral box for 5 minutes to explore the environment and get used to the experimental setup. This also has the aim to reduce the exploration time of the third final phase where the interaction session will be recorded. In the second phase, the same thing was performed for subject B. Finally, both subjects (A and B) were placed in the behavioral box to record for 5 minutes the social interaction session (**Figure 18_Step 3**). Throughout the whole experiment, the cortical activity distributed over the entire cortex and the behavioral repertoire that the animals exhibited were recorded simultaneously using the Miniscope and the Raspberry Pi camera placed under the behavioral box. Plastic containers were used to move the animals from the home cage to the behavioral box. The animal was gently placed inside and once placed in the behavioral box the mouse was released. For the social interaction sessions, both animals were released at the same time. At the end of each session, the behavioral box was cleaned with ethanol 70%, and the door of the enclosure was left open for a few minutes to evaporate ethanol and eliminate the smell of the animal that performed the recording. The plastic containers and all the surfaces where the animal home cages came into contact were cleaned with ethanol 70% between one dyad and the next to avoid olfactory contamination. Once the registrations were completed, the animals were placed in their respective home cage, housed in the animal facilities, and divided according to the interacting dyads for the following session (**Figure 18_Step 4**).

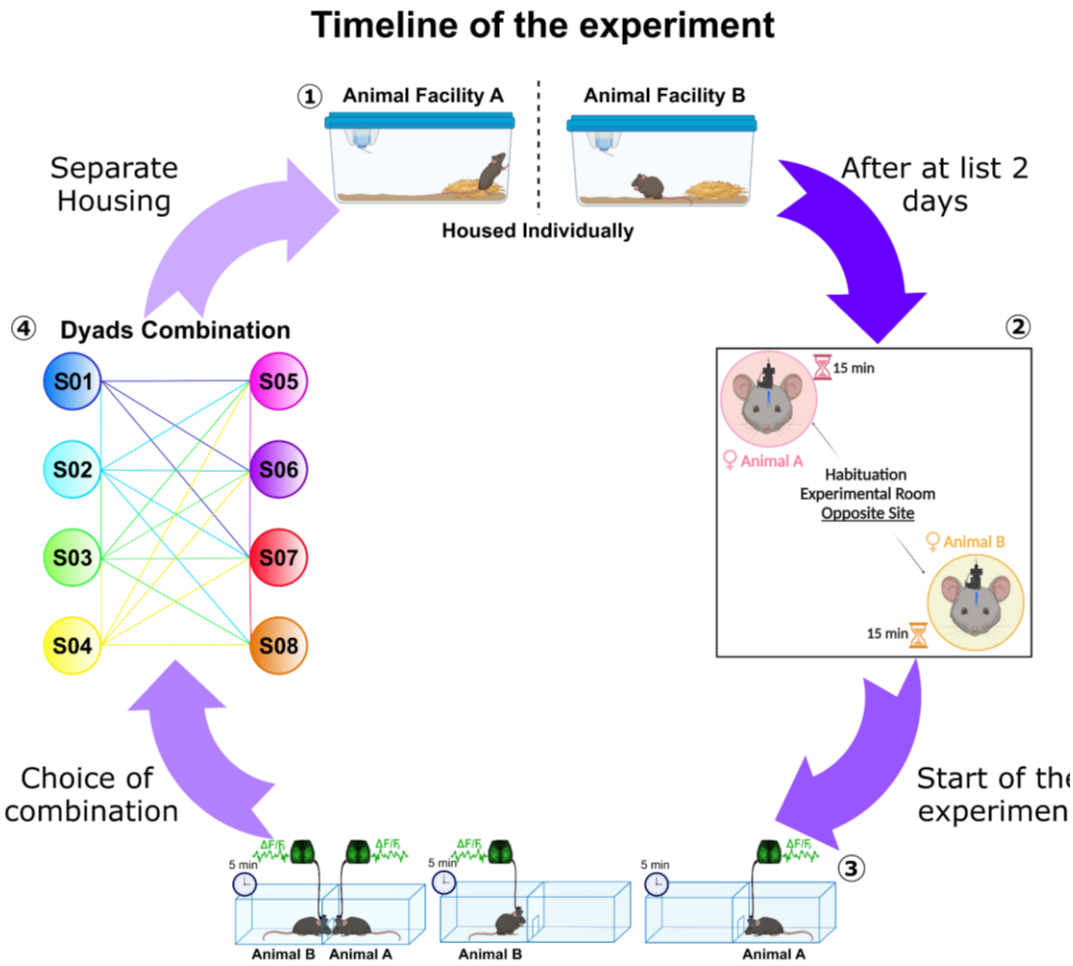

Figure 18: Timeline of the Experiment.

(Step 1) After at least two days of isolation in separate animal facilities, the two interacting subjects are transported to the experimental room, mounted the Miniscope, and acclimatized in their home cages at two opposite sites in the room for at least 15 minutes (**Step 2)**. Animal A is placed individually in the behavioral setup and left free to explore the environment for 5 minutes, the same operation is performed for subject B. Finally, both subjects are placed simultaneously in the setup for the interaction session for 5 minutes (**Step 3)**. After the experiments, new dyad combinations are chosen for the next session, and the animals are separated into different animal facilities (**Step** **4**) to recreate isolation before the next interaction session.

III. Results

1. Miniscope

In this work, a miniaturized single-photon optical system called Miniscope was designed and developed to perform wide-field calcium activity recordings, expressed as fluorescence variation, in rodents in freely moving conditions. The assembly, development, and characterization of the device developed in our laboratory will be shown below.

1.1. Mechanical and Optical Design

All the parts of the Miniscope and the implanted ring were designed using the CAD program (Autodesk Fusion 360). These components were built using a stereo-lithography 3D printer (XFAB 2500HD; DWS System, Vicenza, Italy) using a black photosensitive resin (Invicta DL385; DWS System, Vicenza, Italy) to obtain components isolated from external light. Miniscope (**Figure 19A**) was equipped with 2 blue LEDs (CREE XPEBBL-L1-0000-00301; Cree, Inc., Durham, North Carolina, USA) with a dominant wavelength between 465 and 485 nm, paired with a circular excitation filter (450-490 nm, 4mm DIA, ET 470/40x; Chroma Technology Corp, Bellow Falls, Vermont, USA). This wavelength was necessary to excite the GCaMP6f indicator expressed in the excitatory cortical neurons. An emission filter (500-550 nm, 7mm DIA, ET 525/50m; Chroma Technology Corp, Bellow Falls, Vermont, USA) was inserted before the camera to filter the fluorescence signal. A complementary metal-oxide-semiconductor imaging sensor (Spy Camera for Raspberry Pi 5MP, ID 1937 Adafruit Industries LLC, New York, New York, USA) was mounted on the top of the device to record neocortical activity from both hemispheres.

To mount the Miniscope on the animal's head, an implant ring (**Figure 19B**) with an embedded aluminum bar ("head-post") was developed that is glued to the dorsal surface of the animal's head during surgery to create optical access. This system allows perfect mechanical coupling between the Miniscope and the animal's head. Two screws in the implanted ring allow the Miniscope to be locked, ensuring mechanical stability during freely moving recordings.

1.2. Miniscope: Optical Characterization

After the assembly of the device, optical characterization was performed. A stack of images with the Miniscope and the implanted ring was acquired on a sheet of paper on which a microscope slide was applied to simulate fluorescence.

Knowing the resolution of the Miniscope camera (512 x 512 pixels) and using the ImageJ program (https://imagej.net), calibration of the optical system was performed to calculate the real FOV size inside the slip ring. It has been calculated that the Miniscope presents a FOV of approximately 10.5 mm (**Figure 19D**).

The same stack, using ImageJ, was used to calculate the illumination profile, expressed as gray values across the entire FOV, revealing the sensitivity of the CMOS sensor. The data obtained were plotted on a graph in which the x-axis shows the distance along the field of view (in mm) and in the y-axis the gray values. We can see that the illumination profile is homogeneous in the range of 2 to 8 mm with a gray scale ranging from 0 to 240 (**Figure 19D**).

Using the 1951 USAF resolution test target (R3L3S1P, Positive 1951 USAF Test Target, 3" x 3"; Thorlabs Inc., Newton, New Jersey, USA) the optical resolution was estimated (**Figure 19C**). The optical resolution was calculated by positioning the USAF in 11 different positions, and an average resolution of (31.00 ± 5.01) µm was found, expressed as (mean value ± standard deviation).

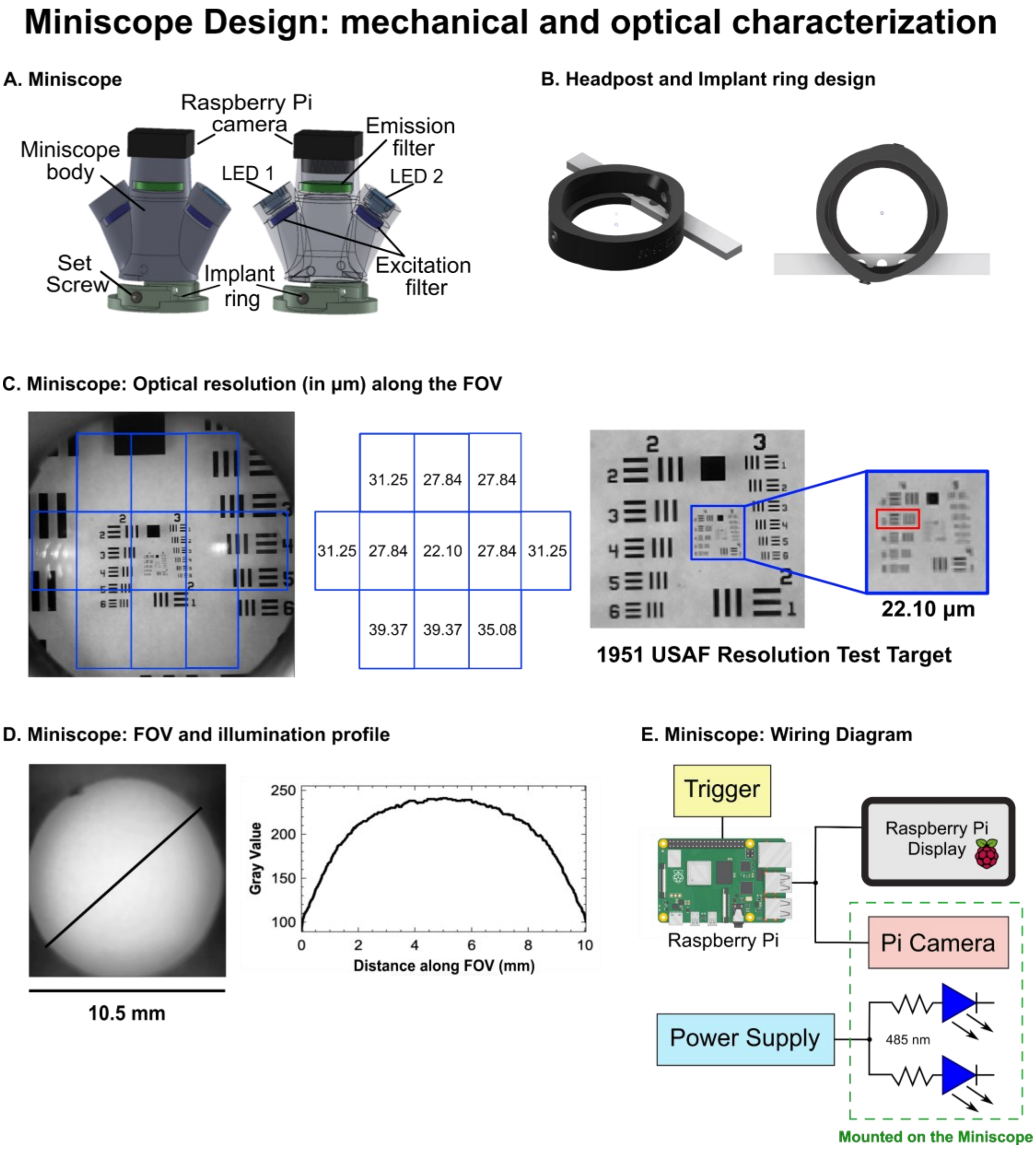

Figure 19: Miniscope Design: Mechanical and Optical Characterization.

(A) Miniscope design with all optical and mechanical components listed. **(B)** Rendering of the head post attached to the implanted ring. **(C)** Optical resolution in µm along the FOV calculated with the 1951 USAF Resolution test target. **(D)** Image of the FOV and Plot Illumination profile along the field of view **(E)** Wiring diagram showing the Raspberry Pi connected to the Raspberry Pi display for viewing both hemispheres and the Raspberry Pi camera used to perform calcium imaging. The 2 blue LEDs (485 nm) are controlled by an external power supply. The green dotted rectangle contains the components mounted on the Miniscope.

1.3. Miniscope Compared to Widefield Microscope: Visual Stimulation Experiment

To characterize the developed device and validate its functionality, visual stimulation experiments were conducted using both the Miniscope and the conventional Widefield epifluorescence microscope as recording systems. A series of visual stimuli were delivered using an LED emitting a series of flashes of white light (n = 10 trials in 1 mouse) lasting 100 ms in the right eye, and simultaneously the cortical response evoked by the stimulus was recorded (**Figure 20A**).Figure 20A shows the sequence of mean activation distributed over both hemispheres recorded with the widefield microscope. Starting from the first image, corresponding to the onset of the stimulus, each frame represents a 120 ms time event. We observe the appearance of a cortical response in the visual cortex of the left hemisphere (contralateral to the eye that received the visual stimulus) starting 120 ms from the onset.

The evoked response expands in the mid-lateral direction until it reaches maximal activation about 240 ms after stimulus onset (**Figure 20B**). In the subsequent frames, the evoked activity tends to decrease until it disappears about 840 ms from the onset. As we can see from the mean activation sequence and as also confirmed in Figure 20B where the frame with maximum activation is depicted, the cortical response evoked by the stimulus occurs primarily in the contralateral hemisphere, while in the ipsilateral hemisphere, there is extremely little fluorescence change.Figure 20C shows the single calcium activity profiles over time, expressed as fluorescence variation, recorded as a response to the individual 10 visual stimuli presented to the subject. As we can see even in the single-trial condition, a cortical response evoked by the stimulus, corresponding to time zero in the graph, can be observed. Finally, Figure 20D shows the activation profile, in the contralateral hemisphere, expressed as percent fluorescence variation (% $\Delta F/F_0$) over a time window ranging from -2 seconds to 3 seconds from stimulus onset. The activation sequence corresponds to the profile obtained from the average of the 10 stimuli presented to the subject. It is evident that at the onset of the stimulus, an almost immediate cortical response is evoked with a maximum fluorescence change of about (2.32 ± 0.55%) expressed as (mean value ± standard deviation), afterward this activity drops below the baseline level to stabilize again in the seconds following the stimulus.

Given the excellent performance of the conventional Widefield epifluorescence microscope, the activity recorded with this system was used as a reference standard to characterize and validate the Miniscope developed in our laboratory. Figure 20E shows the average activation sequence, distributed over both hemispheres, of the stimulus-evoked cortical response recorded with the Miniscope. Averaging the 10 stimuli provided to the subject shows a cortical response in the contralateral hemisphere beginning 120 ms after stimulus onset that extends into the visual cortex reaching maximum activation 200 ms after stimulation onset (**Figure 20F**). Again, the evoked response in the ipsilateral hemisphere is minimal compared to the contralateral one.Figure 20G shows the calcium profiles of individual stimulation trials over time. As reported in the Widefield microscope, a cortical response is also clearly visible in the individual traces in the Miniscope.

Confirmation of a cortical response evoked by the stimulus can be seen in Figure 20H in which the profile obtained from the average of the 10 stimuli previously described. A few milliseconds after the stimulus onset, a cortical response is shown in the visual cortex of the contralateral hemisphere with a fluorescence change (% $\Delta F/F_0$) of about (1.7 ± 0.53%) expressed as (mean value ± standard deviation), thereafter the activity decreases reaching a lower value than the baseline to return to baseline values in the next 3 seconds.

In conclusion, we were able to use both devices to capture a stimulus-evoked cortical response in the contralateral hemisphere. Despite differences in the sensor performance, optical components, and resolution of the two microscopes, the Miniscope was shown to be a system capable of measuring a stimulus-evoked response with qualitative and quantitative characteristics comparable to the Widefield microscope.

Figure 20: Visual Stimulation: Comparison between Widefield and Miniscope.

Cortical responses evoked by visual stimulation recorded with two systems are shown: Widefield microscope **(A-B-C-D)** and Miniscope **(E-F-G-H)**.

(A and E) Mean activation sequence distributed over both hemispheres following visual stimulation of the right eye. **(B and F)** Frame showing maximum cortical activation following the stimulus. **(C and G)** Plot with individual calcium profiles reporting the evoked response in the visual cortex of the contralateral hemisphere. **(D and H)** Plot reporting the average profile of percent fluorescence variation (% $\Delta F/F_0$) over time (-2 to 3 sec) extracted from the visual cortex contralateral to the stimulus averaged over the 10 trials.

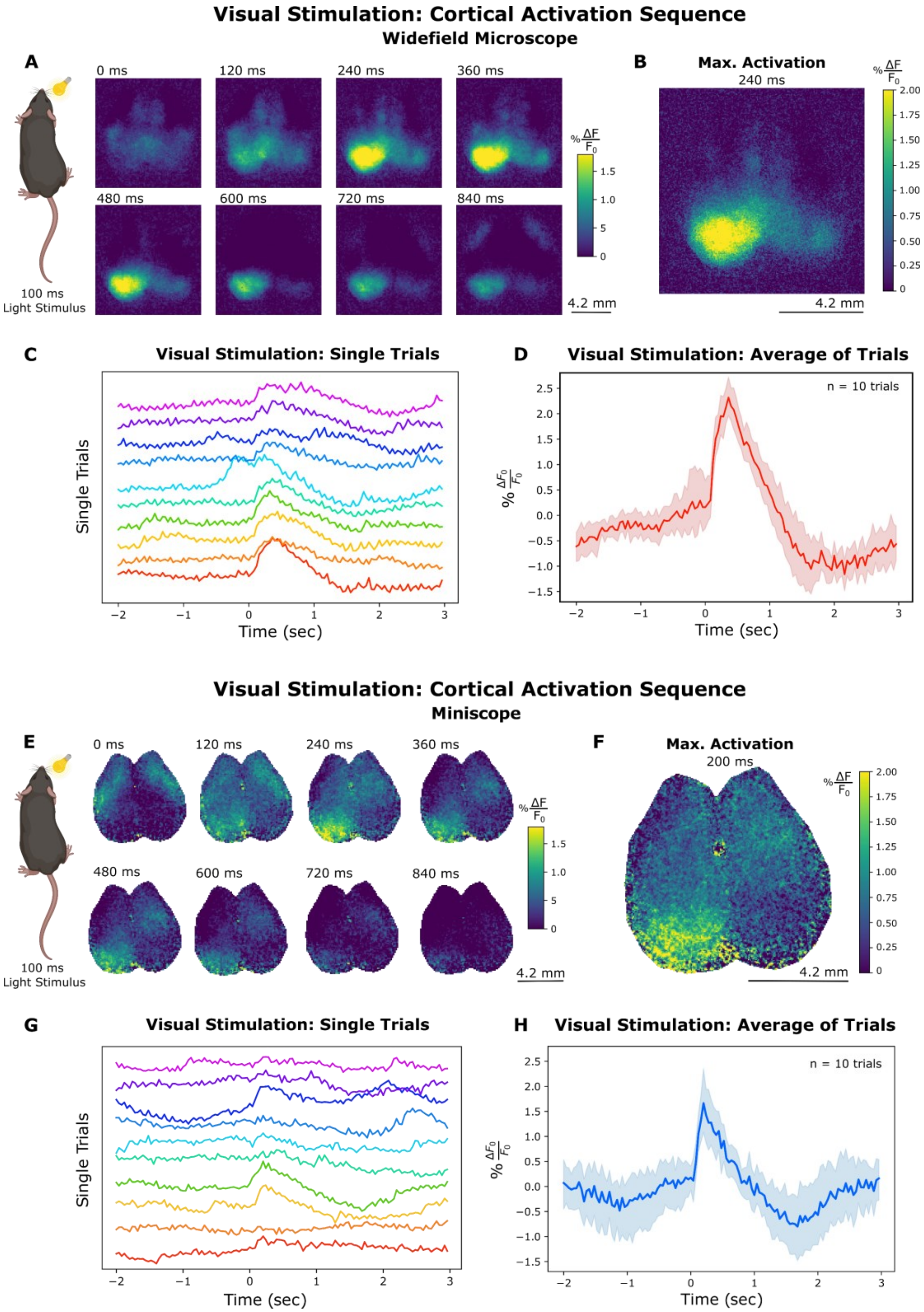
Visual Stimulation: Cortical Activation Sequence
Widefield Microscope
A
0 ms
120 ms
240 ms
360 ms
480 ms
600 ms
720 ms
840 ms
100 ms
Light Stimulus
%ΔF/F0
1.5
1.0
5
0
4.2 mm
B
Max. Activation
240 ms
%ΔF/F0
2.00
1.75
1.50
1.25
1.00
0.75
0.50
0.25
0
4.2 mm
C
Visual Stimulation: Single Trials
Single Trials
−2
−1
0
1
2
3
Time (sec)
D
Visual Stimulation: Average of Trials
n = 10 trials
%ΔF0/F0
2.5
2.0
1.5
1.0
0.5
0.0
−0.5
−1.0
−1.5
−2
−1
0
1
2
3
Time (sec)
Visual Stimulation: Cortical Activation Sequence
Miniscope
E
0 ms
120 ms
240 ms
360 ms
480 ms
600 ms
720 ms
840 ms
100 ms
Light Stimulus
%ΔF/F0
1.5
1.0
5
0
4.2 mm
F
Max. Activation
200 ms
%ΔF/F0
2.00
1.75
1.50
1.25
1.00
0.75
0.50
0.25
0
4.2 mm
G
Visual Stimulation: Single Trials
Single Trials
−2
−1
0
1
2
3
Time (sec)
H
Visual Stimulation: Average of Trials
n = 10 trials
%ΔF0/F0
2.5
2.0
1.5
1.0
0.5
0.0
−0.5
−1.0
−1.5
−2
−1
0
1
2
3
Time (sec)

2. Behavioral Setup

In this section, the new behavioral paradigm developed in our laboratory will be described. Inspired by the linear chamber test developed by Lee and colleagues (E. Lee et al. 2016), a modified version of the behavioral apparatus was built to gather data on exploration and social interaction. A custom-made plexiglass arena (size 740 x 200 x 250 mm) (**Figure 21A**) was made, and inside it was placed a transparent barrier equipped with a gap (size 10 x 100 mm) (Figure 21B) to separate the box into 2 identical compartments. The size of the gap allowed subjects to interact with their noses, while the transparency of the structure ensured visual contact with the other compartment. To record the behavior, a camera was placed under the behavioral box (5MP Camera, Okdo Design the World, London, United Kingdom) (**Figure 21D**). To have a good field of view, the box was raised so that the edges were visible (**Figure 21**). Using 8 posts (4 pcs TR300/M and 4pcs TR250/M; Thorlabs Inc., Newton, New Jersey, USA), 4 vertical supports were built joined by 2 horizontal supports (TR250/M; Thorlabs Inc., Newton, New Jersey, USA) to create a structure on which to place the box. The 4 vertical support, employing pillars posts (4 pcs RS50P4/M; Thorlabs Inc., Newton, New Jersey, USA) and clamping forks (4 pcs CF125C; Thorlabs Inc., Newton, New Jersey, USA), were anchored to the optical table to ensure the immobility and stability of the structure during the execution of the experiments. The entire structure was enclosed by 5 white custom-made hardboard panels (2pcs 900 x 750 mm for the front and back, 2pcs 750 x 450 mm for the laterals, and 1pcs 900 x 450 mm for the top) held together by square construction rails (XE25L900/M, XE25L750/M, XE25L550/M; Thorlabs Inc., Newton, New Jersey, USA). Five sound-absorbing panels (**Figure 21E**) made of polyurethane foam with 50 mm thick pyramids (Akustic Stop 100 x 100 x 5 cm 35 Kg/m^2, NDA The Panels of Silence, Viterbo, Italy) were applied to the outside of the structure to silence the internal environment and not to introduce sound artifacts during the execution of the experiments.

A led strip (Kit Strip LED RGB 21, 6W 3m 24V, TMR Elcart, Milan, Italy) was applied along the internal perimeter of the ceiling to illuminate the whole experimental apparatus with white light. To prevent the light from bothering the animals, sheets of paper were applied to diffuse the light and create a homogeneous illumination. A sheet of transparent red acetate (**Figure 21C**) (as rodents do not see the red spectrum) was applied to the base of the box to prevent the animals from perceiving the height from the optical table and therefore the sense of suspension that causes a high level of stress in rodents.

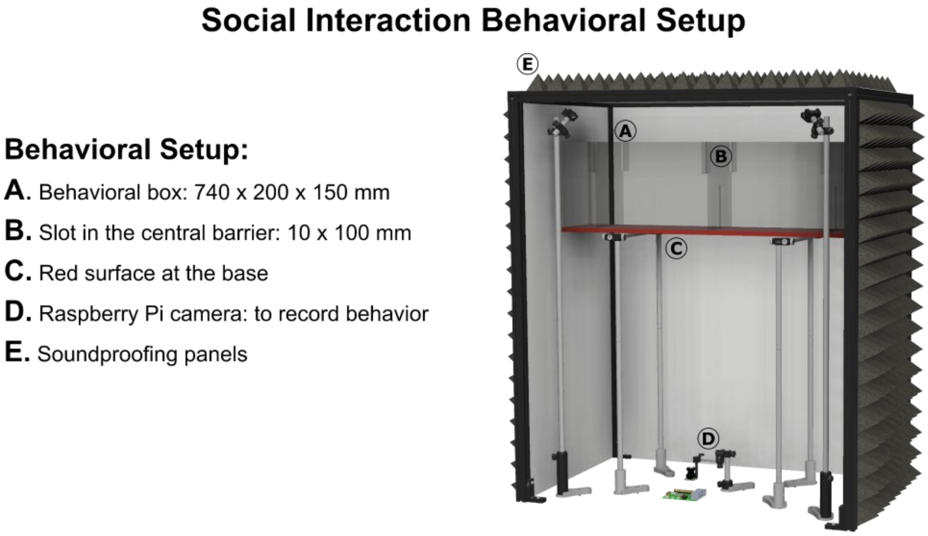

Figure 21: Experimental Setup for Performing Social Interaction Recordings.

(A) The behavioral box was made of translucent plexiglass and consists of two chambers separated by a central barrier equipped with a slot **(B)** to allow subjects to interact with their noses. **(C)** The base of the behavioral box was covered with a translucent sheet of red acetate so that the animals would not perceive the sense of suspension. **(D)** Acquisition system (Raspberry Pi camera) to record the animals' behavior from below. **(E)** The entire experimental setup was enclosed by white hardboard panels and externally lined with soundproofing panels to prevent sound artifacts from altering social interactions.

The 2 LEDs of the Miniscope were wired in parallel using 36-gauge wires (Miniature Insulated Wire 36 AWG, UAA3601, Micron Meters; Tucker, Georgia, USA) and 2 resistors (10 Ohms ± 0,05% 0,25W, 1206; Stackpole Electronics, Inc., Raleigh, North Carolina, USA) were also inserted to balance the current supplied. The entire illumination system was connected to a power supply that provided 300 mA of current to the LEDs.

The CMOS sensor (Spy camera for Raspberry Pi 5MP; Adafruit Industries LLC, New York, New York, USA) of the Miniscope was connected to a slip ring (Slip Ring mini 12 mm Dia, 12 wire, Adafruit Industries LLC, New York, New York, USA) located in the top panel of the experimental apparatus to allow subjects to move freely and rotate on themselves.

A behavioral camera (5MP Camera, Okdo Design the World, London, United Kingdom) (**Figure 21D**) was placed below the behavioral box to record the movement of the subjects. The distance of the behavioral box from the behavioral camera was determined to scan the whole box in the field of view (FOV).

The behavioral camera and the slip rings were connected via flat cable (Cable FFC 15POS 1.00 mm 12”, Molex, Lisle, Illinois, USA) to the Raspberry Pi (Raspberry Pi4 Model B, 4GB; RaspberryPi, Caldecote, United Kingdom), and the videos of the animal’s movements and fluorescence calcium signals from the entire cortex were visualized on Raspberry Pi Display (Display for Raspberry Pi LCD 7-inch touchscreen; RaspberryPi, Caldecote, United Kingdom). Finally, coaxial cables were used to synchronize all recording systems using the data acquisition (DAQ) of National Instruments.

3. Miniscope Validation

After developing and characterizing the Miniscope, validation experiments were performed.

The first test was conducted to analyze and determine the impact that the application of the device has on the rodent's head. The developed system, in addition to the characteristics of a wide field of view, must present a design and weight that is sustainable by the mice without altering or hindering the conventional behavioral repertoire. Subsequently, the mechanical coupling of the Miniscope with the implanted ring was validated to test the stability of the recordings to obtain images free from motion artifacts.

The results obtained from the validation of Miniscope by analyzing both the behavior and the fluorescence signal will be described below.

3.1. Behavioral Tracking in Mice with and without Miniscope

The impact that Miniscope has on animal behavior was assessed. To validate the effect of the system, recording sessions were performed in 2 experimental groups: one bearing the Miniscope on the head (*Miniscope group*) and the second without the device (only with the implanted ring) defined as *Control*.

The records of individual subjects within the box were used for these analyses. In the behavioral videos, a mask was applied to cut only the region of interest of the behavioral box in which the animal was located (**Figure 22A_left**). Videos of the region of interest were used to perform automated tracking of the animal's position using a custom-made blob detector algorithm. To obtain correct position tracking, it is important to have an excellent contrast between the color of the subject and the background of the environment. This was solved by using white hardboard flanks to have the subject black on a white background. The algorithm generated a circular blob around the animal to calculate its centroid (**Figure 22A_center**), this was used to determine the x and y coordinates of the subject's position inside the box. To prevent the algorithm from making evaluation errors, and to include the entire behavioral repertoire of the animal (including rearing or maximum stretching), two criteria were provided: minimum and maximum area of the blob, as limit parameters to perform the tracking. The x and y coordinates of the tracking (**Figure 22A_right**) were used to evaluate the behavior in the 2 experimental groups and initially generate the heatmaps. The heatmaps (**Figure 22B_left**) show, on a colorimetric scale, the time spent by the subjects in the different parts of the box for the 2 experimental groups: *Miniscope* and *Control* (**Figure 22B_right**). In our study we have chosen to divide the region of interest into 2 sub-regions: center the portion of the box near the slot and outer the opposite part. From the heatmaps reported in Figure 22B, we can see that both experimental groups spend more time in the central part than in the outer one. The data obtained from the tracking were plotted to quantify the time spent by the subjects in the 2 sub-regions (outer and center ROI) and to quantify the total distance traveled inside the box during the recording session for both groups. The plot of Figure 22C shows that both groups (*Miniscope* and *Control*) spend more time in the center ROI than in the outer one and this difference is statistically significant with a p-value <0.05.

Finally, the total distance covered by the subjects in the 2 experimental groups was reported in the plot of Figure 22D. From this analysis it emerged that the subjects bearing the Miniscope traveled on average a greater distance inside the box compared to the Control, however, this difference is not statistically significant.

These results provided an assessment of the impact that the Miniscope mounted on the animal's head, compared to the *Control*, has on the behavior of the subjects.

We believe that Miniscope does not hinder natural behavior or limit the ability of animals to explore the environment.

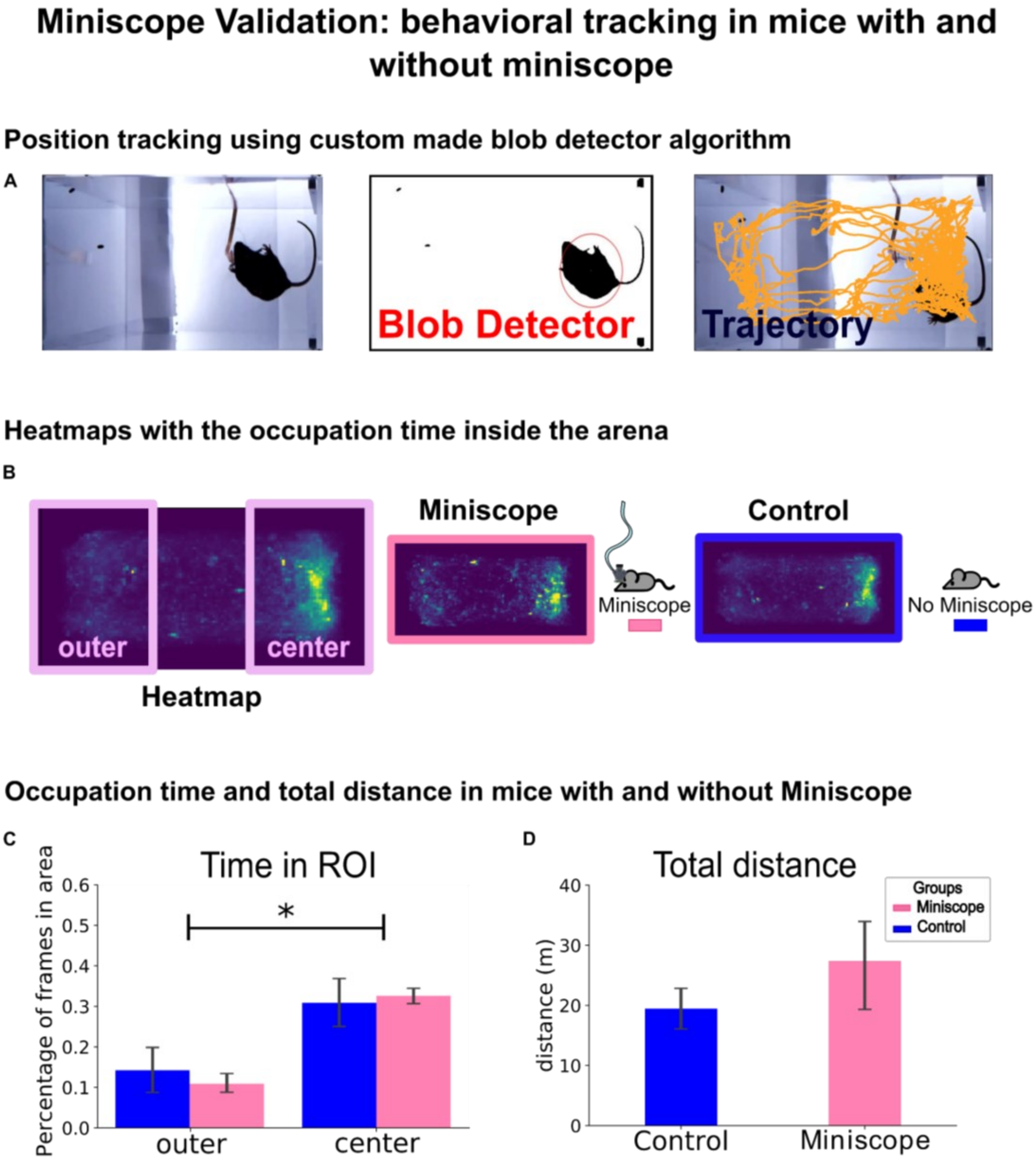

Figure 22: Miniscope Validation: Behavioral Tracking in mice with and without Miniscope.

(A) Bottom view representation of the behavioral chamber containing the mouse with Miniscope. The black mouse on a white background was used for the application of a custom-made algorithm for detecting the animal's centroid and performing subject tracking. **(B)** Heatmaps report the permanence time of the animal in the different parts of the arena in the two experimental conditions: with and without a Miniscope. **(C)** Plots reporting occupation time in the two identified ROIs: outer and center and total distance traveled by the animals with and without Miniscope.

3.2. Image Processing and Fluorescence Signal

Thanks to this device we were able to record the cortical activity distributed on the whole cortex. Using the Thy1-*GCaMP6f* transgenic line, we recorded neuronal response expressed as fluorescence variation which is an indirect indicator of calcium activity. The images related to the calcium activity (**Figure 23A**) were processed to calculate the fluorescence variation expressed as $\Delta F/F_0$. This value was calculated following this formula $\frac{\Delta F}{F_0} = \frac{(F-F_0)}{F_0}$, where F is the value of fluorescence signal per pixel while F0 is the mean fluorescence per pixel over time and generally this ratio is reported as a percentage. To analyze cortical activity on specific regions of interest in the brain during the different sessions and in different subjects, image alignment was necessary (**Figure 23B**). An image has been saved as a reference for each session or subject or for each time the field of view of the image has changed. Using the custom-made alignment tool, each image used as a reference was loaded and the parceling mask (according to the Allen Institute Mouse Brain Atlas) was applied to segment both hemispheres into different regions of interest (**Figure 23C and D**). The program requires the insertion of the field of view of the optical device and knowing that the distance between the two anatomical landmarks (bregma and lambda) is 4.2 mm (**Figure 23B**), it automatically determines the distance of the 2 points to be applied to the image. All the images were processed following these guidelines to obtain a precise alignment between the different acquisitions over time.

To validate the stability and efficiency of the optical system, the calcium fluorescence signal in freely behaving mice was plotted in 2 behavioral states: during locomotion (orange) and the resting phase (red) (**Figure 23E_right**). Figure 23E_left shows the image of the entire field of view aligned with Allen's parceling mask, in which 4 regions of the right hemisphere have been highlighted. Starting from the rostral area we find the Primary motor cortex (MOp_R), Primary somatosensory area- barrel field (SSp-bdf_R), Primary visual area (VISp_R), and Retrosplenial area- dorsal part (RSPd_R). From these 4 cortical regions, percentage changes in fluorescence during the two behavioral conditions in a 10-second time window were plotted (**Figure 23F**). Although the trend of the traces is very similar, during the locomotion phase, there is a variation of the % $\Delta F/F_0$ signal that differs slightly across the 4 cortical regions. This demonstrates that the device presents good sensitivity and stability of fluorescence recordings across different behavioral conditions. Even though the animal is free to move and exhibits a varied behavioral repertoire, the optical system remains stable on the rodent's head without introducing movement artifacts.

Figure 23: Miniscope Validation: Image Processing and Fluorescence Signal.

(A) Left, images of the cortical mantle acquired with the Miniscope, as we can see the wide field of view allows a good portion of both hemispheres to be recorded. The right formula for calculating the fluorescence change $\Delta F/F_0$.
(B) Alignment phase with the positioning of the two anatomical repere points: Bregma and Lambda. **(C)** Application of the parcellation mask of the Allen Brain Atlas used to segment the cortex into the cortical sub-areas and **(D)** cutting of the areas outside the mask.
(E) Image of the cortex with the Allen mask applied in which four cortical areas were highlighted. Starting from the rostral area: Motor Cortex (blue), Somatosensory Cortex barrel field (red), Visual Cortex (orange), and Retrosplenial Cortex (green). **(F)** Calcium profile graph expressed as fluorescence change (% $\Delta F/F_0$) over time of the four previously described cortical areas in two behavioral phases: resting (red rectangle) and locomotion (orange rectangle).

Miniscope Validation: image processing and fluorescence signal

Image processing and fluorescence signal analysis

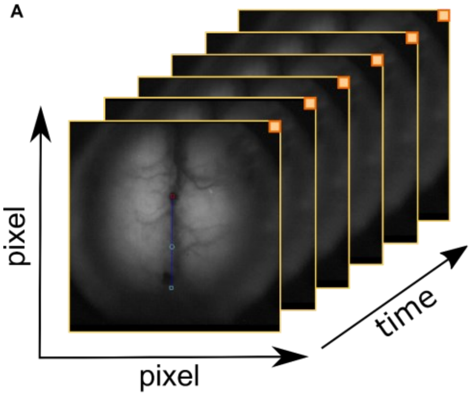

$$\frac{\Delta F}{F_0} = \frac{F - F_0}{F_0}$$

F = Fluorescence signal per pixel
F_0= Average fluorescence per pixel over time

Image alignment and Allen Brain Atlas mask application

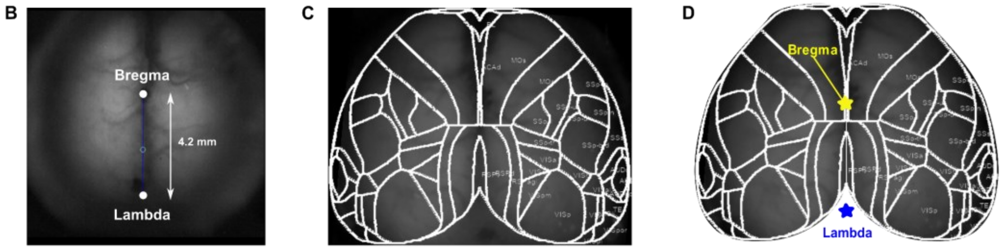

Calcium fluorescence signals in freely behaving mice: locomotion vs rest

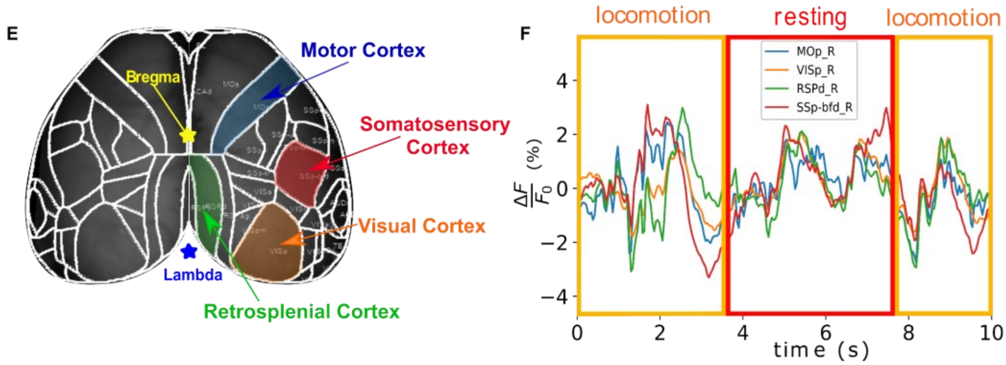

4. Social Interaction: Behavioral Analysis

In this project, studies were carried out to assess and examine social interactions in mouse dyads. One subject was made to engage with a new subject during each recording session.

As anticipated earlier, the tested subjects are kept apart in two different animal facilities to prevent olfactory and visual contact before interaction, and at least two days are allowed to pass between one recording session and the next to increase and foster interactions between dyad members.

Animals are brought individually from the animal facility to the experimental room while keeping them at an appropriate distance to avoid contact between the two test subjects. Both subjects are habituated in the home cage for at least 15 minutes after the Miniscope has been applied. In the first stage of the social interaction test, each subject is placed in the arena chamber with a Miniscope mounted on their heads for a session of environment exploration and acclimation. In the last stage, both subjects are placed in the experimental setup to perform the social interaction recording. Each of these phases has a duration of 5 minutes.

The results of the validation of the developed experimental setup with quantification of nose poke behavioral events will be reported below. Finally, a section will be reported on the segmentation method of the behavioral repertoire chosen to investigate the dynamics of social interaction.

4.1. Quantification of Nose Pokes Events in Interacting vs Solitary Subject

To validate the developed experimental setup and assess any behavioral differences, gap behavior during the initial habituation and social interaction sessions was analyzed. This preliminary analysis provides insight into the functionality of the behavioral paradigm for studying social interactions. Especially, using a customized algorithm based on ROI, the analysis of the gap behavior of the single subject and the couple during the interaction was performed.

The algorithm generated 5 ROIs (**Figure 24A**): ROI 0 called "Gap" which corresponds to the slot in the central barrier, ROI 1 called "Left ROI" a small square near the left side of the gap, ROI 2 called "Right ROI" a small square near the right side of the gap, and finally ROIs 3 and 4, they are bigger squares that include respectively the Left and Right ROIs.

Using the contrast between the white background of the environment and the black of the subjects, the algorithm was able to quantify the number of times the animal passed through these ROIs and how many times it entered the gap. To count the number of inputs, the condition to be validated was that at least 75% of the pixels within these ROIs were black. To evaluate the number of entrances to the gap, the nose poke interactions at the slot were quantified both when the subjects were alone (Alone condition) or both present (Interaction condition).

From this analysis, the duration and number of nose poke interactions in both conditions were evaluated. The plot in Figure 24 B shows in light blue (Alone condition) and yellow (Interaction conditions), the duration (in seconds) of stay in the 3 different ROIs: Gap, Left, and Right. As we can see, when both subjects are present in the behavioral box they spend more time in all three ROIs to perform nose pokes than when they are alone, and in general this difference is statistically significant with a p-value <0.05 (**Figure 24B**).

When we look at the number of entries in the gap with the nose (**Figure 24C**), it was observed that the number of entries is greater in the Interaction vs Alone condition for the Gap ROI; while generally for the Left and Right ROIs the number of inputs remains similar.

However, the difference in entrance in the ROI gap for both conditions is not statistically significant. This could indicate that the subjects are intrigued by the presence of the gap both when they are alone or in a company, but only when a second subject is placed on the other side of the arena, the pair of animals spend more time near the gap to interact with their nose. To further characterize the nose poke event in the Interaction condition, the average duration (expressed in seconds) of the first interaction at the gap was calculated and compared with the average of the subsequent interactions (**Figure 24D_left**). It has been observed that subjects generally spend more time at the gap the first time they meet compared to the subsequent nose pokes. This difference is statistically significant with a p-value <0.05. Finally, to have an overall evaluation of the number of interactions per session, it was observed that on average about 7 nose poke events are performed in each recording session (**Figure 24_right**).

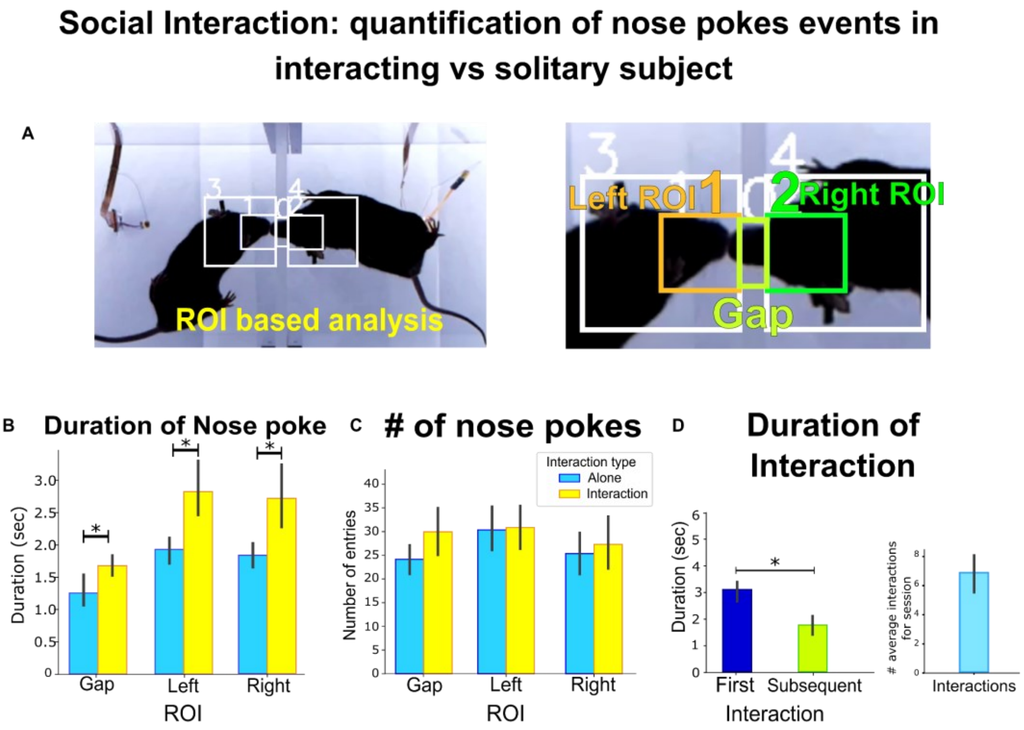

Figure 24: Social Interaction: Quantification of Nose Pokes Events.

(A) Images of a nose poke interaction event with ROI representation for applying the ROI-based analysis algorithm and quantifying the number of interactions. The central ROI corresponds to the Gap, the two smaller ROIs lateral to the Gap are referred to as Left and Right ROIs (1 and 2), and finally, two macro ROIs (3 and 4) that include 1 and 2. **(B)** The plot of the duration of nose poke events in the Gap, Left, and Right ROIs in the Alone (blue) and Interaction (yellow) conditions. **(C)** The plot of the number of nose pokes events in the Gap, Left, and Right ROIs in the Alone (blue) and Interaction (yellow) conditions. **(D)** Left, is a plot showing the duration of the first social interaction compared to subsequent interactions, right graph with the average number of interactions per session.

4.2. Behavioral Segmentation

After validation of the behavioral paradigm, to perform a finer study of the subjects' behavioral repertoire, an ethogram was constructed. While running the ethogram, the behavioral repertoire was segmented to select the types of behavior to be investigated to study the dynamics of social interaction.

BORIS (Friard and Gamba 2016), an easy-to-use event recording software for video encoding and live observations, was used to specifically segment the different behaviors.

Considering the three recording sessions: two for habituation in which the individual subjects are placed in their room and the last in which both subjects are located in their respective chambers for the social interaction session; behavior was divided into two main categories: Interacting Dyads and Surrogate Dyads (**Figure 25**).

For the Interacting Dyads, a further subdivision was performed. The first category was the Gap Interacting (**Figure 25**). By scrolling the video frame by frame, the event in which both subjects (right and left) were simultaneously in the gap was selected. The start of the event was identified as the first frame in which the animal entered the corresponding ROI (right or left) while the end was determined as the first frame in which the animal exited the gap with its nose and began to change head orientation.

The Gap Non-Interacting condition was also included within the Interacting Dyads. In this type of behavior, the moment was selected when only one of the two subjects went to the gap but the companion did not interact (**Figure 25**).

Finally, for the Surrogate Dyads, we used the two single sessions (in which we find the animal in one chamber but the other compartment remains empty) to create a control behavior called "Gap Solitary" (**Figure 25**). This condition was achieved by artificially combining the habituation sessions and identifying when one of the two animals went to the gap.

Once all the videos of the behavior had been observed, thanks to the BORIS software a ".csv" file was downloaded to obtain a data frame showing all the segmentation data such as the beginning and the end of the three behavioral events divided by subject and by session.

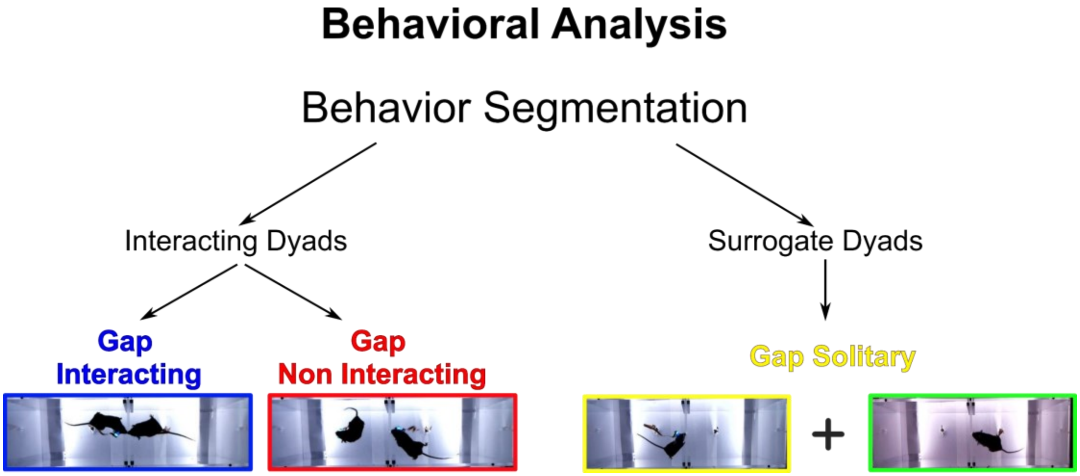

Figure 25: Behavioral Segmentation.

Schematic representation of behavior segmentation. The first macro classification is to divide Interacting Dyads (recordings with both subjects) from Surrogate Dyads (recordings of individual subjects). Two behaviors were classified for the Interacting Dyad: Gap Interacting when both subjects go to the gap to perform a nose poke and Gap Non-Interacting in which only one of the two subjects goes to the gap to perform the nose poke In the Surrogate Dyad, recordings with individual subjects were segmented by going to isolate the time when the individual subject explored the gap with the nose. These recordings were artificially combined to generate a control behavior and simulate the Interacting Dyads.

5. Social Interaction: Wavelet Coherence Transform Analysis

Using the Miniscope, it was possible to record cortical calcium profile, expressed as fluorescence variation ($\Delta F/F_0$), from both hemispheres of both interacting subjects in freely moving conditions. The extracted calcium signal was used to measure inter-brain coupling in all the behavioral conditions described previously (Gap Interacting, Gap Non-Interacting, and Gap Surrogate).

To study and measure the coupling of the two signals, Wavelet Coherence Transform analysis was used since this technique allows measuring the level of synchrony between two-time series as a function of time and frequency. As described previously, the use of this method is related to the power this analysis technique shows. WCT can discover locally blocked-in phase events that may not be detectable with the analysis of time series such as the Fourier Transform, and also by not being required to choose a fixed window in time, solves the problem of non-stationarity of biomedical signals.

Given the freedom of choice offered by this analysis tool in choosing the mother function wavelet, Morlet's wavelet was used in this study because it offers a proper balance between temporal localization and frequency. Morlet’s wavelet is multiplied by the signal (the calcium profile) and integrated at each instant. During the sliding of the mother wavelet over the time series, when the two functions have a more similar profile, their product will be greater, while at points where this does not occur their product will be zero. WCT expresses the relationship between the mother wavelet, at a different level of compression and dilation (varying the scaling factor), and the time series. Once the WCT is performed, we obtain a spectrum like those shown in the (**Figure 26A and B_right**) in which the x-axis shows the time of the entire recording (310 seconds) and the y-axis shows the various frequencies of the calcium profile related to the cortical activity.

Given the type and kinetics of the GCaMP6f indicator, a sampling frequency of 25 Hz was chosen to properly monitor calcium transients. With this sampling, the maximum frequency resolution that can be analyzed by WCT is half which is 12.5 Hz. The level of synchrony between the signals is expressed on a colorimetric scale by the coherence, which takes values between 0 and 1, where 1 indicates perfect synchrony between the two signals while 0 indicates the absence of coherence (**Figure 26**).

This analysis was performed for all acquisitions, either when the subjects were alone or during the interaction session. Thanks to the behavior segmentation performed with BORIS and the Data Frame obtained, the time windows in which the Gap Interacting, Gap Non-Interacting, and Gap Solitary events occurred were cut out from the entire spectrum.

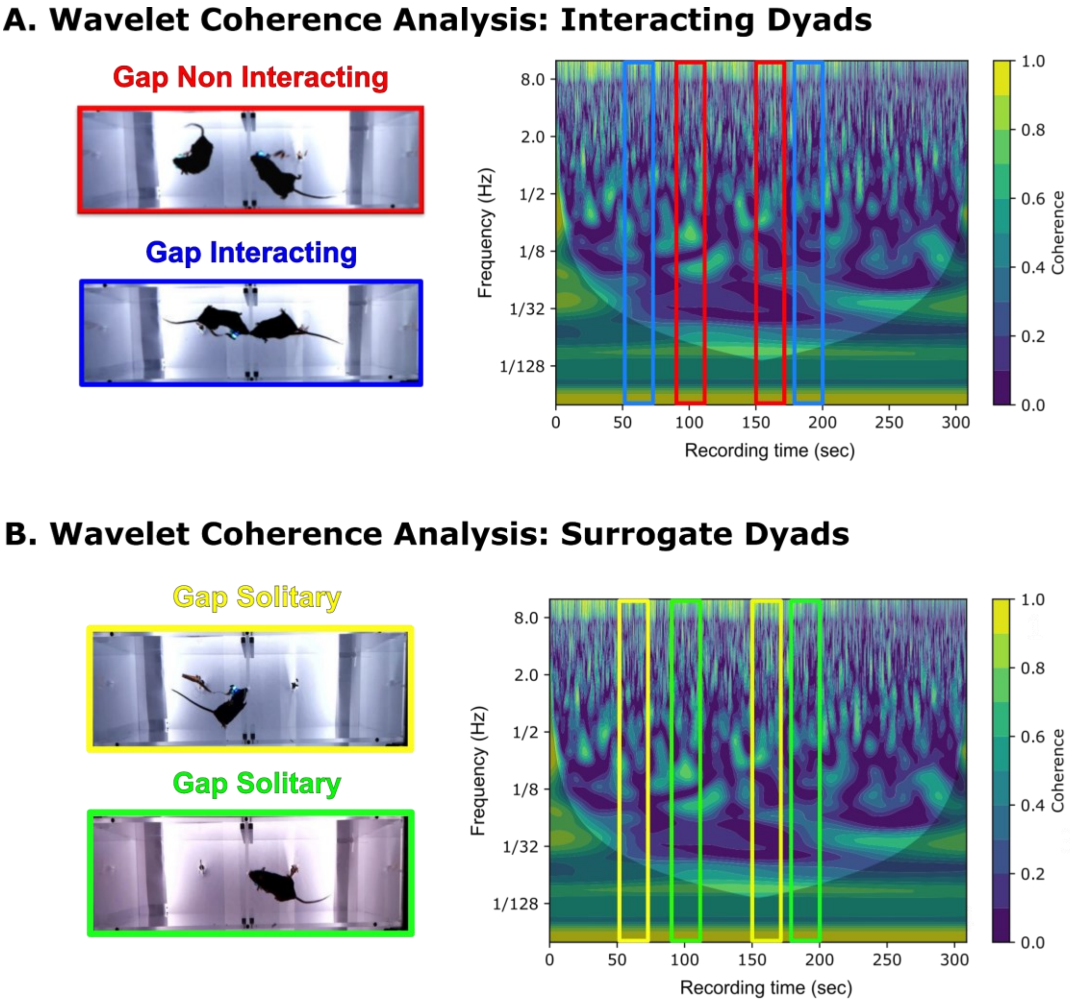

Figure 26: Wavelet Coherence Analysis: Interacting vs Surrogate Dyads.

Representation of Interacting Dyads **(A)** and Surrogate Dyads **(B)**. Left representation of the behavioral events: Gap Interacting and Gap Non-Interacting in **(A)** and Gap Solitary **(B)**.On the right spectra of the Wavelet Transform Coherence in which on the x-axis is shown the time duration of the recording session (310 seconds) while on the y-axis is the oscillation frequency of the two signals. On the colorimetric scale, the level of coherence expressed from 0 (no coherence) to 1 (perfectly coherent) is shown. The time phases in which the related events took place are indicated with red, blue, yellow, and green rectangles.

5.1. Coherence Spectrum Distributed over the Entire Cortex

From the segmentation described in paragraph 4.2, chapter III, the coherence profiles in the different frequencies were extrapolated. In the first analysis, the coherence spectrum distributed over the entire cortex was compared (**Figure 27**). In the graphs shown in Figure 27, the x-axis shows the various frequencies and the y-axis shows the level of coherence. These parameters were investigated in the Gap Interacting condition by comparing it with the control behavior of the Surrogate Dyad (Gap Solitary) and later in the Gap Non-Interacting versus Gap Solitary condition of the Surrogate Dyad.

The lines in the graphs represent the mean coherence profile while the underline band represents the 95% confidence interval. These profiles were obtained by averaging 11 female dyads. In the graph in the Figure 27A, we can see in the Interacting Dyad (Gap Interacting) an increase in the level of coherence in two frequency bands: the first in the infra-slow frequencies (about 1/16 Hz) with a higher level of coherence (about 0.6) than the second peak in the slow frequencies (about 3-4 Hz) with a coherence level of about 0.3. When looking at the coherence profile in the surrogate dyad, we show no increase in coherence in the various frequency bands. When comparing the Gap Non-Interacting with the Surrogate Dyad (**Figure 27B**), again we observe an increase in the coherence level only in the non-interacting dyad.

Looking at the coherence profile in the Surrogate Dyad, we show no increase in coherence in the various frequency bands. When comparing Gap Non-Interacting to the Surrogate Dyad, again we observe an increase in the level of coherence only in the Non-Interacting Dyad (**Figure 27B**). However, in the

Gap Non-Interacting condition, in which only one of the two subjects goes to the gap, we notice a different behavior than in the Gap Interacting. In this case in the Gap Non-Interacting, an increase in coherence in the infra-slow frequency band is observed while the peak in the slow frequencies disappears. Analyzing the coherence of the Gap Non-Interacting in the infra-slow frequencies we notice a lower level of synchrony (about 0.45) than in the Gap Interacting condition (**Figure 27B**).

Given the results and the presence of two coherence peaks during the Gap Interacting condition, to assess the actual coherence level, the coherence variation (ΔC) defined as the difference in coherence between the Gap Interacting and Gap Surrogate distributed over both hemispheres was calculated $(\Delta C = Gap\ Interacting - Gap\ Surrogate)$ (**Figure 27C**). This analysis confirms the presence of two frequency bands that are relevant and statistically significant, and also suggests that the level of synchrony in infra-slow is higher than in slow frequency (**Figure 27C**).

An increase in coherence in the infra-slow frequencies is congruent with the temporal order of the duration of interactions at the gap, also an increase in the level of synchrony has been observed in studies conducted in humans in cooperative and competitive tasks. The presence of coherence in slow frequencies could be correlated with communication between different brain regions, it could be linked to how the different brain areas are coordinated.

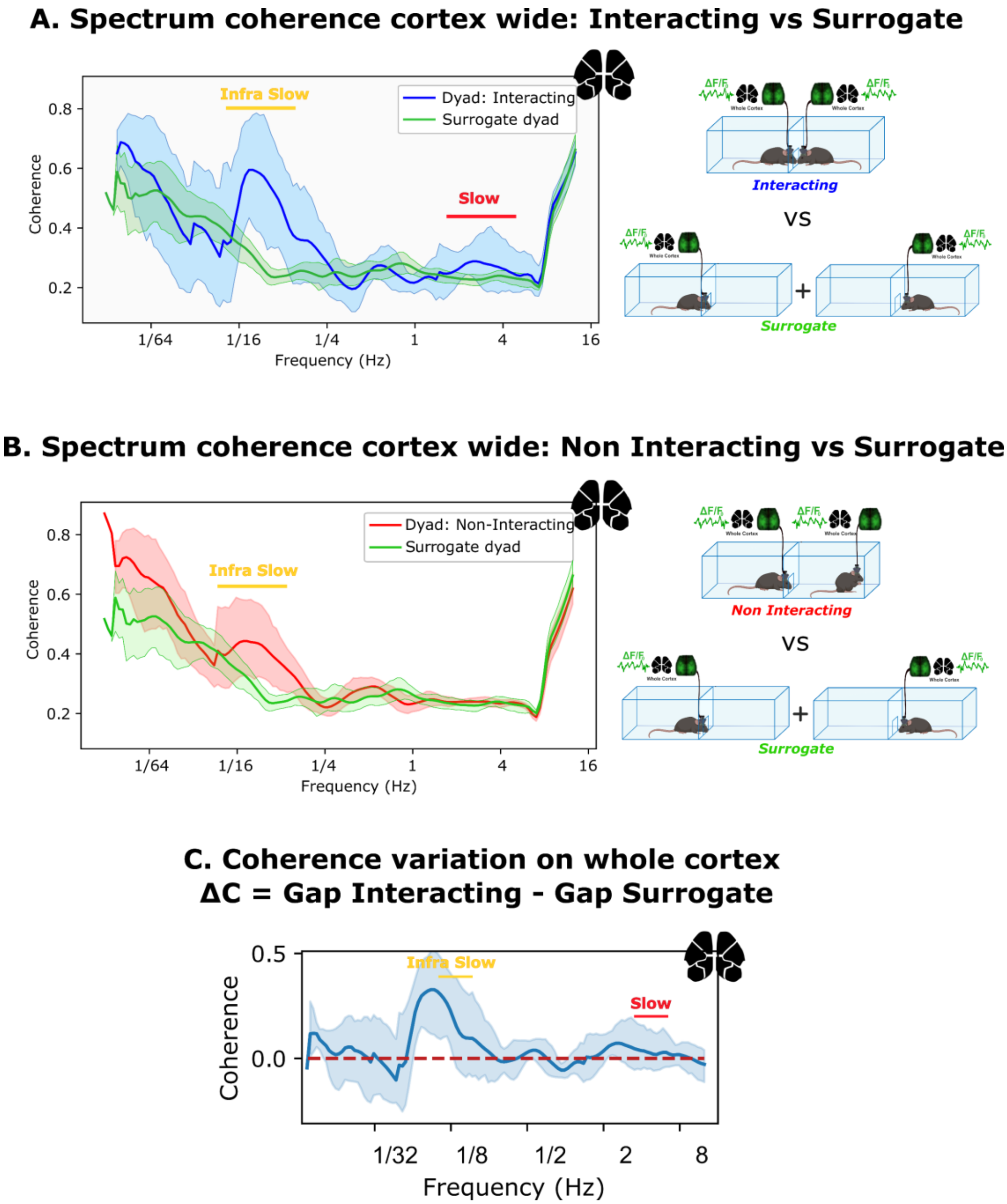

Figure 27: Coherence Spectrum Distributed over the Entire Cortex.

Frequency-dependent coherence spectrum graphs distributed over the entire cortex. **(A)** Comparison between the Interacting Dyad (blue) and the Surrogate Dyad (green) **(B)** between the Non-Interacting Dyad (red) and the Surrogate Dyad (green). **(C)** Graph showing the change in coherence defined as the difference between Gap Interacting and Gap Surrogate as a function of frequency.

5.2. Coherence Spectrum Parceled for Cortex Brain Region

Given the results obtained from the analysis of distributed coherence variation over the entire cortex, in this project, we decided to investigate this phenomenon in detail to try to understand whether this event could also occur in more circumscribed cortical areas. The same WCT analysis was performed by considering parcellated cortical areas. From the parcellation mask of the Allen Brain Atlas (according to the Allen Institute Mouse Brain Atlas), we decided to segment the entire cortex into 4 macro areas that enclose within their areas regions that are homologous or have similar functions.

From this parcellation, the following 4 areas were obtained: a motor, somatosensory, associative, and visual area for the left and right hemispheres. Again, the change in coherence between Gap Interacting and Gap Surrogate was calculated for the different parceled areas (**Figure 28**). In Figure 28A, we can see the 8 graphs showing on the x-axis the frequency in Hz and on the y-axis the coherence variation (ΔC) for the 4 cortical areas of the left and right hemispheres. What emerges from this analysis is that the increase in coherence in infra-slow frequency persists in all cortical areas. What is interesting is that the trend of coherence in the slow frequency band does not remain constant in all brain areas. From these graphs, we can see an increase in the level of coherence only in the visual area of the left and right hemispheres and in the somatosensory region only in the right hemisphere (**Figure 28A**).

Given the relevance of certain cortical areas, a map expressing the level of coherence (on a colorimetric scale) in the different cortical regions in the two bands Infra slow and slow frequency for the two behavioral conditions Gap

Interacting and Gap Surrogate was made to try to quantify this behavior (**Figure 28B**).

Regarding the infra-slow frequency band, we can observe that the level of coherence is higher during the interaction compared to the surrogate dyad, moreover, during Gap Interacting we can also observe a topographic distribution of cortical areas. In Figure 28B, cortical areas where significant inter-brain synchronization emerged between dyad members were connected with black lines. In the infra-slow band, inter-brain synchronization of all cortical areas of both brains is observed during the interaction at the gap while in the slow frequency band, this inter-brain synchronization emerges only in the visual areas of the left and right hemispheres, in the somatosensory areas of the left and right hemispheres, and the associative area only in the right hemisphere (**Figure 28B**). This confirms that only during social interaction at the gap is coupling and synchronization of the two brains observed.

Figure 28: Coherence Spectra Segmented by Brain Region and Coherence Map.

(**A**) Spectra of coherence variation plotted for the macro cortical area as a function of frequency. Starting from the top we find the coherence of the left and right hemispheres of the motor, somatosensory, associative, and visual areas.
(**B**) Coherence map of the different cortical areas in the two behavioral conditions: Gap Interacting vs Gap Surrogate in the Infra-slow and Slow frequency bands. Black lines represent cortical areas where inter-brain coupling emerged.

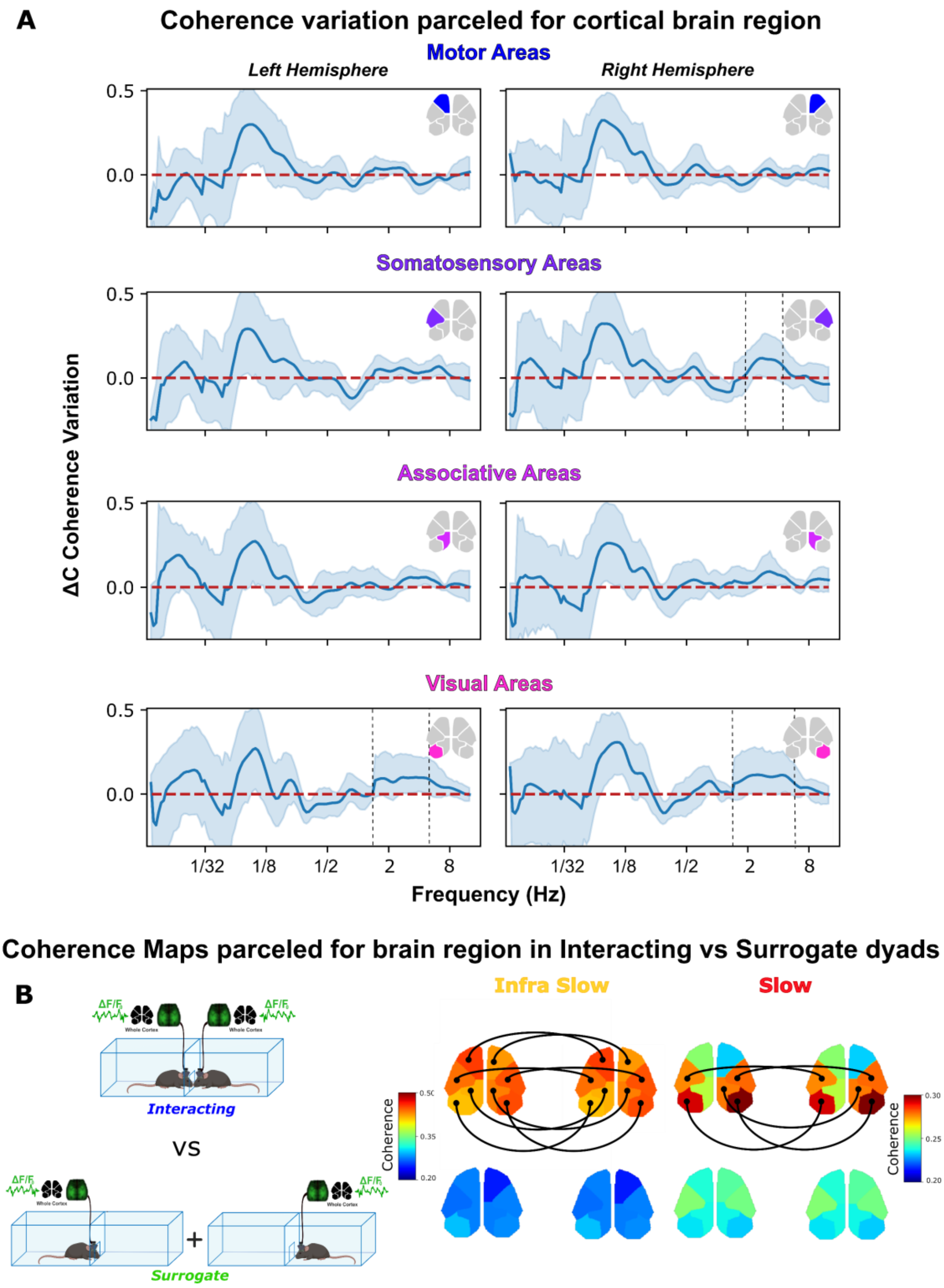
A
Coherence variation parceled for cortical brain region
Motor Areas
Left Hemisphere
Right Hemisphere
Somatosensory Areas
Associative Areas
Visual Areas
ΔC Coherence Variation
0.5
0.0
1/32
1/8
1/2
2
8
Frequency (Hz)
Coherence Maps parceled for brain region in Interacting vs Surrogate dyads
B
ΔF/F
Whole Cortex
Interacting
VS
+
Surrogate
Infra Slow
Slow
Coherence
0.50
0.35
0.20
0.30
0.25
0.20

IV. Discussion

In this project, a miniaturized optical system "Miniscope" was developed to conduct widefield calcium imaging in freely moving rodents. This system was applied to perform a Hyperscanning study and investigate cortical dynamics that coordinate social interactions in mice.

Working on CAD design, it was possible to develop and print a working, compact, and durable 3D device that was compatible with the experimental requirements for performing recordings in freely moving mice. Several versions were made so that the body of the Miniscope with its components would be wearable by animals. As reported in the literature, the miniaturized systems developed in recent years are single-photon GRIN lens-based devices that require implantation of the latter in the brain site to be investigated exhibiting a field of view limited to a few μm^2 or mm^2 (Aharoni and Hoogland 2019; Barbera et al. 2016; Jacob et al. 2018; Liberti et al. 2017). Because the biological question posed involves wide-field calcium imaging distributed over both hemispheres, none of the previously developed systems were compatible with our study. Only recently has a miniaturized microscope with similar features and performance to our needs been developed (Rynes et al. 2021).

The Miniscope developed in our laboratory has adequate mechanical and optical characteristics to answer the experimental question. Thanks to the FOV of about 10.5 mm (corresponding to 512 x 512 pixels) and an optical resolution of less than 20 µm, it was possible to perform wide-field recordings at the mesoscale level with the possibility of monitoring neuronal activity, expressed as fluorescence variation, distributed over the whole cortex. The dual illumination system provided by the two blue LEDs placed at 180° allowed for a symmetrical and homogeneous illumination profile along the field of view with a maximum illumination level in the center between 2 and 8 mm decreasing slightly along the edges. The elaboration of the CAD design and the fabrication of the device with the 3D printer made it possible to decrease the weight of the microscope structure, realizing a sufficiently light device (2.80 grams), lower than systems used in other laboratories with a significantly smaller FOV (Cai et al. 2016; Jacob et al. 2018) and therefore wearable on the head of the mice.

By producing the different components in our laboratory, it was possible to reduce the production time and make continuous improvements that have produced the current design. The 3D development of a very light implant ring with an integrated aluminum head-post made it possible to manipulate the animals easily and to anchor the Miniscope simply in a few seconds without the need to anesthetize the animal or perform craniotomies for the insertion of GRIN lens (Aharoni and Hoogland 2019; Barbera et al. 2016; Cai et al. 2016).

In addition to optical characterization, performing visual stimulation experiments provided more data on the functionality of the system. Since the conventional widefield microscope is the gold standard for performing mesoscale imaging with a wide field of view, the recording of cortical activity distributed over both hemispheres following visual stimulation with this microscope was used as a benchmark to define the performance of the Miniscope. The study found that both systems recorded an evoked response in the contralateral hemisphere reaching maximal activation in comparable times (240 ms vs 200 ms after onset for Widefield vs Miniscope). Although the conventional Widefield microscope recorded a slightly higher mean fluorescence change than the Miniscope, probably conditioned by the different sensor performance and resolution of the two systems, the presence of a clear and readable response in the calcium profiles of the individual trials is an indication of the good quality and performance of the Miniscope in recording the fluorescence change evoked by the stimulus.

After developing a working optical system capable of recording cortical activity on both hemispheres with features comparable to conventional systems, the Miniscope was used to investigate neuronal dynamics related to social interactions in mice. To study social interactions in rodents, after a thorough review of the existing literature on the most used paradigms and conditions to pay attention to when conducting social tests, a revamped custom-made setup was developed. Knowing that the environment in which the behavioral experiments take place must be extremely controlled in terms of lighting, olfactory and sound stimuli, we developed a transparent plexiglass rectangular arena with a central barrier equipped with a slot which allowed the subjects, present in the two compartments, to interact with their nose. The structure, open at the top, made it possible to maintain the continuity of the olfactory stimuli between the two subjects. To prevent external auditory stimuli from frightening or altering the execution of the experiments, as well as the execution of the tests in complete silence, the experimental setup was closed by white hardboard panels (which contributed to the formation of a white background during the recordings used to perform automatic tracking) externally wrapped in soundproofing panels to isolate the environment. A LED strip of white light with adjustable intensity applied along the four edges of the structure ensured homogeneous lighting of the behavioral chamber.

From the results obtained from the optical characterization, we knew that the device had a compact structure and a total weight of fewer than 3 grams, however, to determine the impact of the Miniscope on the behavior of rodents, recordings were performed in which two experimental groups of animals were left free to explore the environment: a group bearing the microscope "*Miniscope* group" compared with the group having only the implant ring "*Control* group".

The results show that in general, the animals of both experimental groups tend to spend a statistically significant time in the central part of the arena near the slot, compared to the opposite area, probably this result could be explained by the structural asymmetry of the behavioral chamber and the presence of the gap in the central barrier. In the analysis of the distance covered by the two groups, it emerged that generally, the subjects with the Miniscope cover a greater distance than the control, however, this difference is not statistically significant. These results show that the head-mounted Miniscope does not hinder the normal behavior of the animals. The design and weight of the device allow the animals to freely explore all spaces of the arena (including the corners of the chamber), allowing the animals to exhibit a broad behavioral repertoire.

Considering that the visual stimulation recordings for performing the system characterization were conducted in head-fixed conditions, to validate the stability and functionality of the Miniscope in freely moving, the image sequences acquired during the exploration of the environment described in paragraph 5, chapter II, were analyzed. The collected images confirm the ability of the system to perform wide-field acquisitions stably without the introduction of motion artifacts to visualize a large part of both cortical hemispheres. Image alignment and application of the Allen Brain Atlas parcellation mask segmented the two cortical hemispheres into the various cortical subregions. The extrapolation of calcium activity profiles, expressed as fluorescence variation (% $\Delta F/F_0$), in different cortical regions distributed along the FOV under two conditions such as locomotion or rest state, confirm that the Miniscope is capable of recording cortical activity stably and with sufficient signal-to-noise ratio during different behavioral states and in different cortical areas.

Given that a commercial or previously tested behavioral paradigm was not used to study social interactions in this project, a validation of the paradigm was performed by quantifying the interaction events at the gap (nose poke) in both the "Alone" and "Interaction" experimental sessions. Quantification was performed with an ROI-based analysis using a custom-made algorithm to quantify the duration and number of nose-poke events at the gap. The algorithm revealed that more nose pokes are present during the “Interaction” condition than during the "Alone" condition, however, this difference is not statistically significant. Analyzing the duration of the nose poke, the data show that when both subjects are inside the arena, they spend more time at the gap interacting with their partner than in the “Alone” condition.

It follows that although the number of nose poke events is similar in both conditions (Alone and Interaction), probably dictated by the animal's curiosity in exploring the gap, the time spent at the gap has statistically significant differences and is strongly influenced by the presence of a second subject on the other side of the arena. In addition to these results, analyzing the first interaction event and comparing it with the subsequent ones showed that the duration of the first interaction is significantly longer than the subsequent one. Since the tests performed predicted the formation of dyads in which a novel subject was presented at each interaction session, the findings imply that under these circumstances, mice spend more time at the gap when they first interact.

After developing and characterizing the Miniscope, generating a behavioral paradigm to study social interactions, these were used to perform a Hyperscanning study in mice and investigate the neuronal dynamics underlying social interactions. Miniscope recordings monitored the cortical activity (expressed as fluorescence variation) in Thy1-GCaMP6f transgenic mice, in which a subpopulation of excitatory cortical neurons express the calcium indicator GCaMP6f. Calcium profiles extrapolated from the acquired images were used to measure the level of inter-brain synchrony between the two interacting subjects. To quantify the level of coupling, WCT analysis was used as a survey technique to measure the level of coherence between the time series of the two interacting subjects as it allowed for measurement as a function of time and frequency. By manually segmenting the behavior, a classification was performed identifying three types of behavior at the gap in the various experimental sessions: Gap Interacting, Gap Non-Interacting, and Gap Surrogate. By performing WCT on the calcium data, coherence spectra distributed over the entire cortex were extrapolated. From the coherence spectra, there was an increase in coherence in two frequency bands, the first in the infra-slow frequencies around 1/16 Hz and the second in the slow frequencies around 4 Hz when both subjects interact at the gap (Gap Interacting). This phenomenon was not detected in the Surrogate Dyads (Gap Surrogate). Examining the behavioral condition in which only one of the two subjects in the dyad goes to the gap (Gap Non-Interacting) and comparing it with the Surrogate Dyad, an increase in coherence was found only in the infra-slow frequencies in the Gap Non-Interacting condition. Similar to the previous case, the same phenomenon was not observed in the Surrogate Dyad. However, if we compare the level of synchrony of the two peaks in the infra-slow frequencies between the Interacting Dyad and the Non-Interacting Dyad, the coherence detected in the Non-Interacting Dyad presents a lower value than that observed in the Gap Interacting; while the coherence peak in the slow frequencies at 4 Hz disappears in the non-interacting dyad. Only when both subjects interact at the gap does an increase in coherence in two frequency bands emerge. The results suggest that inter-brain coupling is modulated by the type of behavior at the gap by highlighting that maximum coherence is achievable only by the physical participation of both subjects at the gap. In the Gap Non-Interacting, although the coherence peak at 4 Hz disappears, lower synchrony is detected in the infra-slow frequency. This could be explained by the fact that, although there is no physical interaction of both subjects, the presence of the partner on the other side of the barrier is a sufficient condition to determine an inter-brain coupling but with a lower level than the Gap Interacting condition.

The coherence peak in slow frequencies at 4 Hz seems to be characteristic only of the behavioral condition of the Interacting Dyad in which both subjects go to the gap. Hyperscanning studies in humans, conducted with various scanning techniques carried out in the last decade, report an increase in the level of inter-brain synchrony in different cortical regions during the execution of social tasks (Astolfi et al. 2011, 2012; Babiloni and Astolfi 2014; Barraza et al. 2020; Cui et al. 2012; Dommer et al. 2012; Funane et al. 2011; Jiang et al. 2012; Liu and Pelowski 2014; Montague et al. 2002). A brain-to-brain coupling to different frequency bands modulated by behavior had been highlighted in a human study using the EGG in which the presence of synchrony between two individuals in the Theta band was highlighted (3-7 Hz) during cooperative and competitive tasks with stronger coupling during competitive interactions, while a brain-to-brain increase in the Gamma frequency band (38-42 Hz) was observed as a hallmark only in cooperative interactions (Barraza et al. 2020).

Inter-brain synchronization during social interactions has been reported in the Dumas study, using dual-EEG setups in which synchronization was detected in the alpha-mu band between the right centroparietal regions, suggesting that these brain areas play a crucial role in social behavior (Dumas et al. 2010).

Using the fNIRS technique to measure the simultaneous activity of two subjects during the execution of a computer-based game, the inter-brain coherence in the right superior frontal cortex emerged between the signals of the two participants only during a cooperative task but not during the competition (Cui et al. 2012).

Considering the Hyperscanning experiments conducted on humans cited in the literature and the results obtained in our study from the wavelet analysis, the presence of an inter-brain coupling at different frequency bands could be explained by the fact that the synchrony between two brains is modulated in frequency according to the type of social task at the gap.

It is clear from these works that most social neurosciences based on Hyperscanning have focused on human studies observing small numbers of subjects due to the difficulties of synchronizing multiple systems and the physical footprint of the instrumentation. The execution of social paradigms using these scanning techniques sometimes requires subjects to remain still, complicating the development of articulate tasks similar to real-life conditions. Until recent years, studies of social interaction conducted in animals have relied primarily on observation of behavior without receiving information about what neural correlates coordinate these events.

Recently, with the advent of miniaturized optical systems, it is becoming possible to monitor neuronal activity in freely-moving conditions, but in the social context, there is little work in which behavior and brain dynamics are simultaneously investigated or at least focused on the analysis of the individual animal.

Although interbrain synchrony correlated with the type of social interaction has been reported in humans, it is not clear whether this interbrain coupling is a phenomenon unique to primates or whether it is present in other animal species including rodents. There is only one work conducted by Kingsbury and colleagues in which by performing microendoscopic calcium imaging they record the activity of a few thousand neurons (through implantation of a GRIN lens) in the dorsomedial prefrontal cortex (dmPFC) in pairs of mice engaged in social interactions in an open field arena. What emerged is a correlation between the neurons of the prefrontal cortex in the two brains dependent on social interaction. The brains of the dyad have neurons in the dmPFC that separately code their behavior and that of the other member of the couple. The correlation of neurons between the two brains predicts the formation of future social interactions and how dominance relationships will form during a competitive task (Kingsbury et al. 2019; Kingsbury and Hong 2020).

Prefrontal cortex neurons are known to be involved in the modulation of behavior during social interactions (Ko 2017; S. A. Lee et al. 2016; Liu et al. 2022; Miura et al. 2020) along with the involvement of subcortical circuits such as the amygdala, hippocampus, hypothalamus, olfactory system, etc. Because these areas have important cortical connections, what is not yet known is what the role or involvement of the entire cortical mantle is in social interactions or whether inter-brain pairings exist when two or more mice are involved in a social task.

In this Hyperscanning study, by developing a Miniscope with a wide field of view, it was possible to monitor neuronal activity in both hemispheres by highlighting inter-brain coupling in two frequency bands: infra-slow and slow as a function of the type of behavior at the gap. Given the results obtained on inter-brain synchrony distributed throughout the cortex, analysis of the synchrony of more circumscribed regions could provide a clearer view of the contribution of individual cortical areas in social interactions. This led to analyze the coherence variation in four macro areas: motor, somatosensory, associative, and visual cortex of the left and right hemispheres during the Gap Interacting condition. The analysis confirmed the presence of inter-brain coupling in the infra-slow frequencies in all cortical areas, while synchrony in the 4 Hz (slow) frequency band was detected in the visual area of both hemispheres and the somatosensory area of the right hemisphere.

Subsequently, it was decided to compare the effective synchronicity of the interacting dyad with the surrogate dyad and represent the level of coherence on a colorimetric scale parceled by cortical area in the two frequency bands.

The results revealed that inter-brain coupling is present only in the Interacting Dyad and that the level of coherence is modulated by the frequency band in different cortical areas. While in the infra-slow frequencies coupling between the signals of the two brains is observed in all cortical areas, in the 4 Hz slow frequency band, coupling emerged in the visual and somatosensory areas of the right and left hemispheres and in the associative area of the right hemisphere. In the motor areas of both hemispheres and the left-associative area, the coupling of the two signals was not detected. These data suggest a different coupling as a function of frequency in the various cortical areas, moreover, in slow oscillations, an asymmetrical involvement of the association areas emerges. A functional asymmetry of neuronal activity between the two hemispheres was reported in a study conducted on mPFC in which left-hemisphere neurons were observed to modulate the effects of stress on social behavior (Lee et al. 2015). To date, no studies have been reported that show an asymmetry in inter-brain coupling modulated in frequency and type of behavior during social interactions.

The involvement of other cortical areas during social behavior could be connected with the activation and processing of information by the mPFC, but to understand it, it will be necessary to study simultaneously the neuronal activity of this specific area with the rest of the cortical mantle.

In conclusion, we believe that the development of a new miniaturized Widefield optical system equipped with: a single photon illumination system, compact size, and weight, has allowed us to move away from the conventional method of imaging under head-fixed conditions, allowing us to develop various behavioral paradigms under conditions similar to the real-life context. The substantial advantage of this system lies in having a sufficiently large field of view to monitor both hemispheres without having to resort to the application of cranial implants or perform a craniotomy for the insertion of a GRIN lens in specific brain areas, thus altering the cerebral cytoarchitecture incurring in inflammatory processes that require long recovery times.

The results obtained on the characterization demonstrate the functionality of the system in performing calcium imaging and detecting the signal in response to stimuli with good accuracy and sensitivity, moreover, behavioral tests confirmed that the developed experimental paradigm allows the study of the dynamics of social interaction with a novel subject and demonstrates the portability of the device on the rodent's head without affecting the normal behavioral repertoire.

Through the combination of the Miniscope and the behavioral paradigm, it was possible to conduct a novel Hyperscanning study where the level of inter-brain synchrony between calcium activity profiles in mice was assessed. This uncovered the presence of coherence coupling modulated by both the type of behavior at the gap and the frequency band.

This platform provides an experimental framework for studying social interactions in an animal model that replicates findings made in human studies. Given the Hyperscanning studies conducted in humans, we believe that these results demonstrate that inter-brain synchrony is not a phenomenon exclusive to primates and provide a pioneering basis for conducting further studies on the neural mechanisms that orchestrate the neuroscience of rodent social interactions.

Unlike Hyperscanning studies in humans, rodents allow a greater variety of investigative techniques to be performed. The developed behavioral paradigm could be used to investigate more thoroughly the origin of the phenomenon of synchrony between the two brains. In the future, it might be interesting to perform interference studies by providing stimulation sets at different frequencies or by going to inhibit the activity of the neural circuits involved during the behavioral event of nose poke interaction. This would provide insight into whether the social interaction event is responsible for inter-brain coupling.

V. Future Perspective

1. Hemodynamic Contribution: Measurement of Reflectance

As reported in the literature, miniaturized head-mounted optical systems for conducting free-moving imaging in mice developed in the last decade, have manifested considerable impact in the field of neuroscience and conspicuous use for studying behavior in more ethological contexts by simulating real-life conditions.

Except for the microscope recently developed by Rynes and colleagues (Rynes et al. 2021), most of the optical calcium imaging devices reported in the literature are compact-sized microscopes that allow neuronal imaging of a few hundred to a few thousand neurons distributed over fields of view limited to a few mm^2 that require implantation of a GRIN lens at the site to be explored and a craniotomy for optical access, severely limiting the brain surface to be investigated. These systems developed to monitor neuronal activity generally use indicators that detect the variation of calcium transients expressed as fluorescence fluctuations.

During recordings, the fluorescence emitted by the calcium indicator "GCaMP" related to the activity of excitatory neurons, carries with it an intrinsic signal from the bloodstream, particularly hemoglobin, which causes an increase in the recorded fluorescence. Increased blood flow is consistent with increased neuronal activation since this system is deputed to transport/exchange oxygen, carbon dioxide, nutrients, and waste substances that must be continuously exchanged for cell survival. It follows that the global fluorescence signal recorded by the camera sensor is derived from both neuronal activity and hemodynamics. It is important to take into account the existence of the optical cross-talk between the recorded fluorescence and the dynamic changes in blood flow absorption caused by hemoglobin to avoid incorrect interpretation of fluorescence data (Ma et al. 2016).

Traditional wide-field microscopes, and especially miniature microscopes, do not take this optical cross-talk into account. In reflectance, the light detected by the chamber sensor is diffusely reflected light. This type of light once it hits the sample (the brain surface), enters and diffuses into the layers below, and emerges on the surface to achieve the sensor. Illumination with wavelengths shorter than 600 nm can highlight the superficial vasculature of the brain with good contrast. If cortical activity changes (e.g. as a result of a stimulus); the intensity of diffusely reflected light will be different.

The change in intensity can be used to map functional regions at the cortical level. In particular, changes in reflectance signal intensity are related to the absorption of light by hemoglobin. Like most biological molecules, hemoglobin has an absorption spectrum in the visible and near-infrared, dependent on the level of oxygenation. This can also be observed colorimetrically, generally, arterial blood (rich in oxygen) is deep red compared to venous blood (more loaded with carbon dioxide) tending to darker brown. Using appropriate wavelengths to measure changes in diffuse reflectance, it is possible to show the contribution, in terms of concentration, of the oxy-, deoxyhemoglobin form and the total hemoglobin (given by the sum of both) that would provide the overall change in local blood volume.

The graph in Figure 29 shows the absorption values, expressed as the extinction coefficient, of the two forms of hemoglobin at different wavelengths. When we excite the GCaMP indicator fluorophore, an illumination source of about 480 nm is used. At this wavelength, looking at the absorption spectrum (**Figure 29**), we notice a higher absorption by oxygenated hemoglobin (red profile) than by deoxyhemoglobin (dashed blue profile), which means that by using blue light, in addition to the fluorescence emission from the GCaMP indicator, we will have a hemodynamic contribution from oxyhemoglobin. By changing the type of illumination and moving into the red spectrum at 635 nm (**Figure 29**), we can see that the dynamics are reversed. In this case, we will have more absorption of deoxyhemoglobin (dashed blue profile) than the oxygenated form (red profile). However, there is a wavelength, between these two bands, around 530 nm that plays a key role here. The 530 nm wavelength (**Figure 29**) corresponds to an isosbestic point of the two hemoglobin absorption spectra. This means that at 530 nm both, HbO and HbR, exhibit the same absorption values measuring the reflectance signal independent of the oxygen concentration of hemoglobin but will be sensitive only to the change in the total concentration of the two forms (HbT) (Ma et al. 2016).

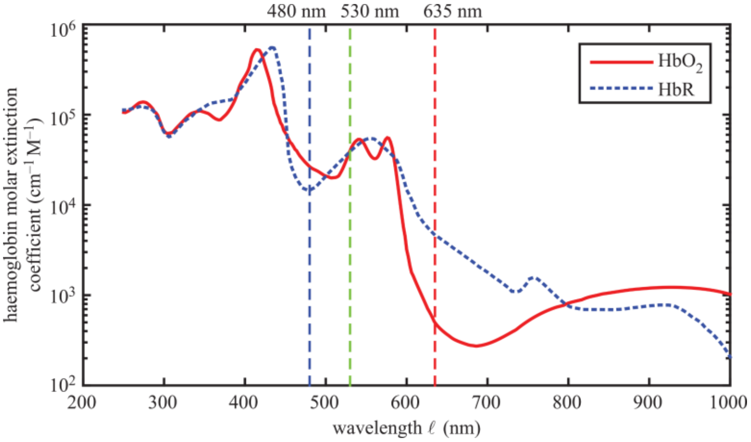

Figure 29: Oxy- and Deoxy-Hemoglobin Absorption Spectrum.

The absorption spectrum of oxygenated hemoglobin [HbO_2] (red) and deoxyhemoglobin [HbR] (blue) at different wavelengths. At 480 nm, greater absorption of oxygenated hemoglobin is observed, while at 635 nm the greatest absorption is of the reduced form of hemoglobin. In the center at 530 nm, the isosbestic point of hemoglobin is observed where the two forms HbO_2 and HbR have the same absorption value making the measurement independent of the oxygenation state. Image modified from **(Ma et al. 2016)**.

Given these conditions, implementing in benchtop and miniaturized widefield epifluorescence microscopes, an additional 530 nm LED providing illumination of the dorsal surface of the brain alternating with the blue LED (stroboscopic illumination), would allow for reflectance measurements independent of changes in oxygenation, determining the hemodynamic contribution and obtaining a fluorescence value dependent only on neuronal activity related to calcium changes.

2. The New Generation of Miniscopes

In recent years only two miniaturized systems have been developed which have integrated a second illumination source, centered in the green wavelength, to record the reflectance signal. The first miniaturized microscope capable of recording intrinsic signals in addition to fluorescence was developed in 2018 to investigate neuronal dynamics in rats with a device weighing 33 grams, a field of view of 7.8 mm in diameter, and a ring with a system of collar LEDs system to provide homogeneous illumination in the green spectrum at 530 nm (Scott et al. 2018). The second miniaturized microscope was developed in 2021 by Rynes and colleagues, where in addition to combining three blue LEDs to perform calcium imaging on mice, a fourth green LED was inserted to measure hemodynamic contribution (Rynes et al. 2021).

The requirement to investigate neuronal activity under less restrictive conditions has resulted in a great development of head-mounted miniaturized systems where over time researchers are working to try to reduce the size, weight, and development costs while increasing spatiotemporal resolution with a good signal-to-noise ratio.

Although technological advances have helped develop wiring systems with increasingly thin and flexible power and data cables, the presence of the latter makes it difficult to study complex behaviors or to record neural activity in large groups of animals without the cables affecting or hindering behavioral outcomes. In addition to the need to detect the reflectance signal to assess the hemodynamic contribution a second limitation to be solved is to reduce the impact of the wiring system.

In 2019, NIDA (National Institute on Drug Abuse) developed a wireless miniaturized fluorescence microscope (wireless miniScope) using the previously developed device as the base system, enabling the recording of neuronal activity with cellular resolution (Barbera et al. 2019). The first attempt at a wireless system had been developed by Liberti and colleagues in 2017, developing a microscope for freely-moving imaging with a wireless configuration in zebra finches (Liberti et al. 2017). Although without the footprint of cables, the size and weight of this system made it usable for neuronal imaging only in large birds or bats but not for small animals such as rodents.

The wireless miniScope developed by Barbera enabled the monitoring of neuronal activity in the dorsal striatum in two interacting subjects (Barbera et al. 2019). This system, using the epifluorescence microscope developed in 2016 as a prototype could acquire images with a frequency of 10 Hz and a field of view of 500 x 500 μm (corresponding to 200 x 200 pixels). The miniScope has a total weight of 3.9 grams which must be added to the weight of the battery (2.2 g to 5 g depending on the model chosen and the type of amperage), as a power supply placed inside a backpack mounted on the animal's back. Despite the many advantages of this system, mounting the device on the animal's head requires light anesthesia of the mouse with isoflurane.

2.1. Miniscope v2: Mechanical and Optical Design

Considering the recent progress in the field of miniaturized systems for conducting calcium imaging in free moving, our laboratory starting from the previously developed model, generated a second version of the microscope called "Miniscope v2" which, in addition to recording fluorescence related to calcium activity, has the peculiarity of detecting the reflectance signal from the hemodynamic component.

The new device features a revamped design and optical components. Excluding the optics and sensor, the Miniscope v2 body and small accessory structures were created and designed with Autodesk Fusion 360 for CAD files later printed in our lab with a stereolithographic 3D printer (XFAB 2500HD; DWS System, Vicenza, Italy) using a black photosensitive material for construction (INVICTA DL385; DWS System, Vicenza, Italy). The assembled Miniscope v2 (**Figure 30**) has a size of about 26.3 x 21.2 x 20.2 mm and a weight of 3.6 grams, has a central cylindrical body with a diameter at the base of about 11 mm and three arms: 2 placed 180° to house the 2 blue LEDs at 480 nm (CREE XPEBBL-L1-0000-00301; Cree, Inc., Durham, North Carolina, USA) and a third arm placed 90° between the two blue LEDs to house the green LED at 530 nm (CREE XPEBGR-L1-0000-00F03; Cree, Inc., Durham, North Carolina, USA) (**Figure 30A**). The three LEDs are positioned at an angle of 50° to the sample plane, and each is positioned at 90° to the axis of the arm. The optical component of this microscope consists of an achromatic doublet lens with a diameter of 3 mm and a focal length of 4.5 mm (#47-721, 3 mm Dia. x 4.5 mm FL, MgF_2 Coated, Achromatic Doublet Lens; Edmund Optics, Inc., Barrington, New Jersey, USA) which was housed inside an externally threaded adapter (Lens adaptor built with the 3D printer) (**Figure**

30B) that provides a mechanical coupling to immobilize the lens inside and screw it into the microscope to adjust focus. A CMOS sensor (MT9V022: 1/3-Inch Wide-VGA CMOS Digital Image Sensor; Aptina Digital Clarity, San Jose, California, USA) (**Figure 30D**) with a field of view of 4.51x 2.88 mm, a pixel size of 6.0 μm, and a maximum frame rate of 60 fps was used for image acquisition. Thanks to the technology of this sensor, it was possible to control the switching on and intensity of the two LEDs by setting a stroboscopic illumination of blue alternating with the green LED to image both fluorescence and reflectance. The sensor integrated into a PCB was housed in a protective structure, to which the mechanical coupling containing the lens was screwed. Finally, the whole system was locked with a screw on the top of the Miniscope v2 (**Figure 30**).

Coupled with the two blue LEDs are the corresponding excitation filters (450-490 nm, 4mm DIA, ET 470/40x; Chroma Technology Corp, Bellow Falls, Vermont, USA) to select the wavelength needed to excite the GCaMP indicator. An emission filter (500-550 nm, 7mm DIA, ET 525/50m; Chroma Technology Corp, Bellow Falls, Vermont, USA) is placed before the lens and CMOS sensor to filter the emitted fluorescence (**Figure 30A and B**). A 2.2 Ω ±5%, 0.5 W resistor (2.2 Ω, 0805 (2012M), ±5%, 0.5 W SMD resistor; TE Connectivity, Berwyn, Pennsylvania, USA) and 36-gauge leads connected to the PCB are soldered to the back of each LED. The LEDs are protected by caps made with the 3D printer, equipped with two small holes for the cables to exit. Finally, the slit for inserting the excitation and emission filters is covered by locking clips to prevent the entry of external light. The same implant ring with aluminum head-post (**Figure 30C**) used in the previous version was used to mount the Miniscope v2 on the animal's head.

2.2. Miniscope v2: Optical Characterization

Also for the Miniscope v2, the first step was to perform an optical characterization of its performance. Recordings were made to determine the device's field of view using a ruler. The acquired images were processed with the ImageJ program (https://imagej.net) for calibration and FOV determination (**Figure 30E**). A FOV of approximately 9 x 9 mm was calculated, an adequate field of view to visualize a good portion of both cortical hemispheres. Using the 1951 USAF resolution test target (R3L3S1P, Positive 1951 USAF Test Target, 3" x 3"; Thorlabs Inc., Newton, New Jersey, USA) the optical resolution was estimated (**Figure 30E**), and an average resolution of (34.10 ± 5.85) µm expressed as (mean value ± standard deviation) was found.

The resolution is sufficient for the biological investigation of our experiments and perform mesoscale imaging of cortical activity. By performing a recording on a white surface, the illumination profile of the device was determined, expressed as grey values across the entire FOV, revealing the sensitivity of the CMOS sensor. The data obtained were plotted on a graph in which the x-axis shows the distance along the field of view (in mm) and in the y-axis the gray values. We can see that the illumination profile is homogeneous in the range of 2 to 8 mm presenting a very wide grayscale ranging from 0 to 40000 (**Figure 30E**).

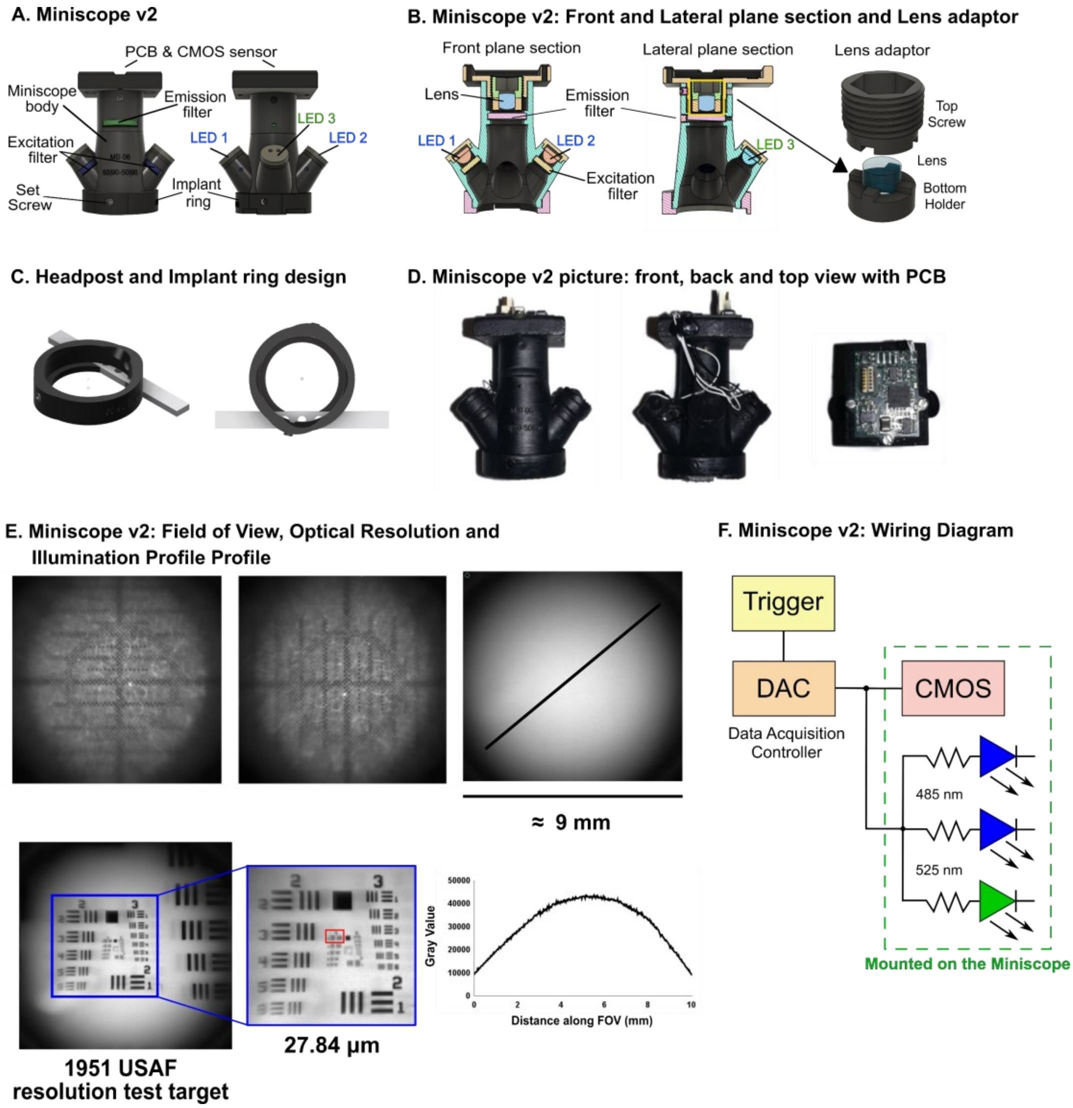

Figure 30: Miniscope v2.

(A) Design of the Miniscope v2 with all optical and mechanical components. **(B)** Front and side section of the Miniscope v2 with the representation of the lens adapter. **(C)**. Implant ring with head-post for mounting the Miniscope v2 on the animal's head. **(D)** Photograph of the Miniscope v2 with front, back, and top views. **(E)** On the top, a representation of FOV was acquired with a Thorlabs ruler and on a white surface. Bottom image of 1951 USAF resolution test target for FOV calculation and illumination profile plot. **(F)** Wiring diagram showing the Data Acquisition Controller (DAC) connected to the CMOS camera and the 3 LEDs (blue and green) for stroboscopic illumination. The green dotted rectangle contains the components mounted on the Miniscope v2.

3. Toward the Wire-free Version

Using the Miniscope v2 as a model, where thanks to the implementation of the green LED and a new CMOS sensor, it is possible to control the LED turn-on and carry out reflectance measurements to ascertain the hemodynamic contribution, the following step we are currently working on is to make it independent of the wiring system and develop the wire-free version. Having to slightly rework the design of the Miniscope v2 to integrate new electronic components and implement an external battery placed on the rodent's back to power the system and make it wire-free, some experiments will be needed to test portability both in terms of physical bulk and heaviness to get confirmation that the new device does not alter the animal's normal behavior. The development of a system that allows strobe imaging to be conducted at two different wavelengths and without wiring components would allow behavioral experiments to be performed in a more ethologically valid context similar to real-world conditions. Studying social interactions with these systems would allow investigation of the neural dynamics underlying social behavior on a larger number of subjects, enabling monitoring of animal behavior under experimental conditions more similar to real life. By testing a larger number of subjects at the same time, we could untether ourselves from the context of dyadic interactions, although ethologically sound, which might be somewhat reductive to the broad concept of social interactions. All this would allow for superior data output while limiting experimental time. We strongly believe that the development of this system could give rise to a variety of experimental paradigms that applied to the study of Hyperscanning on mice could provide a wealth of information in the field of neuroscience.

Bibliography

Acikgoz, Burcu, Bahar Dalkiran, and Ayfer Dayi. 2022. “An Overview of the Currency and Usefulness of Behavioral Tests Used from Past to Present to Assess Anxiety, Social Behavior and Depression in Rats and Mice.” *Behavioural Processes* 200:104670. doi: 10.1016/j.beproc.2022.104670.

Addison, Paul S. 2005. “Wavelet Transforms and the ECG: A Review.” *Physiological Measurement* 26(5):R155-199. doi: 10.1088/0967-3334/26/5/R01.

Adolphs, Ralph. 2010. “What Does the Amygdala Contribute to Social Cognition?” *Annals of the New York Academy of Sciences* 1191(1):42–61. doi: 10.1111/j.1749-6632.2010.05445.x.

Aharoni, Daniel, and Tycho M. Hoogland. 2019. “Circuit Investigations With Open-Source Miniaturized Microscopes: Past, Present and Future.” *Frontiers in Cellular Neuroscience* 13. doi: 10.3389/fncel.2019.00141.

Akerboom, Jasper, Tsai-Wen Chen, Trevor J. Wardill, Lin Tian, Jonathan S. Marvin, Sevinç Mutlu, Nicole Carreras Calderón, Federico Esposti, Bart G. Borghuis, Xiaonan Richard Sun, Andrew Gordus, Michael B. Orger, Ruben Portugues, Florian Engert, John J. Macklin, Alessandro Filosa, Aman Aggarwal, Rex A. Kerr, Ryousuke Takagi, Sebastian Kracun, Eiji Shigetomi, Baljit S. Khakh, Herwig Baier, Leon Lagnado, Samuel S. H. Wang, Cornelia I. Bargmann, Bruce E. Kimmel, Vivek Jayaraman, Karel Svoboda, Douglas S. Kim, Eric R. Schreiter, and Loren L. Looger. 2012. “Optimization of a GCaMP Calcium Indicator for Neural Activity Imaging.” *The Journal of Neuroscience* 32(40):13819–40. doi: 10.1523/JNEUROSCI.2601-12.2012.

Amodio, David M., and Chris D. Frith. 2006. “Meeting of Minds: The Medial Frontal Cortex and Social Cognition.” *Nature Reviews Neuroscience* 7(4):268–77. doi: 10.1038/nrn1884.

Anderson, Steven W., Antoine Bechara, Hanna Damasio, Daniel Tranel, and Antonio R. Damasio. 1999. “Impairment of Social and Moral Behavior Related to Early Damage in Human Prefrontal Cortex.” *Nature Neuroscience* 2(11):6.

Anon. n.d. “Handbook of Optical Filters.” Retrieved December 8, 2022 (https://www.chroma.com/file/handbook-of-optical-filters).

Astolfi, L., J. Toppi, G. Borghini, G. Vecchiato, E. J. He, A. Roy, F. Cincotti, S. Salinari, D. Mattia, B. He, and F. Babiloni. 2012. “Cortical Activity and Functional Hyperconnectivity by Simultaneous EEG Recordings from Interacting Couples of Professional Pilots.” Pp. 4752–55 in *2012 Annual International Conference of the IEEE Engineering in Medicine and Biology Society*. San Diego, CA: IEEE.

Astolfi, Laura, Jlenia Toppi, Fabrizio De Vico Fallani, Giovanni Vecchiato, Febo Cincotti, Christopher Wilke, Han Yuan, Donatella Mattia, Serenella Salinari, Bin He, and Fabio Babiloni. 2011. “Imaging the Social Brain by Simultaneous Hyperscanning during Subject Interaction.” *IEEE Intelligent Systems* 26(5):38–45. doi: 10.1109/MIS.2011.61.

Atsak, Piray, Marie Orre, Petra Bakker, Leonardo Cerliani, Benno Roozendaal, Valeria Gazzola, Marta Moita, and Christian Keysers. 2011. “Experience Modulates Vicarious Freezing in Rats: A Model for Empathy” edited by P. F. Ferrari. *PLoS ONE* 6(7):e21855. doi: 10.1371/journal.pone.0021855.

Baarendse, Petra J. J., Danielle S. Counotte, Patricio O'Donnell, and Louk J. M. J. Vanderschuren. 2013. "Early Social Experience Is Critical for the Development of Cognitive Control and Dopamine Modulation of Prefrontal Cortex Function." *Neuropsychopharmacology* 38(8):1485–94. doi: 10.1038/npp.2013.47.

Baba, Tatsuro. 2012. "Time-Frequency Analysis Using Short Time Fourier Transform." *The Open Acoustics Journal* 5(1):32–38. doi: 10.2174/1874837601205010032.

Babiloni, Fabio, and Laura Astolfi. 2014. "Social Neuroscience and Hyperscanning Techniques: Past, Present and Future." *Neuroscience and Biobehavioral Reviews* 44:76–93. doi: 10.1016/j.neubiorev.2012.07.006.

Babiloni, Fabio, Febo Cincotti, Donatella Mattia, Marco Mattiocco, Fabrizio De Vico Fallani, Andrea Tocci, Luigi Bianchi, Maria Grazia Marciani, and Laura Astolfi. 2006. "Hypermethods for EEG Hyperscanning." Pp. 3666–69 in *2006 International Conference of the IEEE Engineering in Medicine and Biology Society*.

Baillet, Sylvain. 2017. "Magnetoencephalography for Brain Electrophysiology and Imaging." *Nature Neuroscience* 20(3):327–39. doi: 10.1038/nn.4504.

Baker, Phillip M., Sujean E. Oh, Kevan S. Kidder, and Sheri J. Y. Mizumori. 2015. "Ongoing Behavioral State Information Signaled in the Lateral Habenula Guides Choice Flexibility in Freely Moving Rats." *Frontiers in Behavioral Neuroscience* 9.

Barbera, Giovanni, Bo Liang, Lifeng Zhang, Charles R. Gerfen, Eugenio Culurciello, Rong Chen, Yun Li, and Da-Ting Lin. 2016. "Spatially

Compact Neural Clusters in the Dorsal Striatum Encode Locomotion Relevant Information.” *Neuron* 92(1):202–13. doi: 10.1016/j.neuron.2016.08.037.

Barbera, Giovanni, Bo Liang, Lifeng Zhang, Yun Li, and Da-Ting Lin. 2019. “A Wireless MiniScope for Deep Brain Imaging in Freely Moving Mice.” *Journal of Neuroscience Methods* 323:56–60. doi: 10.1016/j.jneumeth.2019.05.008.

Barraza, Paulo, Alejandro Pérez, and Eugenio Rodríguez. 2020. “Brain-to-Brain Coupling in the Gamma-Band as a Marker of Shared Intentionality.” *Frontiers in Human Neuroscience* 14.

Ben-Ami Bartal, Inbal, David A. Rodgers, Maria Sol Bernardez Sarria, Jean Decety, and Peggy Mason. 2014. “Pro-Social Behavior in Rats Is Modulated by Social Experience” edited by R. Fernald. *ELife* 3:e01385. doi: 10.7554/eLife.01385.

Berridge, Michael J., Peter Lipp, and Martin D. Bootman. 2000. “The Versatility and Universality of Calcium Signalling.” *Nature Reviews Molecular Cell Biology* 1(1):11–21. doi: 10.1038/35036035.

Bicks, Lucy K., Hiroyuki Koike, Schahram Akbarian, and Hirofumi Morishita. 2015. “Prefrontal Cortex and Social Cognition in Mouse and Man.” *Frontiers in Psychology* 6. doi: 10.3389/fpsyg.2015.01805.

Bocarsly, Miriam E., Wan-chen Jiang, Chen Wang, Joshua T. Dudman, Na Ji, and Yeka Aponte. 2015. “Minimally Invasive Microendoscopy System for in Vivo Functional Imaging of Deep Nuclei in the Mouse Brain.” *Biomedical Optics Express* 6(11):4546–56. doi: 10.1364/BOE.6.004546.

Bove, Maria, Kevin Ike, Adriaan Eldering, Bauke Buwalda, Sietse F. de Boer, Maria Grazia Morgese, Stefania Schiavone, Vincenzo Cuomo, Luigia Trabace, and Martien J. H. Kas. 2018. “The Visible Burrow System: A Behavioral Paradigm to Assess Sociability and Social Withdrawal in BTBR and C57BL/6J Mice Strains.” *Behavioural Brain Research* 344:9–19. doi: 10.1016/j.bbr.2018.02.003.

Cai, Denise J., Daniel Aharoni, Tristan Shuman, Justin Shobe, Jeremy Biane, Weilin Song, Brandon Wei, Michael Veshkini, Mimi La-Vu, Jerry Lou, Sergio E. Flores, Isaac Kim, Yoshitake Sano, Miou Zhou, Karsten Baumgaertel, Ayal Lavi, Masakazu Kamata, Mark Tuszynski, Mark Mayford, Peyman Golshani, and Alcino J. Silva. 2016. “A Shared Neural Ensemble Links Distinct Contextual Memories Encoded Close in Time.” *Nature* 534(7605):115–18. doi: 10.1038/nature17955.

Canteras, N. S., R. B. Simerly, and L. W. Swanson. 1995. “Organization of Projections from the Medial Nucleus of the Amygdala: A PHAL Study in the Rat.” *The Journal of Comparative Neurology* 360(2):213–45. doi: 10.1002/cne.903600203.

Catarino, Ana, Alexandre Andrade, Owen Churches, Adam P. Wagner, Simon Baron-Cohen, and Howard Ring. 2013. “Task-Related Functional Connectivity in Autism Spectrum Conditions: An EEG Study Using Wavelet Transform Coherence.” *Molecular Autism* 4(1):1. doi: 10.1186/2040-2392-4-1.

Chen, Kunpeng, Zhaoshi Tian, and Lingjie Kong. 2022. “Advances of Optical Miniscopes for in Vivo Imaging of Neural Activity in Freely Moving Animals.” *Frontiers in Neuroscience* 16.

Chen, Shiyuan, Zichen Wang, Dong Zhang, Aiming Wang, Liangyi Chen, Heping Cheng, and Runlong Wu. 2020. "Miniature Fluorescence Microscopy for Imaging Brain Activity in Freely-Behaving Animals." *Neuroscience Bulletin* 36(10):1182–90. doi: 10.1007/s12264-020-00561-z.

Chen, Tsai-Wen, Trevor J. Wardill, Yi Sun, Stefan R. Pulver, Sabine L. Renninger, Amy Baohan, Eric R. Schreiter, Rex A. Kerr, Michael B. Orger, Vivek Jayaraman, Loren L. Looger, Karel Svoboda, and Douglas S. Kim. 2013. "Ultrasensitive Fluorescent Proteins for Imaging Neuronal Activity." *Nature* 499(7458):295–300. doi: 10.1038/nature12354.

Crawley, Jacqueline N. 2004. "Designing Mouse Behavioral Tasks Relevant to Autistic-like Behaviors." *Mental Retardation and Developmental Disabilities Research Reviews* 10(4):248–58. doi: 10.1002/mrdd.20039.

Crawley, Jacqueline N. 2007. "Social Behavior Tests for Mice." 8.

Cui, Xu, Daniel M. Bryant, and Allan L. Reiss. 2012. "NIRS-Based Hyperscanning Reveals Increased Interpersonal Coherence in Superior Frontal Cortex during Cooperation." *NeuroImage* 59(3):2430–37. doi: 10.1016/j.neuroimage.2011.09.003.

Czeszumski, Artur, Sara Eustergerling, Anne Lang, David Menrath, Michael Gerstenberger, Susanne Schuberth, Felix Schreiber, Zadkiel Zuluaga Rendon, and Peter König. 2020. "Hyperscanning: A Valid Method to Study Neural Inter-Brain Underpinnings of Social Interaction." *Frontiers in Human Neuroscience* 14.

Dana, Hod, Tsai-Wen Chen, Amy Hu, Brenda C. Shields, Caiying Guo, Loren L. Looger, Douglas S. Kim, and Karel Svoboda. 2014. "Thy1-GCaMP6 Transgenic Mice for Neuronal Population Imaging In Vivo." *PLOS ONE* 9(9):e108697. doi: 10.1371/journal.pone.0108697.

Davis, Fred D., René Riedl, Jan vom Brocke, Pierre-Majorique Léger, and Adriane B. Randolph, eds. 2017. *Information Systems and Neuroscience: Gmunden Retreat on NeuroIS 2016*. Vol. 16. Cham: Springer International Publishing.

Dommer, Lukas, Natalie Jäger, Felix Scholkmann, Martin Wolf, and Lisa Holper. 2012. "Between-Brain Coherence during Joint n-Back Task Performance: A Two-Person Functional near-Infrared Spectroscopy Study." *Behavioural Brain Research* 234(2):212–22. doi: 10.1016/j.bbr.2012.06.024.

Donello, John E., Jonathan E. Loeb, and Thomas J. Hope. 1998. "Woodchuck Hepatitis Virus Contains a Tripartite Posttranscriptional Regulatory Element." *Journal of Virology* 72(6):5085–92.

Dumas, Guillaume, Jacqueline Nadel, Robert Soussignan, Jacques Martinerie, and Line Garnero. 2010. "Inter-Brain Synchronization during Social Interaction" edited by J. Lauwereyns. *PLoS ONE* 5(8):e12166. doi: 10.1371/journal.pone.0012166.

Ernst, Monique, and Julie L. Fudge. 2009. "A Developmental Neurobiological Model of Motivated Behavior: Anatomy, Connectivity and Ontogeny of the Triadic Nodes." *Neuroscience & Biobehavioral Reviews* 33(3):367–82. doi: 10.1016/j.neubiorev.2008.10.009.

Ervin, Kelsy S. J., Jennifer M. Lymer, Richard Matta, Amy E. Clipperton-Allen, Martin Kavaliers, and Elena Choleris. 2015. "Estrogen

Involvement in Social Behavior in Rodents: Rapid and Long-Term Actions.” *Hormones and Behavior* 74:53–76. doi: 10.1016/j.yhbeh.2015.05.023.

Ferezou, Isabelle, Florent Haiss, Luc J. Gentet, Rachel Aronoff, Bruno Weber, and Carl C. H. Petersen. 2007. “Spatiotemporal Dynamics of Cortical Sensorimotor Integration in Behaving Mice.” *Neuron* 56(5):907–23. doi: 10.1016/j.neuron.2007.10.007.

Flusberg, Benjamin A., Axel Nimmerjahn, Eric D. Cocker, Eran A. Mukamel, Robert P. J. Barretto, Tony H. Ko, Laurie D. Burns, Juergen C. Jung, and Mark J. Schnitzer. 2008. “High-Speed, Miniaturized Fluorescence Microscopy in Freely Moving Mice.” *Nature Methods* 5(11):935–38. doi: 10.1038/nmeth.1256.

Friard, Olivier, and Marco Gamba. 2016. “BORIS: A Free, Versatile Open-Source Event-Logging Software for Video/Audio Coding and Live Observations.” *Methods in Ecology and Evolution* 7(11):1325–30. doi: 10.1111/2041-210X.12584.

Funane, Tsukasa, Masashi Kiguchi, Hirokazu Atsumori, Hiroki Sato, Kisou Kubota, and Hideaki Koizumi. 2011. “Synchronous Activity of Two People’s Prefrontal Cortices during a Cooperative Task Measured by Simultaneous near-Infrared Spectroscopy.” *Journal of Biomedical Optics* 16(7):077011. doi: 10.1117/1.3602853.

Ghanbari, Leila, Russell E. Carter, Mathew L. Rynes, Judith Dominguez, Gang Chen, Anant Naik, Jia Hu, Md Abdul Kader Sagar, Lenora Haltom, Nahom Mossazghi, Madelyn M. Gray, Sarah L. West, Kevin W. Eliceiri, Timothy J. Ebner, and Suhasa B. Kodandaramaiah. 2019. “Cortex-Wide Neural Interfacing via Transparent Polymer Skulls.”

Nature Communications 10(1):1500. doi: 10.1038/s41467-019-09488-0.

Ghosh, Kunal K., Laurie D. Burns, Eric D. Cocker, Axel Nimmerjahn, Yaniv Ziv, Abbas El Gamal, and Mark J. Schnitzer. 2011. “Miniaturized Integration of a Fluorescence Microscope.” *Nature Methods* 8(10):871–78. doi: 10.1038/nmeth.1694.

Glover, Gary H. 2011. “Overview of Functional Magnetic Resonance Imaging.” *Neurosurgery Clinics* 22(2):133–39. doi: 10.1016/j.nec.2010.11.001.

Goense, Jozien, Yvette Bohraus, and Nikos K. Logothetis. 2016. “FMRI at High Spatial Resolution: Implications for BOLD-Models.” *Frontiers in Computational Neuroscience* 10.

Grinsted, A., J. C. Moore, and S. Jevrejeva. 2004. “Application of the Cross Wavelet Transform and Wavelet Coherence to Geophysical Time Series.” *Nonlinear Processes in Geophysics* 11(5/6):561–66.

de Groot, Andres, Bastijn JG van den Boom, Romano M. van Genderen, Joris Coppens, John van Veldhuijzen, Joop Bos, Hugo Hoedemaker, Mario Negrello, Ingo Willuhn, Chris I. De Zeeuw, and Tycho M. Hoogland. 2020. “NINscope, a Versatile Miniscope for Multi-Region Circuit Investigations” edited by M. R. Carey, K. M. Wassum, and D. J. Cai. *ELife* 9:e49987. doi: 10.7554/eLife.49987.

Gunaydin, Lisa A., Logan Grosenick, Joel C. Finkelstein, Isaac V. Kauvar, Lief E. Fenno, Avishek Adhikari, Stephan Lammel, Julie J. Mirzabekov, Raag D. Airan, Kelly A. Zalocusky, Kay M. Tye, Polina Anikeeva, Robert C. Malenka, and Karl Deisseroth. 2014. “Natural

Neural Projection Dynamics Underlying Social Behavior." *Cell* 157(7):1535–51. doi: 10.1016/j.cell.2014.05.017.

Hari, Riitta, and Miiamaaria V. Kujala. 2009. "Brain Basis of Human Social Interaction: From Concepts to Brain Imaging." *Physiological Reviews* 89(2):453–79. doi: 10.1152/physrev.00041.2007.

Harikrishna, Ette, Komalla Ashoka Reddy, Ette Harikrishna, and Komalla Ashoka Reddy. 2021. *Use of Transforms in Biomedical Signal Processing and Analysis*. IntechOpen.

Herman, James P., and Kellie L. Tamashiro. 2017. "The Visible Burrow System: A View from across the Hall." *Physiology & Behavior* 178:103–9. doi: 10.1016/j.physbeh.2017.01.021.

Hirsch, Joy, Xian Zhang, J. Adam Noah, and Yumie Ono. 2017. "Frontal Temporal and Parietal Systems Synchronize within and across Brains during Live Eye-to-Eye Contact." *NeuroImage* 157:314–30. doi: 10.1016/j.neuroimage.2017.06.018.

Hitti, Frederick L., and Steven A. Siegelbaum. 2014. "The Hippocampal CA2 Region Is Essential for Social Memory." *Nature* 508(7494):88–92. doi: 10.1038/nature13028.

Insel, Thomas R., and Russell D. Fernald. 2004. "HOW THE BRAIN PROCESSES SOCIAL INFORMATION: Searching for the Social Brain." *Annual Review of Neuroscience* 27(1):697–722. doi: 10.1146/annurev.neuro.27.070203.144148.

Jacob, Alexander D., Adam I. Ramsaran, Andrew J. Mocle, Lina M. Tran, Chen Yan, Paul W. Frankland, and Sheena A. Josselyn. 2018. "A Compact Head-Mounted Endoscope for In Vivo Calcium Imaging in

Freely Behaving Mice.” *Current Protocols in Neuroscience* 84(1):e51. doi: 10.1002/cpns.51.

Jakupovic, Jasmina, Ningdong Kang, and Michael J. Baum. 2008. “Effect of Bilateral Accessory Olfactory Bulb Lesions on Volatile Urinary Odor Discrimination and Investigation as Well as Mating Behavior in Male Mice.” *Physiology & Behavior* 93(3):467–73. doi: 10.1016/j.physbeh.2007.10.005.

Jares-Erijman, Elizabeth A., and Thomas M. Jovin. 2003. “FRET Imaging.” *Nature Biotechnology* 21(11):1387–95. doi: 10.1038/nbt896.

Jiang, J., B. Dai, D. Peng, C. Zhu, L. Liu, and C. Lu. 2012. “Neural Synchronization during Face-to-Face Communication.” *Journal of Neuroscience* 32(45):16064–69. doi: 10.1523/JNEUROSCI.2926-12.2012.

Kaidanovich-Beilin, Oksana, Tatiana Lipina, Igor Vukobradovic, John Roder, and James R. Woodgett. 2011. “Assessment of Social Interaction Behaviors.” *Journal of Visualized Experiments : JoVE* (48):2473. doi: 10.3791/2473.

Keysers, Christian, Ewelina Knapska, Marta A. Moita, and Valeria Gazzola. 2022. “Emotional Contagion and Prosocial Behavior in Rodents.” *Trends in Cognitive Sciences* 26(8):688–706. doi: 10.1016/j.tics.2022.05.005.

Kim, Do Gyeong, Edson Luck Gonzales, Seonmin Kim, Yujeong Kim, Keremkleroo Jym Adil, Se Jin Jeon, Kyu Suk Cho, Kyoung Ja Kwon, and Chan Young Shin. 2019. “Social Interaction Test in Home Cage as a Novel and Ethological Measure of Social Behavior in Mice.”

Experimental Neurobiology 28(2):247–60. doi: 10.5607/en.2019.28.2.247.

Kingsbury, Lyle, and Weizhe Hong. 2020. "A Multi-Brain Framework for Social Interaction." *Trends in Neurosciences* 43(9):651–66. doi: 10.1016/j.tins.2020.06.008.

Kingsbury, Lyle, Shan Huang, Jun Wang, Ken Gu, Peyman Golshani, Ye Emily Wu, and Weizhe Hong. 2019. "Correlated Neural Activity and Encoding of Behavior Across Brains of Socially Interacting Individuals." *Cell* 178(2):429-446.e16. doi: 10.1016/j.cell.2019.05.022.

Ko, Jaewon. 2017. "Neuroanatomical Substrates of Rodent Social Behavior: The Medial Prefrontal Cortex and Its Projection Patterns." *Frontiers in Neural Circuits* 11.

Kogan, Jeffrey H., Paul W. Franklandand, and Alcino J. Silva. 2000. "Long-Term Memory Underlying Hippocampus-Dependent Social Recognition in Mice." *Hippocampus* 10(1):47–56. doi: 10.1002/(SICI)1098-1063(2000)10:1<47::AID-HIPO5>3.0.CO;2-6.

Konvalinka, Ivana, and Andreas Roepstorff. 2012. "The Two-Brain Approach: How Can Mutually Interacting Brains Teach Us Something about Social Interaction?" *Frontiers in Human Neuroscience* 6.

Lee, Eunee, Jiso Hong, Young-Gyun Park, Sujin Chae, Yong Kim, and Daesoo Kim. 2015. "Left Brain Cortical Activity Modulates Stress Effects on Social Behavior." *Scientific Reports* 5(1):13342. doi: 10.1038/srep13342.

Lee, Eunee, Issac Rhim, Jong Won Lee, Jeong-Wook Ghim, Seungjoon Lee, Eunjoon Kim, and Min Whan Jung. 2016. "Enhanced Neuronal Activity in the Medial Prefrontal Cortex during Social Approach Behavior." *The Journal of Neuroscience* 36(26):6926–36. doi: 10.1523/JNEUROSCI.0307-16.2016.

Lee, Eun-Hwa, Jin-Young Park, Yunjin Lee, and Pyung-Lim Han. 2018. "Sociability and Social Novelty Preference Tests Using a U-Shaped Two-Choice Field." *Bio-Protocol* 8(10):e2853. doi: 10.21769/BioProtoc.2853.

Lee, Seon A., Kevin S. Holly, Vladislav Voziyanov, Stephanie L. Villalba, Rudi Tong, Holly E. Grigsby, Edward Glasscock, Francis G. Szele, Ioannis Vlachos, and Teresa A. Murray. 2016. "Gradient Index Microlens Implanted in Prefrontal Cortex of Mouse Does Not Affect Behavioral Test Performance over Time." *PLOS ONE* 11(1):e0146533. doi: 10.1371/journal.pone.0146533.

Lehr, Andrew B., Arvind Kumar, Christian Tetzlaff, Torkel Hafting, Marianne Fyhn, and Tristan M. Stöber. 2021. "CA2 beyond Social Memory: Evidence for a Fundamental Role in Hippocampal Information Processing." *Neuroscience & Biobehavioral Reviews* 126:398–412. doi: 10.1016/j.neubiorev.2021.03.020.

Liang, Bo, Lifeng Zhang, Giovanni Barbera, Wenting Fang, Jing Zhang, Xiaochun Chen, Rong Chen, Yun Li, and Da-Ting Lin. 2018. "Distinct and Dynamic ON and OFF Neural Ensembles in the Prefrontal Cortex Code Social Exploration." *Neuron* 100(3):700-714.e9. doi: 10.1016/j.neuron.2018.08.043.

Liberti, William A., L. Nathan Perkins, Daniel P. Leman, and Timothy J. Gardner. 2017. “An Open Source, Wireless Capable Miniature Microscope System.” *Journal of Neural Engineering* 14(4):045001. doi: 10.1088/1741-2552/aa6806.

Liberti, William A., Tobias A. Schmid, Angelo Forli, Madeleine Snyder, and Michael M. Yartsev. 2022. “A Stable Hippocampal Code in Freely Flying Bats.” *Nature* 604(7904):98–103. doi: 10.1038/s41586-022-04560-0.

Lichtman, Jeff W., and José-Angel Conchello. 2005. “Fluorescence Microscopy.” *Nature Methods* 2(12):910–19. doi: 10.1038/nmeth817.

Likhtik, Ekaterina, Joseph M. Stujenske, Mihir A Topiwala, Alexander Z. Harris, and Joshua A. Gordon. 2014. “Prefrontal Entrainment of Amygdala Activity Signals Safety in Learned Fear and Innate Anxiety.” *Nature Neuroscience* 17(1):106–13. doi: 10.1038/nn.3582.

Lindenberger, Ulman, Shu-Chen Li, Walter Gruber, and Viktor Müller. 2009. “Brains Swinging in Concert: Cortical Phase Synchronization While Playing Guitar.” *BMC Neuroscience* 10(1):22. doi: 10.1186/1471-2202-10-22.

Liu, Tao, and Matthew Pelowski. 2014. “A New Research Trend in Social Neuroscience: Towards an Interactive-Brain Neuroscience.” *PsyCh Journal* 3(3):177–88. doi: 10.1002/pchj.56.

Liu, Tiaotiao, Chengxi Qi, Wenwen Bai, Xin Tian, and Xuyuan Zheng. 2022. “Behavioral State-Dependent Oscillatory Activity in Prefrontal Cortex Induced by Chronic Social Defeat Stress.” *Frontiers in Neuroscience* 16.

Lo, Liching, Shenqin Yao, Dong-Wook Kim, Ali Cetin, Julie Harris, Hongkui Zeng, David J. Anderson, and Brandon Weissbourd. 2019. "Connectional Architecture of a Mouse Hypothalamic Circuit Node Controlling Social Behavior." *Proceedings of the National Academy of Sciences* 116(15):7503–12. doi: 10.1073/pnas.1817503116.

Ma, Ying, Mohammed A. Shaik, Sharon H. Kim, Mariel G. Kozberg, David N. Thibodeaux, Hanzhi T. Zhao, Hang Yu, and Elizabeth M. C. Hillman. 2016. "Wide-Field Optical Mapping of Neural Activity and Brain Haemodynamics: Considerations and Novel Approaches." *Philosophical Transactions of the Royal Society B: Biological Sciences* 371(1705):20150360. doi: 10.1098/rstb.2015.0360.

Makino, Hiroshi, Chi Ren, Haixin Liu, An Na Kim, Neehar Kondapaneni, Xin Liu, Duygu Kuzum, and Takaki Komiyama. 2017. "Transformation of Cortex-Wide Emergent Properties during Motor Learning." *Neuron* 94(4):880-890.e8. doi: 10.1016/j.neuron.2017.04.015.

Martínez-Torres, Sara, Maria Gomis-González, Alba Navarro-Romero, Rafael Maldonado, and Andrés Ozaita. 2019. "Use of the Vsoc-Maze to Study Sociability and Preference for Social Novelty in Rodents." *Bio-Protocol* 9(20):e3393. doi: 10.21769/BioProtoc.3393.

Michel, Christoph M., and Denis Brunet. 2019. "EEG Source Imaging: A Practical Review of the Analysis Steps." *Frontiers in Neurology* 10.

Miura, Isamu, Eric T. N. Overton, Nobuhiro Nakai, Takakazu Kawamata, Masaaki Sato, and Toru Takumi. 2020. "Imaging the Neural Circuit Basis of Social Behavior: Insights from Mouse and Human Studies." *Neurologia Medico-Chirurgica* 60(9):429–38. doi: 10.2176/nmc.ra.2020-0088.

Montagni, Elena, Francesco Resta, Emilia Conti, Alessandro Scaglione, Maria Pasquini, Silvestro Micera, Anna Letizia Allegra Mascaro, and Francesco Saverio Pavone. 2018. "Wide-Field Imaging of Cortical Neuronal Activity with Red-Shifted Functional Indicators during Motor Task Execution." *Journal of Physics D: Applied Physics* 52(7):074001.

Montague, P. Read, Gregory S. Berns, Jonathan D. Cohen, Samuel M. McClure, Giuseppe Pagnoni, Mukesh Dhamala, Michael C. Wiest, Igor Karpov, Richard D. King, Nathan Apple, and Ronald E. Fisher. 2002. "Hyperscanning: Simultaneous FMRI during Linked Social Interactions." *NeuroImage* 16(4):1159–64. doi: 10.1006/nimg.2002.1150.

Moy, S. S., J. J. Nadler, A. Perez, R. P. Barbaro, J. M. Johns, T. R. Magnuson, J. Piven, and J. N. Crawley. 2004. "Sociability and Preference for Social Novelty in Five Inbred Strains: An Approach to Assess Autistic-like Behavior in Mice." *Genes, Brain, and Behavior* 3(5):287–302. doi: 10.1111/j.1601-1848.2004.00076.x.

Müller, Viktor, and Ulman Lindenberger. 2014. "Hyper-Brain Networks Support Romantic Kissing in Humans." *PLOS ONE* 9(11):e112080. doi: 10.1371/journal.pone.0112080.

Murakami, Tomonari, Takashi Yoshida, Teppei Matsui, and Kenichi Ohki. 2015. "Wide-Field Ca(2+) Imaging Reveals Visually Evoked Activity in the Retrosplenial Area." *Frontiers in Molecular Neuroscience* 8:20. doi: 10.3389/fnmol.2015.00020.

Nadler, J. J., S. S. Moy, G. Dold, N. and Simmons, A. Perez, N. B. Young, R. P. Barbaro, J. Piven, T. R. Magnuson, and J. N. Crawley. 2004.

“Automated Apparatus for Quantitation of Social Approach Behaviors in Mice.” *Genes, Brain and Behavior* 3(5):303–14. doi: 10.1111/j.1601-183X.2004.00071.x.

Nagai, Takeharu, Shuichi Yamada, Takashi Tominaga, Michinori Ichikawa, and Atsushi Miyawaki. 2004. “Expanded Dynamic Range of Fluorescent Indicators for Ca2+ by Circularly Permuted Yellow Fluorescent Proteins.” *Proceedings of the National Academy of Sciences of the United States of America* 101(29):10554–59. doi: 10.1073/pnas.0400417101.

Nakai, Junichi, Masamichi Ohkura, and Keiji Imoto. 2001. “A High Signal-to-Noise Ca2+ Probe Composed of a Single Green Fluorescent Protein.” *Nature Biotechnology* 19(2):137–41. doi: 10.1038/84397.

Nöbauer, Tobias, Oliver Skocek, Alejandro J. Pernía-Andrade, Lukas Weilguny, Francisca Martínez Traub, Maxim I. Molodtsov, and Alipasha Vaziri. 2017. “Video Rate Volumetric Ca2+ Imaging across Cortex Using Seeded Iterative Demixing (SID) Microscopy.” *Nature Methods* 14(8):811–18. doi: 10.1038/nmeth.4341.

Ohkura, Masamichi, Masanori Matsuzaki, Haruo Kasai, Keiji Imoto, and Junichi Nakai. 2005. “Genetically Encoded Bright Ca2+ Probe Applicable for Dynamic Ca2+ Imaging of Dendritic Spines.” *Analytical Chemistry* 77(18):5861–69. doi: 10.1021/ac0506837.

Okuyama, Teruhiro, Takashi Kitamura, Dheeraj S. Roy, Shigeyoshi Itohara, and Susumu Tonegawa. 2016. “Ventral CA1 Neurons Store Social Memory.” *Science* 353(6307):1536–41. doi: 10.1126/science.aaf7003.

Payne, Lisa, and John Kounios. 2009. “Coherent Oscillatory Networks Supporting Short-Term Memory Retention.” *Brain Research* 1247:126–32. doi: 10.1016/j.brainres.2008.09.095.

Prevedel, Robert, Young-Gyu Yoon, Maximilian Hoffmann, Nikita Pak, Gordon Wetzstein, Saul Kato, Tina Schrödel, Ramesh Raskar, Manuel Zimmer, Edward S. Boyden, and Alipasha Vaziri. 2014. “Simultaneous Whole-Animal 3D-Imaging of Neuronal Activity Using Light-Field Microscopy.” *Nature Methods* 11(7):727–30. doi: 10.1038/nmeth.2964.

Quaresima, Valentina, and Marco Ferrari. 2019. “Functional Near-Infrared Spectroscopy (FNIRS) for Assessing Cerebral Cortex Function During Human Behavior in Natural/Social Situations: A Concise Review.” *Organizational Research Methods* 22(1):46–68. doi: 10.1177/1094428116658959.

Quarta, Eros, Alessandro Scaglione, Jessica Lucchesi, Leonardo Sacconi, Anna Letizia Allegra Mascaro, and Francesco Saverio Pavone. 2022. “Distributed and Localized Dynamics Emerge in the Mouse Neocortex during Reach-to-Grasp Behavior.” *Journal of Neuroscience* 42(5):777–88. doi: 10.1523/JNEUROSCI.0762-20.2021.

Rajoub, Bashar. 2020. “Chapter 2 - Characterization of Biomedical Signals: Feature Engineering and Extraction.” Pp. 29–50 in *Biomedical Signal Processing and Artificial Intelligence in Healthcare*, *Developments in Biomedical Engineering and Bioelectronics*, edited by W. Zgallai. Academic Press.

Ramirez Pacheco, Julio, Deni Torres Román, and Homero Toral Cruz. 2012. “Distinguishing Stationary/Nonstationary Scaling Processes Using

Wavelet Tsallis q -Entropies." *Mathematical Problems in Engineering* 2012:1–18. doi: 10.1155/2012/867042.

Redolfi, Nelly, Paloma García-Casas, Chiara Fornetto, Sonia Sonda, Paola Pizzo, and Diana Pendin. 2021. "Lighting Up Ca2+ Dynamics in Animal Models." *Cells* 10(8):2133. doi: 10.3390/cells10082133.

Ricceri, Laura, Caterina Michetti, and Maria Luisa Scattoni. 2016. "Chapter 17 - Mouse Behavior and Models for Autism Spectrum Disorders." Pp. 269–93 in *Neuronal and Synaptic Dysfunction in Autism Spectrum Disorder and Intellectual Disability*, edited by C. Sala and C. Verpelli. San Diego: Academic Press.

Ryan, Bryce C., Nancy B. Young, Sheryl S. Moy, and Jacqueline N. Crawley. 2008. "OLFACTORY CUES ARE SUFFICIENT TO ELICIT SOCIAL APPROACH BEHAVIORS BUT NOT SOCIAL TRANSMISSION OF FOOD PREFERENCE IN C57BL/6J MICE." *Behavioural Brain Research* 193(2):235–42. doi: 10.1016/j.bbr.2008.06.002.

Rynes, Mathew L., Daniel A. Surinach, Samantha Linn, Michael Laroque, Vijay Rajendran, Judith Dominguez, Orestes Hadjistamoulou, Zahra S. Navabi, Leila Ghanbari, Gregory W. Johnson, Mojtaba Nazari, Majid H. Mohajerani, and Suhasa B. Kodandaramaiah. 2021. "Miniaturized Head-Mounted Microscope for Whole-Cortex Mesoscale Imaging in Freely Behaving Mice." *Nature Methods* 18(4):417–25. doi: 10.1038/s41592-021-01104-8.

Sah, P., E. S. L. Faber, M. Lopez De Armentia, and J. Power. 2003. "The Amygdaloid Complex: Anatomy and Physiology." *Physiological Reviews* 83(3):803–34. doi: 10.1152/physrev.00002.2003.

Sakkalis, Vangelis, Theofanis Oikonomou, Ellie Pachou, Ioannis Tollis, Sifis Micheloyannis, and Michalis Zervakis. 2006. “Time-Significant Wavelet Coherence for the Evaluation of Schizophrenic Brain Activity Using a Graph Theory Approach.” Pp. 4265–68 in *2006 International Conference of the IEEE Engineering in Medicine and Biology Society*.

Scholkmann, Felix, Lisa Holper, Ursula Wolf, and Martin Wolf. 2013. “A New Methodical Approach in Neuroscience: Assessing Inter-Personal Brain Coupling Using Functional near-Infrared Imaging (FNIRI) Hyperscanning.” *Frontiers in Human Neuroscience* 7.

Scott, Benjamin B., Stephan Y. Thiberge, Caiying Guo, D. Gowanlock R. Tervo, Carlos D. Brody, Alla Y. Karpova, and David W. Tank. 2018. “Imaging Cortical Dynamics in GCaMP Transgenic Rats with a Head-Mounted Widefield Macroscope.” *Neuron* 100(5):1045-1058.e5. doi: 10.1016/j.neuron.2018.09.050.

Silverman, Jill L., Mu Yang, Catherine Lord, and Jacqueline N. Crawley. 2010. “Behavioural Phenotyping Assays for Mouse Models of Autism.” *Nature Reviews Neuroscience* 11(7):490–502. doi: 10.1038/nrn2851.

Skocek, Oliver, Tobias Nöbauer, Lukas Weilguny, Francisca Martínez Traub, Chuying Naomi Xia, Maxim I. Molodtsov, Abhinav Grama, Masahito Yamagata, Daniel Aharoni, David D. Cox, Peyman Golshani, and Alipasha Vaziri. 2018. “High-Speed Volumetric Imaging of Neuronal Activity in Freely Moving Rodents.” *Nature Methods* 15(6):429–32. doi: 10.1038/s41592-018-0008-0.

Stokes, George Gabriel. 1852. “XXX. On the Change of Refrangibility of Light.” *Philosophical Transactions of the Royal Society of London* 142:463–562. doi: 10.1098/rstl.1852.0022.

Tallini, Yvonne N., Masamichi Ohkura, Bum-Rak Choi, Guangju Ji, Keiji Imoto, Robert Doran, Jane Lee, Patricia Plan, Jason Wilson, Hong-Bo Xin, Atsushi Sanbe, James Gulick, John Mathai, Jeffrey Robbins, Guy Salama, Junichi Nakai, and Michael I. Kotlikoff. 2006. “Imaging Cellular Signals in the Heart in Vivo: Cardiac Expression of the High-Signal Ca2+ Indicator GCaMP2.” *Proceedings of the National Academy of Sciences of the United States of America* 103(12):4753–58. doi: 10.1073/pnas.0509378103.

Tian, Lin, S. Andrew Hires, Tianyi Mao, Daniel Huber, M. Eugenia Chiappe, Sreekanth H. Chalasani, Leopoldo Petreanu, Jasper Akerboom, Sean A. McKinney, Eric R. Schreiter, Cornelia I. Bargmann, Vivek Jayaraman, Karel Svoboda, and Loren L. Looger. 2009. “Imaging Neural Activity in Worms, Flies and Mice with Improved GCaMP Calcium Indicators.” *Nature Methods* 6(12):875–81. doi: 10.1038/nmeth.1398.

Torrence, Christopher, and Gilbert P. Compo. 1998. “A Practical Guide to Wavelet Analysis.” *Bulletin of the American Meteorological Society* 79(1):61–78. doi: 10.1175/1520-0477(1998)079<0061:APGTWA>2.0.CO;2.

Torrence, Christopher, and Peter J. Webster. 1999. “Interdecadal Changes in the ENSO–Monsoon System.” *Journal of Climate* 12(8):2679–90. doi: 10.1175/1520-0442(1999)012<2679:ICITEM>2.0.CO;2.

Ueda, Yoshibumi, Showming Kwok, and Yasunori Hayashi. 2013. “Application of FRET Probes in the Analysis of Neuronal Plasticity.” *Frontiers in Neural Circuits* 7:163. doi: 10.3389/fncir.2013.00163.

Wallace, Damian J., and Jason N. D. Kerr. 2019. “Circuit Interrogation in Freely Moving Animals.” *Nature Methods* 16(1):9–11. doi: 10.1038/s41592-018-0275-9.

Yang, Mu, Jill L. Silverman, and Jacqueline N. Crawley. 2011. “Automated Three-Chambered Social Approach Task for Mice.” *Current Protocols in Neuroscience* Chapter 8:Unit 8.26. doi: 10.1002/0471142301.ns0826s56.

Yang, Weijian, and Rafael Yuste. 2017. “In Vivo Imaging of Neural Activity.” *Nature Methods* 14(4):349–59. doi: 10.1038/nmeth.4230.

Yizhar, Ofer, Lief E. Fenno, Matthias Prigge, Franziska Schneider, Thomas J. Davidson, Daniel J. O’Shea, Vikaas S. Sohal, Inbal Goshen, Joel Finkelstein, Jeanne T. Paz, Katja Stehfest, Roman Fudim, Charu Ramakrishnan, John R. Huguenard, Peter Hegemann, and Karl Deisseroth. 2011. “Neocortical Excitation/Inhibition Balance in Information Processing and Social Dysfunction.” *Nature* 477(7363):171–78. doi: 10.1038/nature10360.

Zatka-Haas, Peter, Nicholas A. Steinmetz, Matteo Carandini, and Kenneth D. Harris. 2021. “Sensory Coding and the Causal Impact of Mouse Cortex in a Visual Decision” edited by M. Vinck, J. I. Gold, and K. Svoboda. *ELife* 10:e63163. doi: 10.7554/eLife.63163.

Zhang, Lifeng, Bo Liang, Giovanni Barbera, Sarah Hawes, Yan Zhang, Kyle Stump, Ira Baum, Yupeng Yang, Yun Li, and Da-Ting Lin. 2019. “Miniscope GRIN Lens System for Calcium Imaging of Neuronal Activity from Deep Brain Structures in Behaving Animals.” *Current Protocols in Neuroscience* 86(1):e56. doi: 10.1002/cpns.56.

Zhang, Mingming, Tao Liu, Matthew Pelowski, and Dongchuan Yu. 2017. “Gender Difference in Spontaneous Deception: A Hyperscanning Study Using Functional near-Infrared Spectroscopy.” *Scientific Reports* 7(1):7508. doi: 10.1038/s41598-017-06764-1.

Zhang, Zhihua, and John Moore. 2011. “Intrinsic Feature Extraction in the COI of Wavelet Power Spectra of Climatic Signals.” Pp. 2354–56 in *2011 4th International Congress on Image and Signal Processing*. Shanghai, China: IEEE.

Ringraziamenti

Desidero ringraziare il Prof. Francesco Saverio Pavone - relatore della mia tesi - per l'opportunità che mi ha dato, per il supporto scientifico che mi ha fornito durante questo percorso e per avermi permesso di raggiungere questo traguardo.

Vorrei ringraziare Letizia - co-supervisor della mia tesi- per la fiducia espressa in questi anni e per la continua stima e apprezzamento dimostrati nei miei confronti. Mi hai accolto da studentessa durante la Laurea Triennale accompagnandomi fino al traguardo del Dottorato e per questo te ne sono riconoscente.

Un ringraziamento particolare va ad Alessandro - *Ale* - per il continuo supporto e la pazienza dimostrata in questi anni. Lo ringrazio per essere stato un punto di riferimento, per essere stato sempre disponibile per qualsiasi dubbio, incertezza, perplessità e per avermi dato numerosi consigli. Un ingegnere che si trova a dover lavorare con una biologa, sfida decisamente ardua. Sono consapevole di non averti reso la vita facile ma da te ho imparato moltissimo e perciò ti ringrazio per tutto quello che mi hai insegnato.

Ringrazio Eros, sei stato la prima persona che mi ha permesso di conoscere il mondo della Neurofotonica, un ambito a me sconosciuto. Abbiamo iniziato a piccoli passi ma se oggi sono qui a scrivere questi ringraziamenti lo devo anche a te, per aver creduto in me prima ancora che io credessi in me stessa. Hai reso questo lavoro una passione, un qualcosa che amo fare.

Vorrei ringraziare la Prof. Valeria Gazzola e il Prof. Christian Keysers per la meravigliosa opportunità che mi hanno dato accogliendomi nel loro gruppo di ricerca al Netherlands Institute for Neuroscience. Siete due Leader e Ricercatori fantastici. Insieme a tutti i ragazzi del Social Brain Lab siete stati una seconda famiglia durante quei mesi di lontananza da casa. Porterò sempre nel cuore la vostra energia, positività e spirito di gruppo. Mi avete aiutato ad affrontare limiti e paure permettendomi di crescere non solo dal profilo scientifico ma anche sul lato personale. Grazie per tutto quello che mi avete insegnato e lasciato, non lo dimenticherò mai.

Jessica.